Bioinspired Stimuli-Responsive Color-Changing Systems

*Golnaz Isapour and Marco Lattuada**

Stimuli-responsive colors are a unique characteristic of certain animals, evolved as either a method to hide from enemies and prey or to communicate their presence to rivals or mates. From a material science perspective, the solutions developed by Mother Nature to achieve these effects are a source of inspiration to scientists for decades. Here, an updated overview of the literature on bioinspired stimuli-responsive color-changing systems is provided. Starting from natural systems, which are the source of inspiration, a classification of the different solutions proposed is given, based on the stimuli used to trigger the color-changing effect.

1. Introduction

It is hard not to be mesmerized by the extraordinary ability of certain animals to change colors in response to a threat, to signal their presence to others, or to camouflage with the environment, in order to hide from potential predators or preys. Examples include some cephalopods and chameleons, which can adapt their colors to the surrounding background in an instant; beetles that change their colors depending of the level of humidity; zebra fish changing their appearance depending on the light conditions, just to name a few. All these creatures share one common feature: they use responsive structural colors.

Two types of coloration exist in nature: pigmentary coloration and structural coloration. Pigmentary coloration, i.e., coloration due to chemical hues or dyes, is probably the most common form of coloration available in natural systems. On the contrary, structural coloration, i.e., coloration caused by microstructural features of a material that interfere with certain wavelengths of light, is less common, but offers some distinctive advantages. Structural colors are highly durable, since they are not affected by pigment photochemical degradation, and are characterized by striking brilliance, metallic luster, purity of colors, and opalescence.

In principle, any material with a refractive index (RI) higher than that of the surroundings can display a wide palette of structural colors, provided that it possesses the proper microstructure. Structural colors are created by the presence of different microstructural features, such as diffraction gratings, photonic crystals, selective mirrors, crystal fibers, spiral coils, and surface gratings, just to cite the most commonly encountered ones. These elements use different mechanisms to produce a color. For example, diffraction gratings are periodic structures that split and diffract light into several beams travelling in different directions, thus creating a structural color, which depends on the spacing between the structures, as well as the direction of observation. Photonic crystals, on the other hand, are 2D or 3D periodic structures with low- and high-refractive-index parts, leading to only selective wavelengths to be reflected by the crystal. Many animals and plants use a combination of different structural colorations' mechanisms, sometimes also including pigmentary coloration, to achieve the desired colors combination.

Understanding the mechanism of structural coloration has led scientists to develop artificial systems that mimic the performance of natural ones.[1–4] Colloidal crystals are typically made of monodispersed spherical particles, assembled usually in face-centered cubic structures. They have been investigated both from a fundamental point of view, as well as for their ability to produce a variety of iridescent colors, depending on the particles size and spacing. Alternatively, colloidal crystals have been used as templates to prepare inverse opals. First, either a monomer solution or an inorganic material precursor infiltrates in the interstices left empty by the particles and then it is solidified by polymerization or through a sol–gel process. Finally, the template particles are removed and leave empty holes in the solidified matrix. Inverse opals have complementary optical properties to those of the original colloidal crystal templates, because the voids left by the particles are now the low-refractive-index structures. Bragg stacks, i.e., periodic assemblies consisting of alternating layers of two materials with very different refractive indices and a well-defined thickness, are another example of a man-made structure that mimics the behavior of diffraction gratings. Their optical properties are determined by the ratio between the refractive indices of the two materials and by the thickness of the layers. The use of biomimicry to try and replicate the structural colors of living systems is quite challenging, because much still has to be learned from the perfection and the complexity of the architectures used by Mother Nature.

Stimuli-responsive structural colors have an obviously more complex architecture.[4] They require the ability to change the microstructure in response to a stimulus. This implies, for example, changing the particles' size or the spacing among particles in a colloidal crystal, changing the thickness of some

G. Isapour, Prof. M. Lattuada
Department of Chemistry
University of Fribourg
Chemin du Musée 9, CH-1700 Fribourg, Switzerland
E-mail: marco.lattuada@unifr.ch

layers in a Bragg stack, or using pigment dislocation, as it occurs in cephalopods. The mimicry of such natural systems has been heavily pursued in the literature,[1,3] because stimuli-responsive structural colors could have potential applications for the creation of smart sensors, of cloaking devices, of intelligent textiles, just to mention a few examples. While research in this area has been carried out for the past three decades, a wide range of novel results have appeared and continue to be published in the literature. In our opinion, the quantity and quality of new results are so overwhelming that we decided to dedicate this review to provide a general overview of the research efforts, made especially in the last 5–6 years, in the field of bioinspired systems showcasing stimuli-responsive structural colors. **Table 1** summarizes some of the advances in the stimuli-responsive structural colors' systems highlighted throughout this work, grouped together based on the structural features that they are based on, and clearly indicating, the stimulus used to trigger the color change.

The work is structured as follows: first, a brief introduction to some of the fundamental physical concepts necessary to understand the behavior of the systems described in this work is presented. This is followed by a review of natural systems showing switchable structural colors, focusing on explaining their mechanisms, and on those works that have provided new insight into the field. Afterward, man-made systems are reviewed by categorizing them by the stimulus used to induce the color switch. We begin with systems based on hydrogels, because the wide variety of chemistry associated with them allows for a variety of stimuli to be used as triggers for the color change, and because they are an almost omnipresent component in artificial stimuli-responsive systems. After covering all the most important stimuli used as triggers (such as temperature (T), pH, electrical and magnetic fields, light, and mechanical force), natural systems artificially modified will be discussed, before the concluding remarks.

2. Fundamental Physical Concepts

We begin by briefly reviewing some fundamental physical concepts, which will be recalled frequently during the work. Structural colors are obtained when a material possesses microstructural features that can interfere with certain wavelengths of light. These microstructural features require a certain level of periodicity in the structure, at least over a given range of length scales. As schematized in **Figure 1**a–c, periodicity in a structure can occur in one, two, or three dimensions. The presence of periodicity results in constructive interference in the light reflected by the structures, for specific wavelengths, depending on the geometry and optical properties of the materials. This gives rise to specific colors of light being preferentially reflected or transmitted by the material.

In order to exemplify the underlying physics, we will consider first what happens in the case of Bragg stacks, i.e., a structure with 1D periodicity, and then to colloidal crystals, which are a common example of a 3D periodic structure. Most of the systems considered here can be rationalized in a similar fashion.[115]

Golnaz Isapour obtained her Bachelor's degree in polymer engineering from Amirkabir University of Technology in Iran. After working in a polymer composite company for a few years, Golnaz moved to Norway to obtain a Master's degree in polymer chemistry from the University of Oslo. She then joined the group of Prof. Marco Lattuada, at the University of Fribourg. Her Ph.D. project aims at designing novel materials with stimuli-responsive color-changing ability that mimic natural systems, using responsive particles as building blocks.

Marco Lattuada received a Master's degree in chemical engineering from Politecnico di Milano, Italy. He obtained a Ph.D. in chemical engineering from ETH, Zurich, under the guidance of Prof. Massimo Morbidelli. He then moved to MIT, where he carried out a postdoc for over 2 years in Prof. Alan Hatton's group. He then moved back to ETH Zurich, where he worked as a senior scientist and group leader for about 6 years, before moving to the University of Fribourg, at the Adolphe Merkle Institute, where he obtained a prestigious Swiss National Science Foundation Professor-founded professorship, to start his independent career. He is currently a Professor in the Department of Chemistry at the University of Fribourg, Switzerland. His research activity is a balanced combination of experimental and modeling work, aiming at engineering smart nano- and microparticles, and at exploiting their self-assembly, with the objective to design novel soft materials.

Bragg stacks, i.e., multilayer structures made of two materials (with different refractive indices) deposited in alternating layers, are an example of a system that is commonly used to produce structural colors. By considering the schematics in Figure 1d, where two materials, A and B, with refractive indices n_A and n_B, respectively, form alternating layers with thicknesses d_A and d_B, constructive interference between the light reflected by the layers is only possible if the wavelength satisfies the following condition

$$\lambda = \frac{2}{m}\left(n_A d_A \cos(\theta_A) + n_B d_B \cos(\theta_B)\right) \quad (1)$$

where θ_A and θ_B are the angles of refraction of the light in the two materials, and m is an integer number. Any change in

Table 1. Highlighted stimuli-responsive structural colors systems throughout this work, classified according to their structure and the stimuli used to trigger the color change.

Structure	Materials and setup	Application target	Stimuli
Hydrogel bulk	– PS microspheres immobilized into polyacrylamide (PAm) supraballs hydrogels[5] – High-aspect-ratio silicon nanocolumns attached or free-standing embedded in PAm gel[6] – Micrometer scale silicon plates coated on one side with Au or Ag (micromirrors) embedded in poly(acrylamide-*co*-acrylic acid) (PAm-*co*-PAA)[7] – Silk-fibroin inverse opals[8] – Fe_3O_4@C colloidal nanoparticles embedded in polyacrylamide glycol gel[9] – Fe_3O_4@SiO_2 colloids colloidal nanoparticles embedded in a composite matrix of PEGMA and PEGDA[10]	Sensors, artificial muscles[6,7]	Humidity, humidity, and pH[7]
(Thin) Films	– Synthetic melanin nanoparticle films[11] – Stacks of alternately deposited thin films of phosphatoantimonic acid, $H_3Sb_3P_2O_{14}$, nanosheets and TiO_2 or SiO_2 nanoparticles[12] – An $HSbP_2O_8$/TiO_2 multilayer structure not only humidity responsive, but also able to distinguish between chemically similar solvent vapors[13] – Alternating thin films of PMMA and PNIPAM-*co*-PGMA[14] – Macroporous PHEMA/PETPTA films[15] – Fe_3O_4@SiO_2 colloids dispersed in the mixture of PEGMA, PEGDA, and TPM (3-trimethoxysilyl-propyl-methacrylate)[16] – A 2D nanocomposite made of silk and titanate nanosheets[17] – Inverse opal hydrogels thin films with PEGDA[18]	Sensors, environmental monitoring, anticounterfeit labeling[14,16]	Humidity, Humidity and temperature[14]
Chiral nematic	– A mesoporous chiral nematic composite of cellulose nanocrystals and a poly(urea formaldehyde)[19] – Nanocrystalline cellulose in PAm hydrogel[20]	Biosensing, optics, functional membranes, soft templates for new materials	Humidity and pressure,[19] Humidity, pH, ionic strength, solvent polarity[20]
Hydrogel bulk	– Inverse opals with PNIPAM microfluidic hydrogel[21] – Silica nanoparticles embedded in poly(*N*-isopropylacrylamide-*co*-*N*-methylolacrylamide)[22] – Microfluidic PNIPAM hydrogel balls containing PS colloidal crystals[23] – Ag/Au nanoparticles coupled with the inverse opal of P(NIPAM-*co*-MA) hydrogel[24] – Inverse opal of MMAA–BIS polymer filled with thermosensitive liquid crystals (LC)[25] – Inverse opal hydrogel based on HEMA, 4-acryloyl morpholine (ACMO), and NIPAM monomers[26] – Au nanoparticles assembled on P(NIPAM-*co*-AAm)[27]	Sensors, active loading and controlled release of drug,[21] energy-saving multicolor displays,[25] plasmonic on/off valve systems for flow control systems[27]	Temperature, Temperature and NIR light,[24] Temperature and voltage,[25] Temperature and pH[27]
(Thin) Films	– 1D free-standing flexible films made of Fe_3O_4@PVP in a PNIPAM matrix[28] – Stacks of alternate films of PNIPAM and poly(*para*-methyl styrene)[29] – Free-standing films of P(NIPAM–AAc) colloidal crystals modified by HEMA[30] – 1D photonic stacks of P(NIPAM-*co*-AA) and TiO_2 layers[31] – Inverse opal film of poly (2-(2-methoxyethoxy)ethyl methacrylate) P(MEO2)[25] – Casts of PS-*b*-P2VP solutions[32] – Diffraction grating composed of nanoemulsions of PNIPAM brush on SPIONS[33]	Sensors, displays[25,30]	Temperature, Temperature and pH,[30,31] Temperature and solvent[25]
Colloidal particles	– PNIPAM brush-coated silica particles[34] – PNIPAM microgel photonic crystals[35] – PNIPAM microgels copolymerized with pH-responsive fluorescein and rhodamine derivatives[36] – Core–shell microgels of PS-P(NIPAM-*co*-AA)[37]	Sensors, displays	Temperature, Temperature and pH[36,37]
Hydrogel bulk	– PS crystalline colloidal arrays incorporated in PAm[38] – Inverse opal hydrogel of P(HEMA-*co*-AA)[39] using PS microspheres as a template – Embedded (PEG)-crosslinked poly((methyl vinylether)-*co*-maleic acid) (PMVE-*co*-MAA) hydrogels in titania/graphene oxide (TiO_2/GO) 1D photonic crystals[40] – Inverse opal hydrogel consisting of 2-hydroxyethyl methacrylate, *N*-isopropylacrylamide, acrylic acid using PS microspheres as a template[41] – PNIPAM gel particles confined in the inverse opal hydrogel consisting of HEMA, AA, and EGDM[42] – Fe_3O_4@PVP immobilized in PNIPAM hydrogel balls[43] – Fe_3O_4@C nanoclusters introduced into a PAm–PAA matrix[44] – Inverse opals of supraballs based on polyionic liquids sensitive to different counterions (e.g., BF_4^-, PF_6^-, Tf_2N^-, NO_3^-, and ClO_4^-)[45] – 2D photonic films and 3D photonic (microfluidic) supraballs to detect 11 kinds of metal ions (Al^{3+}, Zn^{2+}, Cd^{2+}, Li^+, Mg^{2}+, Pb^{2+}, Mn^{2+}, Co^{2+}, Ni^{2+}, Fe^{3+}, and Cu^{2+})[46] – Photonic gel composed of SiO_2 colloidal crystals embedded in PEGMA/EG gel to distinguish alcohol homologs, isomers, and organic solvents[47]	Sensors, displays[42,43]	pH, pH and ionic strength,[38,39,44] pH and temperature,[41,42] counterions,[45,46] alcohol homologs, isomers and organic solvents[47]

Table 1. Continued.

Structure	Materials and setup	Application target	Stimuli
(Thin) Films	– Ultrathin polymer gel film with P2VP gel infiltrated in monolayers of PS[48] – 2D Au nanosphere array attached onto a polyacrylic acid (PAA) hydrogel film[49] – 1D photonic crystals flakes consisting of P(HEMA-*co*-MA) matrix and multilayers of Ag nanoparticles[50] – *Morpho* butterfly wing as a template coated by PMA[51] – *Papilio paris* wing as a template coated by P(AA-*co*-Am)[52] – PMA integrated into the natural gyroid structure of the *C. rubi* butterfly wing[53] – CLC polymer containing crown ether moieties sensitive to Ca^{2+} concentration[54]	Sensors	pH, counterion[54]
Colloidal particles	– 2D free-standing hydrogel films of chitosan (with a thickness of 8 μm), with PS colloidal monolayers of 500 nm in diameter attached on both the surfaces[55] – Ultrathin poly(acrylamide-*co*-acrylic acid) (PAm-*co*-PAA) films' PS colloidal crystals incorporated[56] – Photosensitive PS/AgBr hybrid colloidal crystals prepared with a co-deposition method for gas sensing[57]	Sensors,[55] antiforgery[56]	pH,[55] ionic strength,[56] UV light, and bromine gas[57]
Etalons	– Etalons of P(NIPAM-*co*-AA) microgels in a photoacid *o*-nitrobenzaldehyde (*o*-NBA) solution[58] – P(NIPAM-*co*-AA)-based etalon[59]	Displays, controlled/triggered drug delivery system, sensors	UV light,[58] pH, and temperature[59]
Hydrogel bulk	– An ink consisting of Fe_3O_4@SiO_2, a solvation liquid (ethanol), and a photocurable resin[60] – Fe_3O_4@SiO_2 incorporated into microspheres (hydrogel balls) made of a photocurable resin (PEGDA)[61] – Fe_3O_4@PVP immobilized in PNIPAM hydrogel balls[43] – Aqueous suspension of inverse opals of ETPTA-3-(trimethoxysilyl)-propylmethacrylate (TPM) dispersed in an aqueous ferrofluid of Fe_3O_4 nanocrystals[62] – An on/off reflection switch based on P(S-*co*-AA) nanoparticles of different sizes dispersed in an aqueous ferrofluid made of highly surface-charged Fe_3O_4 nanocrystals.[63] Triple-responsive Janus supraballs (temperature, magnetic, and fluorescence responsive) based on PS colloidal crystals, CdS quantum dots, and PNIPAM hydrogels[64]	Forgery protection, structurally colored design materials and printing technology,[60] switchable color display, signage, bio- and chemical detection, magnetic field sensing,[43,61] magnetic field strength estimation[62]	Magnetic field, magnetic field and temperature[43]
Films	– Films of PETPTA containing Fe_3O_4@C[65] – Films of EG/PDMS containing Fe_3O_4@C[66] – Agarose hydrogel film containing Fe_3O_4@SiO_2 core/shell colloids[67]	Anticounterfeiting labels, displays[67]	Magnetic field
Colloidal particles	– Fe_3O_4@SiO_2 photonic nanochains[68,69] – Microfluidic Janus microspheres of the photocurable resin ETPTA coated by a thin ferromagnetic iron layer and alternate layers of silica and titania[70] – Fe@SiO_2 nanoellipsoids[71] – Fe_3O_4@PVP in organic media[72] – Microfluidic PEGDA microspheres containing Fe_3O_4@SiO_2[73] – Ferrimagnetic Fe_3O_4@SiO_2 nanorod-based liquid crystals[74]	Anticounterfeiting, signage, energy-efficient color displays, sensors	Magnetic field
Fiber	– Stretchable/squeezable PDMS fiber containing carbon encapsulated Fe_3O_4@C embedded in ethylene glycol droplets[75]	None-powered and functionalized fibers for camouflage	Magnetic field
Colloidal particles	– Negatively charged ZnS– silica core–shell colloidal crystals stabilized by PVP[76] – Fe_3O_4@SiO_2 core–shell nanoparticles with hydrophobic surface dispersed in a low-dielectric medium[77] – Hollow Fe_3O_4@C[78] – Crystalline colloidal arrays composed of monodispersed particles of the copolymer PMMA–PS[79] – Colloidal photonic crystal composed of PS nanoparticles and modified ITO electrode with ion exchange resins[80]	Displays	Electric field
Chiral nematic	– Films of polymer-stabilized CLC made of E7 (Merck) mixed with a prepolymer (NOA65) and a chiral dopant (R5011, Merck)[81] – Oblique helicoidal (heliconical) structured CLC made of two dimeric, LCs (1′,7′-bis(4-cyanobiphenyl-4′-yl)heptane (CB7CB) and 1-(4-cyanobiphenyl-4′-yl)-6-(4-cyanobiphenyl-4′-yloxy)hexane (CB6OCB), and a standard LC pentylcyanobiphenyle (Merck), doped with a left-handed chiral additive S811 (Merck)[82] – LCE based on micropatterned inverse opal films based on a mixture of a nematic diacrylate monomer and a monoacrylate mesogenic monomer[83] – Alternate layers of TiO_2 nanoparticles and an LCE base on 4-cyanophenyl-4-(allyloxy) benzoate, 4-methoxyphenyl-4-(allyloxy)benzoate, and 4-((trimethylsilyl)oxy)phenyl-4-(allyloxy)benzoate, and a top layer a fluorescent dye (rhodamin B)[84]	Optical elements and color information, displays	Electric field, Electric field and temperature[83]

Table 1. Continued.

Structure	Materials and setup	Application target	Stimuli
EC device	– EC device covering RGB from 450 to 750 nm wavelength range provided from P3HT for red, PEDOT for blue, PANBS for green, and PDHFA for yellow covering below 450 nm completing the visible color spectrum[85] – An EC device in the form of fiber consisting of (PEDOT), poly(3-methylthiophene) (P3MT), and poly(2,5-dimethoxyaniline)[86] – A rainbow-like EC device with two viologens (4,4′-bipyridine derivatives –nonpolymer electroactive component) with five different multiswitchable colors based on four-zoned electrodes[87] – EC device based on electroactive polyamides with *N*,*N*,*N*′,*N*′-tetraphenyl-*p*-phenylenediamine and tetraphenylbenzidine units in the backbone and heptyl viologen (HV) in the supporting electrolyte[88] – EC device made of TiO_2 inverse opals[89] – EC device made of PS-*b*-P2VP coated on the ITO bottom electrode with a fluoropolymer spacer filled with 2,2,2-trifluoroethanol (TFE) electrolyte[90] – EC device consisting of highly ordered Au-core/Ag-shell nanodomes integrated in a porous SiO_2 film[91] – EC films based on surface plasmon polaritons with polyaniline (PANI) and poly(2,2-dimethyl-3,4 propylenedioxythiophene) thin films integrated with Au nanoslit arrays assembled on the electrode[92]	Energy-saving displays,[85,89–91] electrochromic fibers for wearable devices,[86] smart windows,[87,88] mechanical chameleon,[91] applications ranging from catalysis to Photovoltaics[92]	Electric field
e-skins	– e-skin consisting of artificial chromatophores layers, ultrathin silicon diode, and the PDMS layer and the Ag layer equipped with photodetectors and actuators[93] – Highly stretchable, tactile sensing e-skin equipped with a pressure sensor based on organic EC device (as chromatophore cells), with an elastic pyramidal-microstructured layer (as tactile sensing) and PDMS layer, both layers coated by single-wall carbon nanotubes[94]	Wearable products for consumer, industrial, and military applications, smart robots[94]	Electric field, Electric field and pressure[94]
Hydrogel-based elastomers	– Fe_3O_4@C embedded in a hydrogel made of soft copolymer of *N*-hydroxymethyl acrylamide and *N*-vinylcaprolactam[95] – Fe_3O_4@C embedded in a hydrogel based on Am and EG[96] – Fe_3O_4@C embedded in PAm hydrogel[97] – Tough photonic hydrogel made of PAA network introduced into the PAm layer of a PDGI/PAm gel[98] – Metastable SiO_2 colloidal crystals embedded in the PEGMA/EG gel[99]	Sensors, high-precision displays, fingerprinting materials	Mechanical force, Mechanical force and organic solvents,[97] Mechanical force and temperature and pH[98]
Colloidal-particle-based elastomers	– (PEA-*co*-MMA) colloidal particles embedded in PEA elastomer[100] – PS core, poly(ethyl acrylate-*co*-allyl methacrylate) interlayer, PEA-poly(isobutyl methacrylate) shell[101] – PS core in (PDEGMEMA-*co*-PEA) film[102] – Core–interlayer–shell particles (PS core, poly(ethyl acrylate-*co*-allyl methacrylate) interlayer, PEA shell) embedded in poly(butanediol diacrylate)) elastomer film[103] – Mechanochromic photonic papers made of silica photonic crystals embedded in PEGMA and EG matrix[104]	Sensors, rewritable 3D optical data storage, tunable laser action,[101] security materials[102,104]	Mechanical force, Mechanical force and light and temperature[101]
PDMS-based elastomers	– Patterned 1D array of gold nanoparticles integrated into PDMS[105] – TiO_2 nanoparticles layer coating on an ≈60 μm thick PDMS membrane[106] – Highly stretchable, tactile sensing e-skin based on organic EC device, with an elastic pyramidal-microstructured layer and PDMS layer; both layers coated by single-wall carbon nanotubes[94]	Optical strain sensors, visualization devices,[106] e-skin[94]	Mechanical force
LCE-based elastomers	– LCE film made of A6OCB (6-((4′-cyano-[1,1′-biphenyl]-4-yl)oxy)hexyl acrylate), 4-(4-(hexyloxy)cyclohexyl)phenyl-4-((6-(acryloyloxy)hexyl)oxy)benzoate and hexane-1,6-diyl diacrylate and single-layer close packed array of silver nanoparticles on top of the film[107] – LCE bilayers of PS film on top a poly(methylhydrosiloxane) showing surface wrinkling patterns[108]	Smart environmental-responsive devices, thermal-camouflage skin, color-changing actuators	Mechanical force and temperature
Fibers	– Optical reflectors made of 2D graphene nanoplatelets on a single glass fiber surface integrated in the epoxy resin[109] – PS nanoparticles electrophoretic-deposited onto continuous aligned-carbon-nanotube sheets, which are rolled on an elastic PDMS fiber and eventually embedded in a layer of PDMS[110] – Photonic fiber based on Fe_3O_4@C super-paramagnetic nanoclusters embedded in a PAm matrix[111] – Hollow multilayer fiber photonic fiber made of PDMS and polyisoprene–polystyrene triblock copolymer[112] – Spandex fibers dip-coated by PS core–PMMA interlayer– PEA shell microspheres[113]	Optical deformation sensors, wearable electronic clothes, smart fabrics	Mechanical force

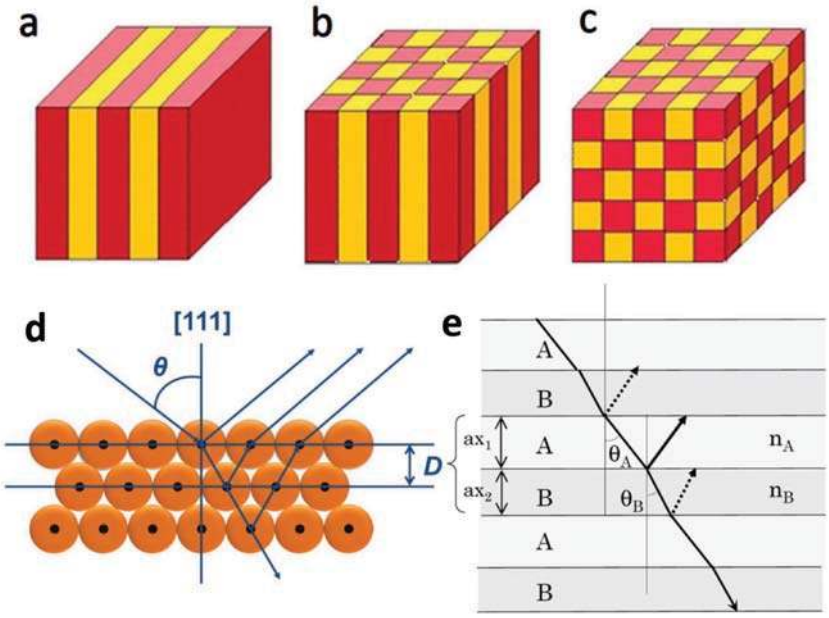

Figure 1. Periodic structures: a) 1D, b) 2D, c) 3D, d) interference patterns of Bragg Stacks,[114] and e) colloidal crystals. a–c,e) Adapted with permission.[4] Copyright 2013, Royal Society of Chemistry. d) Reproduced under the terms of the CC-BY Creative Commons attribution license.[114] Copyright 2013, The Authors; published by MDPI.

spacing of the materials or in their refractive index leads to a change in the wavelength of the reflected light that experiences a constructive interference.

In the case of photonic (colloidal) crystals, the explanation is even more intuitive, as one can refer to the familiar Bragg's law, commonly used to interpret diffraction from an ordered array of spherical particles. Figure 1e is used as a reference. Assuming an ordered configuration of identical spheres, such as the one depicted in the figure, the wavelength λ of light reflected by the array of spheres, which determines the color seen by an observer looking at the crystal, is given by

$$\lambda = 2D\sqrt{{n_{\text{eff}}}^2 - \cos(\theta)^2} \tag{2}$$

where D is the spacing between the planes, n_{eff} is the effective refractive index of the sphere assembly, and θ is the angle of the incident light. According to Equation (2), the wavelength of the radiation reflected by the crystal depends on the spacing between the layers of spheres, on the refractive index of the particles, and on the incident angle of the radiation. By tuning these parameters, different reflected colors appear. To change on demand the wavelength of the reflected light, one or more of these parameters need to vary.

Artificially stimuli-responsive systems are most often based on soft materials, very often swollen and crosslinked polymer networks, which can change their volume in response to a stimulus. This can be used, for example, in a Bragg stack, where at least one of the materials can swell or shrink in response a stimulus. Analogous argument can be used when dealing with colloidal crystals, except that in this case there are two possible scenarios. In the first case, ordered structures made of colloidal particles can be prepared by tightly packing highly monodispersed particles together, as depicted in Figure 1e. The reflected color is dictated by the size of the particles, and an increase in the particles size leads to an increase in the spacing D. By infiltrating a soft material in the interstices left free by the particles, a change in their spacing can be induced by a change in volume of the soft material. If the particles are themselves made of a soft material, their volume change in response to a stimulus leads to the same effect, and to a corresponding color variation.[116]

A second route is instead based on preparing a colloidal crystal of particles in a liquid state, where ordering is induced by a strong repulsion between the particles. This strong repulsion is most often of electrostatic origin, or of steric origin, or combination of both (electrosteric). A change in the repulsive interactions leads to either a change in the colloidal crystal structure or even to a loss of the order and to the corresponding disappearance of the structural color. These changes are caused, for example, by a change in the ionic strength, in the pH, or in the surface charge of the particles, or the application of an external field, introducing a new interaction among the particles.[117] In case of metastable particles, any subtle motion, slight friction, or shearing force can cause a reversible transformation of assembled–disassembled particles' states.[118]

3. Switchable Structural Coloration in Nature

Structural coloration in animals and plants has been a great source of inspiration for researches in the design of artificial materials able to retain their coloration, without having pigments or dyes and with the ability to even switch their colors on demand. There are plenty of examples of creatures with structural coloration on their skin, wings, cuticles, feathers, and leaves.[4,119–122] These topics have been the subject of numerous reviews, and will not be dealt with here. Our focus here is on those systems which are able to change their color rapidly (within a few seconds) in response to a stimulus. Understanding the origin of such responsive coloration, the basic physics behind it and the mechanisms of color change in nature help to develop bioinspired strategies for fabrication of smart color-changing materials with similar functionality.[4,120,123]

There are three major mechanisms that are utilized by living creatures to have stimuli-responsive coloration.

3.1. Bragg Stacks Changing Spacing

The first mechanism is the change in spacing, orientation, or refractive index between ordered layers in a Bragg stack. Several examples are worth mentioning. *Morpho* butterflies are well known for their brilliant iridescent colors. The coloration originates from hierarchical nanostructures of scales on the wings.

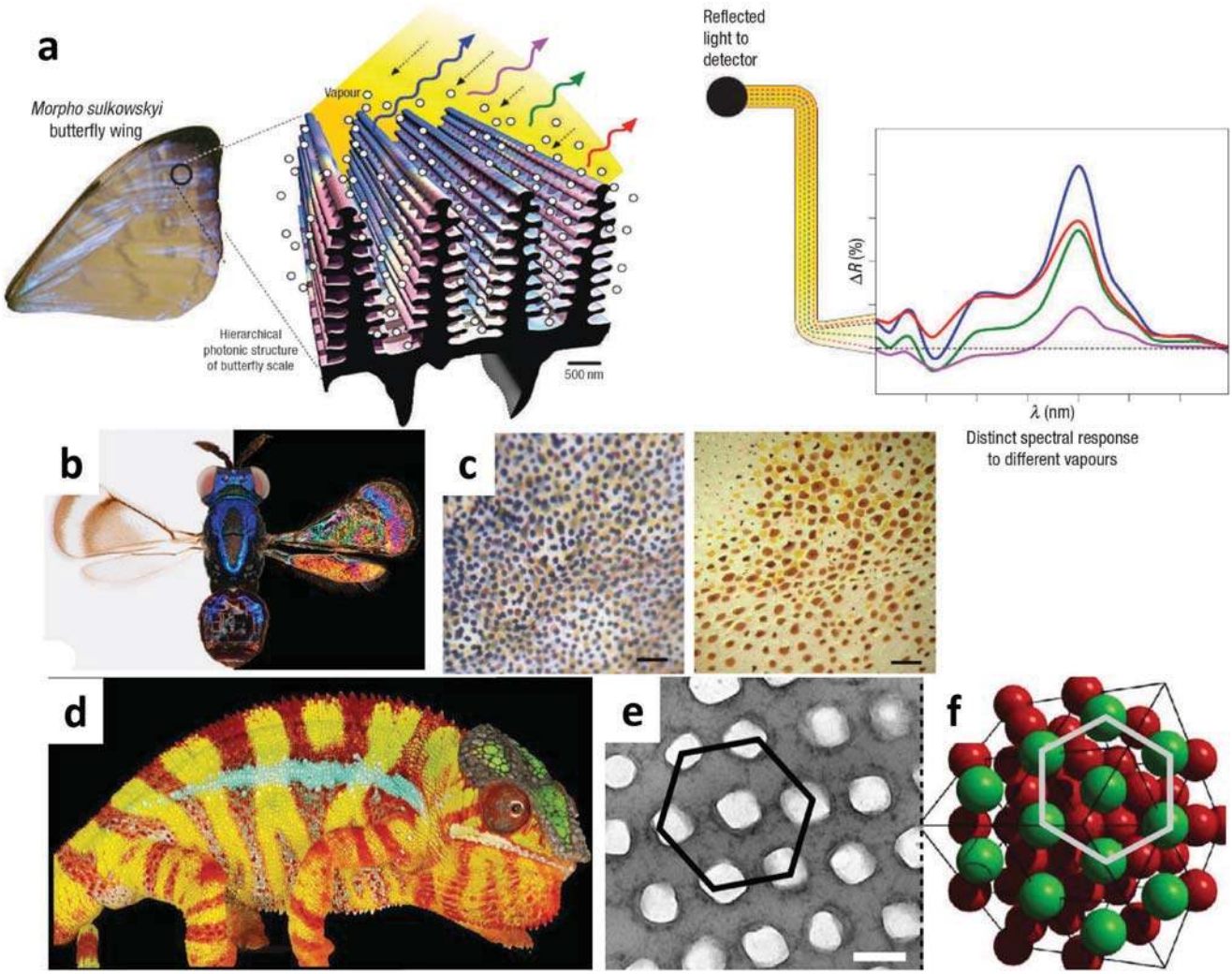

Figure 2. a) A highly selective vapor-responsive system based on hierarchical photonic structures inspired by *M. sulkowskyi* iridescent scales. Differential reflectance spectra ΔR, provide information about the nature and concentration of the vapors: $\Delta R = 100\% \times (R/R_0 - 1)$, where R is a spectrum collected from scales upon vapor exposure and R_0 is a spectrum collected from scales upon exposure to a carrier gas (dry N_2). Reproduced with permission.[124] Copyright 2007, Springer Nature. b) The dramatic effect of changing background reflections on wing interference patterns visibility in *Closterocerus coffeellae*. Reproduced with permission.[125] Copyright 2010, National Academy of Sciences. c) Chromatophores of (left) dorsal mantle and (right) ventral mantle of the cuttlefish *Sepia officinalis*. Scale bar is 1.5 mm. Reproduced with permission.[126] Copyright 2008, Springer Nature. d) The panther chameleon (*Furcifer pardalis*). e) Transmission electron microscopy (TEM) small ≈ 130 nm guanine crystallites. f) Face-centered cubic geometry of the crystallites. d–f) Reproduced under the terms of the Creative Commons Attribution 4.0 International License.[127] Copyright 2015, Macmillan Publishers Limited.

The studies on the iridescence in *Morpho sulkowskyi* butterfly show that the higher visible reflectance is due to a more regular lamellar structure compared to other *Morphos* butterflies.[124] These authors have shown that the iridescence changes in response to different vapors; the higher the vapor pressure, the higher the differential reflectance spectra (ΔR) between the test vapor and the carrier gas. The different spatial periodicity on the wing regions results in different reflectance at different wavelengths (**Figure 2**a).

Eliason and Shawkey have studied, for the first time, the dynamic color changes in a keratinous biophotonic nanostructure.[128] They have shown the iridescent color of the *Theobroma bicolor* feather barbule changes rapidly and reversibly from blue–green to yellow–green in response to humidity and as a result of swelling of the keratin cortex.

Beetles are also known to change the structural colors of their cuticle in response to humidity. *Tmesisternus isabellae* changes the iridescent color—which originates from a multilayer in the scale interior—from golden to red when exposed to a wet environment. Upon water uptake, the periodic multilayers swell and constructive interference results in a different reflected wavelength.[129] A similar behavior has been observed in the beetle *Charidotella egregia*.[130] The nanostructure of the beetle *Hoplia coerulea* is composed of a solid thin flat slab of chitin and a porous layer made of parallel rectangular rods.[131] When exposed to humidity, the scale changes from bright blue to emerald green due to the increased refractive index contrast between chitin and water as opposed to air (pores) in the dry state.

The neon tetra fish change their structural color in response to alteration in light conditions. Their lateral stripe has a blue–green color (λ_{peak} = 490 nm) in the light-adapted state and it turns indigo (λ_{peak} = 400 nm) in the dark-adapted state. It has been found that the origin of the structural color is the stacks of intracellular guanine crystals intercalated with cytoplasm, which reflect light through constructive interference.[132] When the crystal arrays tilt, the spacing of guanine crystals (RI = 1.83) and cytoplasm (RI = 1.33) changes and, as a result, the reflectance spectrum changes too. The *Anolis* lizard is able to rapidly change the brightness of its stripes along its body in response to a mild mechanical force (handling and restraint);[133] it turns from brown to pale blue and green on some parts and to a lighter brown on some other parts along its body. Light exposure also acts as a stimulus for this luminance change.

3.2. Background Effect: Camouflage Ability

Wing interference pattern is another interesting phenomenon observed in some insects with transparent wings. Vivid color patterns are observed through thin-film interference in the wings against backgrounds with certain light properties, while they turn invisible when the background is changed (Figure 2b).[125] This offers another mechanism to design materials with camouflage ability, which is one of the main functions of color change.[134] A quantitative study on the color change and pattern of camouflage in flounders has been reported, in which the degree of spectral match between flounder and background with high-resolution optical instrument has been investigated.[135] Flounders attain the background appearance in terms of color, intensity, and pattern.

White coloration has an important contribution in camouflage of biophotonic structures. It is found that *Sepia officinalis,* a type of cuttlefish, can produce a bright white color on its skin through "leucophores," which are special cells containing organic spheres.[136] On top of the white background created by leucophores, different cells, called chromatophores, provide dark patterns that create contrast, thanks to the luminescence of pigment granules, located inside sacks that are retractable and expandable in a controlled manner by the cuttlefish. Meanwhile, there are colorless cells called "iridophores" containing stacks of thin plates, which act as structural light reflectors. The hierarchy of dermal coloration in *S. officinalis,* i.e., the white-scattering leucophores underneath, iridophores in the middle and chromatophores on top and all acting in harmony, results in the camouflage and color change effect in the cuttlefish (Figure 2c).[126,137] The concept of adaptive coloration and mechanisms of reflection, diffusion, and absorption of light by leucophores, iridophores, and chromatophores, and alteration in texture and morphology of the skin in cephalopods (squid, cuttlefish, and octopus) have been thoroughly reviewed so far.[138] Nevertheless, there are still major challenges in the fabrication of smart materials with exactly the same functionality as the one shown by these creatures.

3.3. Colloidal Crystals Spacing Alteration

Last mechanism is the one displayed by chameleons, which have always been a great source of inspiration in design and fabrication of color-changing systems. A thorough set of experiments combining microscopy, photometric videography, and photonic-bandgap modeling on panther chameleons, in particular, has been conducted.[127] It has been found that there are two populations of iridophores in the dermal structure of the chameleons, each having different morphologies. The underneath layer, which is made of rather disordered guanine nanocrystals, contributes to the near-infrared (IR) reflection of light, while the upper layer, which is made of guanine nanocrystals arranged in a triangle lattice, is responsible for the rapid color change through changing the spacing in the lattice (Figure 2d). Similarly Goda has shown that the rapid color change in the chameleon sand tilefish *Hoplolatilus chlupatyi* originates from a change of spacing between the intracellular reflecting platelets (iridophores).[139] It is found that the color changes from blue to red in response to an increase in K^+ ion concentration in 0.5 s, and to addition of norepinephrine within 1 s. Sapphirinid male copepods change their color both in intensity and wavelength in response to changes in the light conditions. It is shown that this color change originates from changing the spacing between ordered layers of hexagonally shaped guanine crystals. Some types of the copepods can gain camouflage and become transparent against any background.[140]

A common denominator of most biophotonic structures is the presence of guanine crystals. The high reflectivity of many living organisms is due to the extremely high refractive index (RI = 1.83) of guanine crystals. Therefore, understanding guanine-based optics can inspire novel design and fabrication of advanced optical materials. In this respect, the morphology, functionality, and architecture of guanine crystals in organisms and their role in the light manipulation, e.g., scatterers, mirrors, reflectors, and photonic crystals, have been investigated.[141] The morphology of these platelet-forming crystals is beautifully controlled by certain organisms. For instance, in the white widow spider (*Latrodectus pallidus*), coherent scattering from thick dense layers of guanine crystals results in a white color. Disordered multilayer reflectors of guanine crystals in the Japanese Koi fish (*Cyprinus carpio*) reflect a silver color. 3D photonic crystal structures in chameleons and well-aligned multilayer reflectors in neon tetra fish are other examples that have been mentioned before.

4. Artificial Materials

We will begin now to review the most important examples recently proposed in the literature of man-made systems displaying stimuli-responsive structural color-changing features. The classification is made based on the stimulus used to trigger the color-changing mechanisms.

On top of this, inspired by the three mechanisms used by living creatures, outlined in the previous section, we have classified, whenever possible, all systems according to the same structural principles, to establish a clear connection with the natural source of inspiration.

4.1. Gas- and Liquid-Responsive Systems

Gas-responsive systems that are sensitive to small concentrations of certain gas molecules (H_2O, NH_3, NO_2, CO_2, etc.), as well as liquid-responsive systems to detect the amount of a

liquid (water or organic dispersants), are common colorimetric sensors used in safety applications, high-tech and quality control of water/air.[5,9,10,18,57,142] Increased colorimetric sensitivity can be achieved with an optimal fabrication process, e.g., with 1D, 2D, or 3D photonic crystals and functionalized materials. In particular, hydrogel-based systems are a class of materials that have been well studied in tunable structural color systems and will be the focus of this work.

Hydrogels are networks of crosslinked hydrophilic polymer chains, in which the chains are connected through a variety of mechanisms, such as physical entanglement, electrostatic forces, and covalent bonds. The polymer network can swell and take up a great volume of water. The possibility of controlling the degree of hydration and the reversible swelling and contraction of hydrogels make them applicable in various fields, including drug delivery, tissue engineering, sensors, and actuators. The chemical nature of the polymer chains dictates the physicochemical properties of the swelling mechanism and its kinetics. As a result, different types of hydrogels have been synthesized for various applications.[2,143,144] Among these, responsive hydrogels have attracted a great deal of attention in the past few decades. External stimuli such as temperature, pH, humidity, light, electric field, magnetic field, electrolytes, or certain small molecules can be used to trigger a responsive hydrogel to change its volume, which is associated with a change in hydrophobicity, optical, electrical, magnetic, or mechanical properties of the hydrogel.

Inspired by nature, synthetic melanin nanoparticles (NPs)' thin films have been prepared for the first time, which show a rapid reversible color change in response to a change in the humidity level. When the nanoparticles swell upon water uptake in a humid environment, the thin-film thickness increases and the reflection peak wavelength shifts from 475 to 530 nm when relative humidity (RH) is increased from 10% to 90%.[11]

Moving to a more complex architecture, hydrogel-actuated integrated responsive systems (HAIRS) introduce a composite material prepared by integrating high-aspect-ratio (HAR) silicon nanocolumns as a hard element with a hydrogel layer as a soft element, which acts like a synthetic muscle. The humidity-responsive polyacrylamide (PAm) gel is grafted to an Si/SiO_2 substrate via the polyglycidyl methacrylate (PGMA) anchoring layer (**Figure 3**). This complex and yet robust microstructure is able to change its optical pattern by reversibly tilting the nanocolumns based on the humidity level.[6] The nanocolumns can be free-standing or attached on the substrate. The architecture based on high-aspect-ratio structures and the fabrication of hybrid systems composed of nanostructured surfaces combined with responsive hydrogels have been reviewed in details.[145] The key steps in the design of HAIRS are soft lithography, used to replicate high-aspect-ratio structures, and substrate

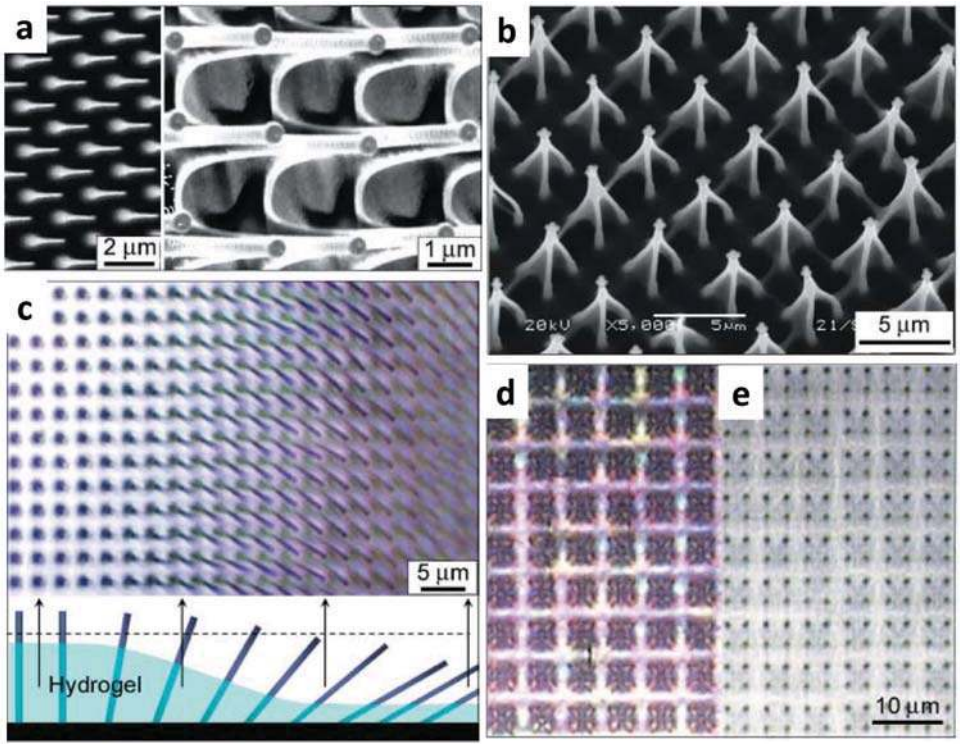

Figure 3. Microscopy study of a hydrogel-actuated integrated responsive systems (HAIRS). a) Scanning electron microscopy (SEM) images of characteristic conical features at the bottom of the nanocolumns formed by the hydrogel layer. b) Optical microscopy image of the drying edge of the nanocolumns in the hydrogel taken perpendicular to the surface. The clarification of the actuation mechanism is shown schematically below the microscopy image. A dashed line in the schematic corresponds to the focal plane in the image. The degree of hydration or swelling of the polymer layer decreases gradually across the sample from left to tilted. c) An example of a complex nanocolumn system in the hydrogel pattern, showing an array of microtraps, in which every group of four attached nanocolumns is held together by the hydrogel. d,e) Optical microscopy imaging microtraps shown in panel (c) in a d) dry and e) a wet state. The switching of the nanocolumns from bent fourfold clusters to a vertical orientation is clear. Reproduced with permission.[6] Copyright 2007, American Association for the Advancement of Science.

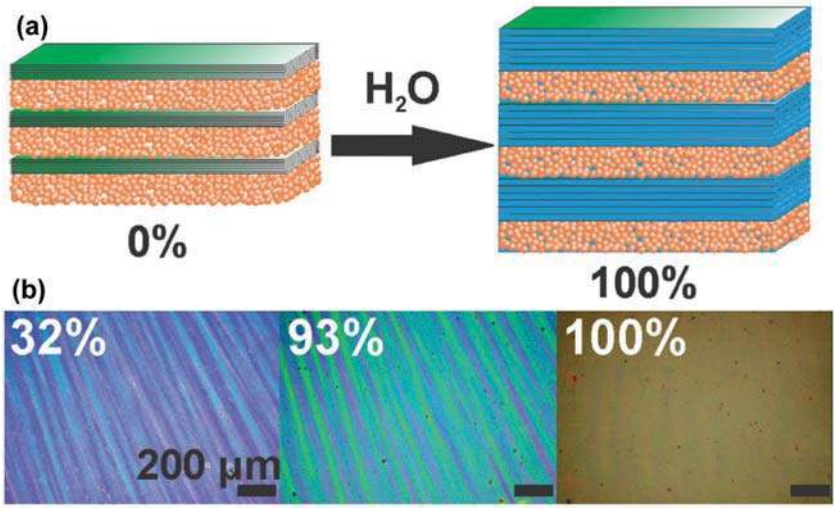

Figure 4. SiO_2 /H3Sb3 P2O14 Bragg stacks. a) Optical humidity sensing features b) Microscopy images of the surface at relative humidity values of 32%, 93%, and 100%, respectively. Reproduced with permission.[12] Copyright 2015, Wiley-VCH.

modification, used to anchor the hydrogel. The system can be responsive in or out of liquid depending on the hydrogel of choice.[145] Various design strategies can be applied in the concept of HAIRS. Taking advantage of plasmonic coatings on the nanostructured surface, micromirrors can be designed. They represent another application of these hybrid systems, and they are investigated in the development of next-generation active optics components. Optical properties can reversibly switch in response to the environment.[7]

Bragg stacks have been one of the well-known strategies in photonics design, in particular, for electronic devices. A highly humidity-responsive touchless positioning interface has been fabricated by phosphatoantimonic acid ($H_3Sb_3P_2O_{14}$) nanosheets.[12] In a humid environment, the bulk material is delaminated into 2D nanosheets in the form of a stable liquid crystalline suspension with anisotropic optical properties (**Figure 4**). The alternative layer in the Bragg stacks is made of either TiO_2 or SiO_2 nanoparticles, to provide a sufficiently high RI difference. Similarly, a photonic $HSbP_2O_8/TiO_2$ multilayer structure has been developed, which is not only humidity responsive, but also able to distinguish between chemically similar solvent vapors.[13] Photonic paper through alternating thin films of poly(methyl methacrylate) (PMMA) and poly(*N*-isopropyl acryl amide)-*co*-polyglycidyl methacrylate (PNIPAM-*co*-PGMA has been prepared.[14] The paper is crosslinked with a pattern so that it only displays the pattern in water (as ink) because of high RI difference of the layers. The color can be tuned by changing the crosslinking density and the ink (water) temperature.

A different strategy has been employed, for the first time, to fabricate colloidal photonic crystals supraballs of about 200 µm in diameter, which consist of polystyrene (PS) microspheres immobilized into PAm hydrogel matrix in an ordered colloidal crystal configuration.[5] Compared to the conventional film-type colloidal photonic crystals, the superball approach takes advantage of having a maximal packing fraction of PS microspheres and a long-range order. By increasing the humidity from 25% to 100%, the PAm hydrogel matrix swells, thus increasing the spacing among the particles. This causes a reflection peak shift from 495 nm (blue) to 654 nm (red).[5]

Siloxane-containing photonic prints have also been fabricated, in which a pattern that develops a visual contrast based on a different crosslinking degree or a different hydrophobization with the background is created with lithographical methods.[16] The pattern only displays when the print is dipped in water and disappears when it is dry. The film is made by Fe_3O_4@SiO_2 nanoparticles embedded in an ordered configuration (i.e., as a colloidal crystal in poly(ethylene glycol) diacrylate (PEGDA), poly(ethylene glycol) methacrylate (PEGMA), and 3-trimethoxysilyl-propyl-methacrylate (TPM), which is later photopolymerized). The reason for showing and hiding the pattern is that the reflection wavelength difference between the pattern and the background becomes significant because of their different degrees of swelling. Similar approach for preparing photonic papers with a writing–erasing feature has been also proposed.[14] With a different approach, photonic gels have been developed as sensors to distinguish alcohol homologs, isomers, and organic solvents with similar structures and physical properties. The photonic gels are composed of SiO_2 colloidal crystals embedded in PEGMA/EG gel, and are able to detect/differentiate the analyte based on the dynamic reflection spectra.[47]

Cholesteric liquid crystals (CLCs) or chiral nematic liquid crystals (LCs) are a special class of materials used as colorimetric sensors, owing to the helical arrangement of their molecular directors, which selectively reflect the incident light. A variety of CLC materials exist in nature, such as chiral biopolymers, condensed DNA phases, and plant cell walls. Light is separated along the helicoidal axis into right-handed and left-handed circularly polarized components. If the pitch of the helix changes by a stimulus, CLCs can be used as smart color-changing systems. CLC-based coatings with the ability to change color have been prepared. When placed in water, within about 30 s they change their color and retake their original color in about 2–3 min when left to dry at ambient conditions.[146] To prepare these responsive patterned CLC coatings, a chiral dopant, nematic mesogens, and polymerizable molecules (benzoic acid derivatives) are mixed together with a photoinitiator (**Figure 5**). After polymerization, the mesogens are trapped into a hydrogel matrix, which swells and contracts upon contact with water and drying, respectively. By using different concentrations of the chiral dopant in the CLCs, which is the responsible component for the cholesteric molecular order, a different colored coating is prepared.

Cellulose nanocrystals (CNCs) are known to be a natural source to prepare CLCs. CNCs are typically 100–200 nm long and 5–15 nm in width.[147] In water, they form chiral nematic liquid crystalline phase at sufficiently high concentrations, and when they are dried they display iridescent colors. The helical pitch of CNCs can be changed by various external means or by co-assembly them with stimuli-responsive materials. Photonic

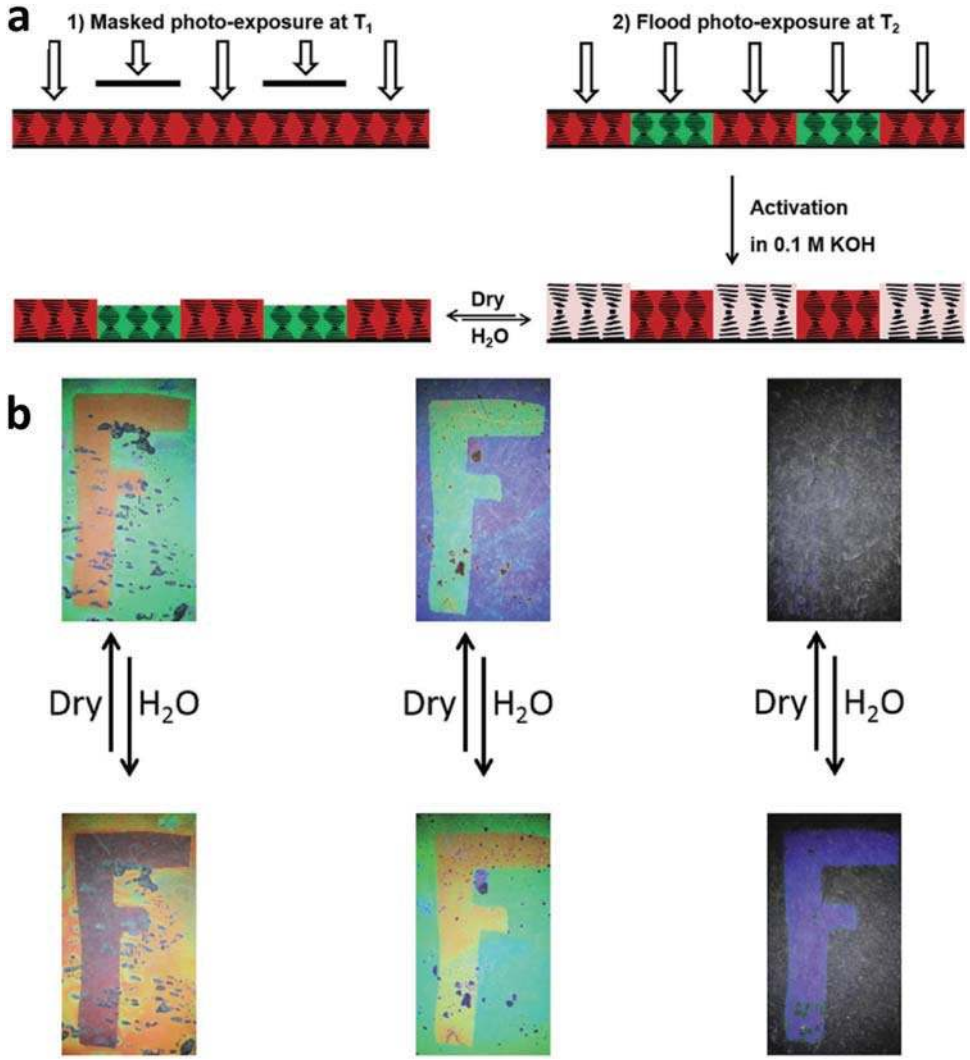

Figure 5. a) Top: schematic representation of the manufacturing method for a patterned cholesteric liquid crystals (CLC) coating. The mixture was partially polymerized in a red-reflecting CLC phase at T_1 during the masked photoexposure step. Subsequent flood exposure at T_2 polymerizes a green-reflecting CLC phase and ensures full polymerization. Bottom: activation with an alkaline solution leads to a patterned water-responsive dual colored changing CLC polymer coating. b) Optical images showing three different polymer salt coatings with the letter "F" in ambient conditions (RH = 40%, T = 20 °C) and in the wet state. The coatings were made as follows: left—20 °C mask, 50 °C flood exposure; middle—20 °C mask, 50 °C flood exposure; and right—20 °C mask, 100 °C flood exposure. The size of the images is 17 mm × 9 mm. Reproduced with permission.[146] Copyright 2015, Royal Society of Chemistry.

multilayer films with co-assembly of CNCs and poly(ethylene glycol)(PEG) have been prepared.[148] The films have different colors depending on the CNC/PEG ratio and reversibly change their colors in the order of seconds as the environment humidity is changed. For a CNC/PEG ratio of 80/20, as RH is increased from 30% to 100%, the green composite film uniformly turns to dark red and then transparent where the multilayer structure is swelled due the highest water uptake. Inspired by the shell structure of the *Chrysina* genus of beetles, a composite structure consisting of a uniaxially oriented polyamide-6 (as a half-wave retarder) sandwiched between CNCs/PEGDA layers has been developed. The composite can go through a simultaneous and reversible 3D deformation and a shift of the Bragg diffraction by a change in the humidity.[149] Similarly, CNC nanocomposite hydrogels with acrylamide (Am)[20] or mesoporous poly(urea formaldehyde)[19] have been prepared, in which the reflection peak is reversibly shifted when the hydrogels uptake the solvent medium (ethanol, methanol, acetone, or isopropanol) and swell to various extents.

A different design principle for the preparation of stimuli-responsive colloidal crystals is to use the inverse opals design. A typical fabrication method to make inverse opals is to incorporate colloidal crystals made of PS microspheres[39,41] or silica nanoparticles[42,150c] in a hydrogel matrix. After removal of the templating particles, an ordered crystal arrangement of pores, i.e., an inverse opal is created. Such porous hydrogels are practical choices to prepare responsive systems that can go through a fast volume transition. Inspired by the Hercules beetle that changes its cuticle's color in response to humidity, thin-film hydrogels of PEGDA inverse opal have been made. The color

of the nanoporous structure changes from blue–green to red in response to an increased humidity.[18]

Using a different fabrication approach, a scalable and roll-to-roll compatible doctor-blade technology has been employed to prepare a reversible vapor detector based on macroporous poly(ethoxylated trimethylolpropane triacrylate) (PETPTA) films.[15] They have used monodispersed silica colloids (225 nm in size) as a template, which are then etched away and result in the macroporous polymer film. A layer of poly(2-hydroxyethyl methacrylate) (PHEMA) coats the porous film and finally the macroporous PHEMA/PETPTA composite films are prepared. Upon condensation of vapors in the porous film, the reflection peak shifts because of the swelling of PHEMA and changing the RI of the diffractive medium. An increase in ethanol vapor pressure (diffractive medium) from 0 to 1 P_0 (where P_0 is the saturation vapor pressure of ethanol at 25 °C, which is equal to 60 mmHg) drives a redshift in the diffraction peak from 500 to 595 nm.

4.2. Temperature-Responsive Systems

In aqueous systems, which are one of the main foci of this review, PNIPAM is the most commonly investigated temperature-responsive polymer. It has a lower critical solution temperature (LCST) of about 32 °C, and for this reason it has been investigated repeatedly in the last 40 years, especially in the form of polymer brushes, hydrogels, and microgels. Research on the synthesis of monodispersed PNIPAM microgels,[151] colored thin films formed by microgels,[152] microgel size, colloidal crystal formation, colloidal stability, ionic strength effects on PNIPAM microgels, and their optical properties,[153] as well as the phase behavior, and rheology of the microgels,[154] is well documented in the literature. There have been various strategies to modify the thermochromic behavior for sensing applications as well.[155]

Chiappelli and Hayward have prepared Bragg stacks of PNIPAM film as the low RI (≈1.5) layer and poly(*para*-methyl styrene) as the high RI layer (≈1.6).[29] By adjusting the number of layers in the stacks, fabrication parameters (spin coating, ultraviolet (UV) exposure duration, and intensity) and tailoring the properties in each layer various reflection behaviors can be achieved upon changing the temperature.

An angle-independent thermoresponsive material with an amorphous array of PNIPAM brush-coated silica nanoparticles has been prepared.[34] In another study, a high-temperature-induced hydrophobic assembly method has been introduced as a simple strategy to create ordered self-assembly of PNIPAM microgels. In the resulting colloidal crystal, the effect of sedimentation time and temperature, solvent quality, and crosslinking degree on the reflected structural color has been investigated.[35] A non-thermosensitive comonomer together with *N*-isopropylacrylamide (NIPAM) has been used to change the volume transition temperature, and silica photonic crystals have been embedded into it to make a thermosensitive photonic gel.[22] Taking the idea of immobilizing nanocrystals in a PNIPAM hydrogel matrix,[156] microfluidic hydrogel balls containing PS colloidal crystals have been prepared, which beautifully display a thermoresponsive color change due to altering the colloidal crystals spacing.[23]

A thermochromic photonic gel based on 2-hydroxyethyl methacrylate (HEMA), 4-acryloyl morpholine (ACMO), and NIPAM monomers has been prepared.[26] The pores are created by periodic structures of PS microspheres of 230–235 nm in diameter. The effect of different molar ratios of HEMA:BIS:NIPAM:ACMO on the temperature-driven swelling of the inverse opal has been investigated. Since P(ACMO) is also a temperature-responsive hydrogel (LCST ≈ 95 °C) the reflection peak of the copolymer gel is changed with temperature. It is found that, compared to NIPAM-only gels, ACMO-containing gels show more uniform $d\lambda_{peak}/dT$ within the temperature range of 10–80 °C over the entire visible light spectra, as well as a smaller hysteresis of the λ_{peak} on the heating and cooling cycle.

According to Bragg's diffraction law, the reflected structural color is angle dependent and this associates with long-range order of the periodic structures. However, fabricating photonic materials that show certain colors independent of observation angles is for some applications an advantage or even a first requirement. Carbon black has been used in the PNIPAM inverse opals to correct the overall magnitude of the scattering coming off the amorphous nanopores.[150b] As a result, the inverse opal hydrogel displays bright angle-independent structural color. There are several strategies to prepare angle-independent structural colors which can be applied in many responsive systems. Inspired by nature, there have been studies in that area as well;[157] nanostructured amorphous colloidal array with short-range order that displays homogeneous, angle-independent, although in most cases nonbrilliant, yet tunable colors[34,158] or beads containing nanocrystals.[159]

Temperature-responsive inverse opals with PNIPAM hydrogel (LCST ≈ 32 °C) have been prepared, in which templates of silica nanoparticles self-assemble in microfluidic droplets of sizes from several to hundreds of micrometers.[21] The silica nanoparticles are packed in crystalline order, which is essential to show structural colors. The presence of macropores left from the SiO_2 provides passages for active drug loading and release by changing the temperature. The hydrogel volume change is associated with changing the average refractive index or spacing between nanopores and the reflection peak changes as a result (**Figure 6**a).

Takeoka has reviewed a new strategy to prepare optical composites, which display reversible angle-independent structural colors based on Christiansen effect. This describes the reduced scattering of multiphase microstructures at wavelengths where their refractive indices match.[25] A porous poly (2-(2 methoxyethoxy)ethyl methacrylate) P(MEO2) membrane is impregnated and slightly swollen with a mixture of solvents and exhibits different colors depending on the composition or temperature of the solvents (Figure 6b). The same mechanism is observed with *N*-methyl methacrylamide (MMAA)–*N,N′*-methylene-bisacrylamide (BIS) porous polymer filled with thermosensitive LC droplets because of a mismatch between the LC droplets and the porous polymer. By a change of temperature or potentially applying an electric field, refractive index of the LC changes and the transmittance wavelength peak shifts.[25]

A large class of multiresponsive materials has been developed, using functionalized building blocks combined with responsive materials. Two pH-responsive fluorescent dyes were synthesized and then copolymerized with NIPAM to add a

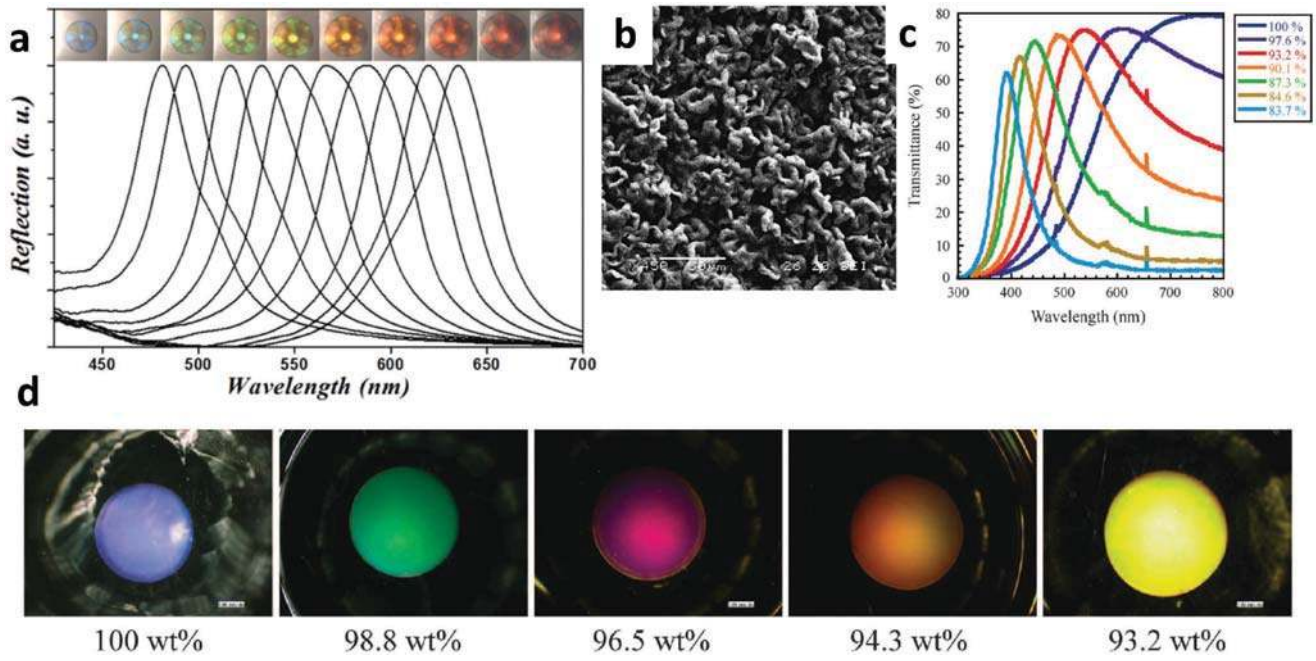

Figure 6. Porous systems. a) The reflection images and spectra of a PNIPAM hydrogel inverse opal hydrogel during a dynamic temperature decrease process. Reproduced with permission.[21] Copyright 2015, Royal Society of Chemistry. b) SEM image of a porous polymer membrane composed of poly(MEO2). c) Solvent composition dependence of the transmission spectra and d) optical photographs of the same polymer membrane in different toluene–acetone mixed solvents at 20 °C. b–d) Reproduced with permission.[25] Copyright 2016, Springer Nature.

color-changing pH response to the standard PNIPAM thermal response.[36] The system of microgels dispersed in an aqueous solution shows both a temperature-responsive change in turbidity, and a pH-responsive change in fluorescence.

Creating hybrid systems consisting of hydrogels and plasmonic nanoparticles (AgNPs or AuNPs) has been a successful strategy to increase the light absorption and introduce unique optical properties in the hydrogels. PNIPAM hydrogels as one of the well-studied temperature-responsive color-changing systems have been coupled with plasmonic nanoparticles, since the latter induce a heat buildup in the hydrogel systems as a result of the light absorption. A design strategy for a thermo-photochromic composite consisting of photonic poly(*N*-isopropylacrylamide-*co*-methacrylic acid) (P(NIPAM-*co*-MA)) copolymer and plasmonic nanoparticles has been proposed.[24] The gold/silver nanoparticles coupled with the inverse-opal-responsive hydrogel increase the sensitivity of the temperature response and make it possible to show a full color response over the entire visible spectrum in the system (Figure 10a). It is also demonstrated that by increasing the temperature, a molecular conformation transformation of PNIPAM happens that induce conformation rotation from intermolecular hydrogen bond into intramolecular hydrogen bond.[24]

4.3. Ion-Responsive Systems

Among hydrogels-, which are one of the foci of this work, temperature is one of the most convenient stimuli to be used to induce a structural color change. However due to the large quantities of water in hydrogels, pH and electrolytes are also both natural stimuli that can be used to elicit a change in swelling conditions. Hydrogels containing charged moieties display swelling behavior strongly dependent on pH and ionic strength, both of which can be used to tune the electrostatic part of the osmotic pressure that determines the equilibrium state of the hydrogel.

pH-responsive Bragg stacks based on maleic-acid-containing hydrogels ($pK_a \approx 1.8$) have been reported. By embedding the (PEG)-crosslinked poly((methyl vinylether)-*co*-maleic acid) (PMVE-co-MAA) hydrogels in titania/graphene oxide (TiO_2/GO) 1D photonic crystals, pH-responsive TiO_2/GO Bragg stacks are fabricated.[40] TiO_2, a pregel solution and GO were spun alternatively and finally the Bragg stacks was baked to form the gel. The resulting multilayer photonic crystals exhibit six times faster response compared to simple TiO_2/GO Bragg stacks.

Bragg stacks with dual-responsive behavior have also been reported. Gao and Serpe have prepared etalons of P(NIPAM-*co*-AA) microgels in a photoacid *o*-nitrobenzaldehyde (*o*-NBA) solution.[58] The system shows a color change induced by UV light exposure, which causes a pH change in the acrylic-acid-containing ($pK_a \approx 4.3$) system (Figure 8c). The Bragg stacks approach has also been used to prepare P(NIPAM-*co*-AA)-based photonic structures. The concept has been employed to prepare a multilayer system by alternatively spin-coating of NIPAM–AA polymer precursor and TiO_2 layer as a high-refractive-index component.[31] The multilayer system is baked at higher temperature resulting in 1D photonic stacks that change the structural color of the system by changing temperature and at different pH values.

Using plasmonic nanoparticles, 1D photonic crystals flakes (d = 5 mm) consisting of P(HEMA-*co*-MA) matrix and

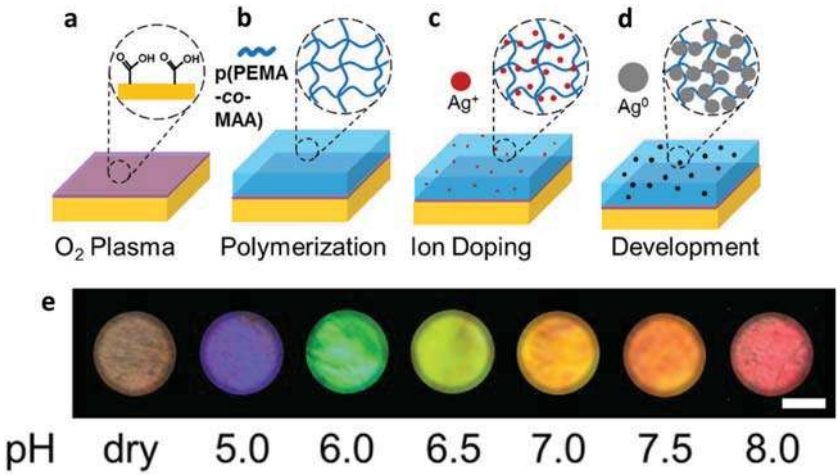

Figure 7. Laser writing of free-standing 1D photonic crystal flakes sensors. a) Treatment of the PMMA surface with O_2 plasma to render the surface hydrophilic. b) Free radical copolymerization of HEMA, ethylene dimethacrylate (EDMA), and MA on the O_2-plasma treated PMMA substrate. c) Diffusion of Ag^+ ions into the p(HEMA-*co*-MA) matrix. d) The formation of Ag nanoparticles within the matrix through reduction of Ag^+ ions using a photographic developer. e) Photographs of free-standing flakes from pH 5.0 to 8.0. The images were taken under white light illumination. Scale bar is 3 mm. Reproduced with permission.[50] Copyright 2016, American Chemical Society.

multilayer AgNPs have been fabricated.[50] By increasing the pH from 4 to 7, the hydrogel containing MA (p*K*a ≈ 4.6) swells and the AgNPs lattice spacing is changed and, as a result, the diffraction peak shifts from 500 to 620 nm with 0.1 pH unit sensitivity. The immobilization of AgNPs in the hydrogel matrix has been elaborated as well (**Figure 7**). A slightly different photonic system was developed before by the same group as a divalent metal ions' detector.[160] The polymer matrix for Ag^+ diffusion is poly(acrylamide-*co*-carboxylic acid) (PAM) hydrogel. A single laser pulse is used to pattern the matrix and form a slanted diffraction grating of periodic AgBr nanocrystals within the PAM matrix functionalized with 8-hydroxyquinoline. As the concentration of the detected ions is changed, the lattice spacing is tuned, and as a result the diffraction spectrum is shifted.

Colloidal crystals with pH-responsive behavior have also been prepared in several occasions. 2D free-standing hydrogel films of chitosan (pK_a ≈ 6.5) (with a thickness of 8 μm) have been developed, in which PS colloidal monolayers of 500 nm in diameter are attached on both surfaces.[55] They have investigated advantages of the 2D colloidal structure over 3D arrangement. The strategy of using colloidal monolayers on both surfaces introduced an anticurling feature and enhanced diffraction intensity to the composite, compared to traditional hydrogel films having the monolayer on one side. Because of the pH-dependent swelling behavior of chitosan, by decreasing the pH from 6.88 (the higher limit of chitosan swelling) to 2.07, the diffraction peak is shifted from 508 to 648 nm.

Several colloidal crystals with dual-responsive behavior have been prepared by using modified P(NIPAM-*co*-AA) microgels. The microgels have HEMA polymerizable methacrylic groups on their surface.[30] When the microgels self-assemble in a highly ordered crystalline structure, the surface-bonded vinyl groups are polymerized by UV-initiated free radical polymerization resulting in the formation of dually responsive photonic films consisting of immobilized colloidal crystals microgels (**Figure 8**a). Color-changing core–shell microgels of PS-P(NIPAM-*co*-AA) have also been prepared. The color change is rapid across the entire visible spectrum.[37] The stop band can be tuned with temperature at a rate of 60 nm s^{-1}. The core–shell microgels are mixed with an aqueous concentrated suspension of PAm as a depleting agent and then self-assembled into photonic crystals on a glass substrate. With the PAm as the depleting agent, together with the strongly scattering PS cores, and rapidly swelling–deswelling P(NIPAM-*co*-AA) shell, this system shows a uniform change in structural color upon heating (Figure 8b).

Another type of pH-responsive system is based on poly-(2-vinyl pyridine) (P2VP) hydrogels. P2VP microgels alone can display bright structural colors.[161] (PS–P2VP) hybrid systems have also been studied frequently. An ultrathin polymer gel film with P2VP gel infiltrated in monolayers of PS colloidal crystals has been prepared using a controlled spin-coating method.[48] The film exhibits distinct reflective colors upon pH-induced swelling and deswelling of P2VP (pK_a ≈ 4) gel, which is associated with a change in the thickness of the gel layer. At acidic pH, e.g., 2.44, where P2VP is swelled, the reflection peak is 663 nm, while as the pH is increased to 4.36 and 6.05, the reflection peak is shifted to 584 and 544 nm, respectively.

Studies on the thermochromic behavior of the PS-*b*-P2VP gel which was made of casts of PS-*b*-P2VP solutions show that the color change is originated from a temperature-induced change in the pK_a of P2VP.[32] The color of the gel clearly changes as the temperature increases, a phenomenon associated with a change in spacing between the PS blocks and P2VP blocks domains. At higher pH values when the P2VP domains are collapsed upon increasing the temperature, the domain spacing is reduced until no visible light is reflected and the gel looks clear. A similar system has been developed by controlled infiltration of SiO_2 nanoparticles in the hydrogel block.[162] It is found that this modification allows an expansion of the stop band across the entire visible spectrum.

Electrolyte-responsive hydrogels are ideal candidates for chemical classifiers, biosensors, and antiforgery applications, if they are designed to show a quick response and high-accuracy performance. pH-responsive acrylic-based hydrogels are one the most used polymers in that area. Ultrathin poly(acrylamide-*co*-acrylic acid) (PAm-*co*-PAA) films incorporated with PS colloidal crystals have been developed.[56] 2D assemblies of PS particles in the hydrogel display bright structural colors that change when exposed to salt-containing solutions of different concentrations (**Figure 9**). The color change originates from a change in lattice spacing caused by the electrostatic effect of the salt.

Incorporating PS crystalline colloidal arrays in a responsive hydrogel network has been a classic way in the preparation of photonic gels.[38,39] Once the hydrogel volume changes upon applying the stimuli, the crystalline colloidal array lattice constant

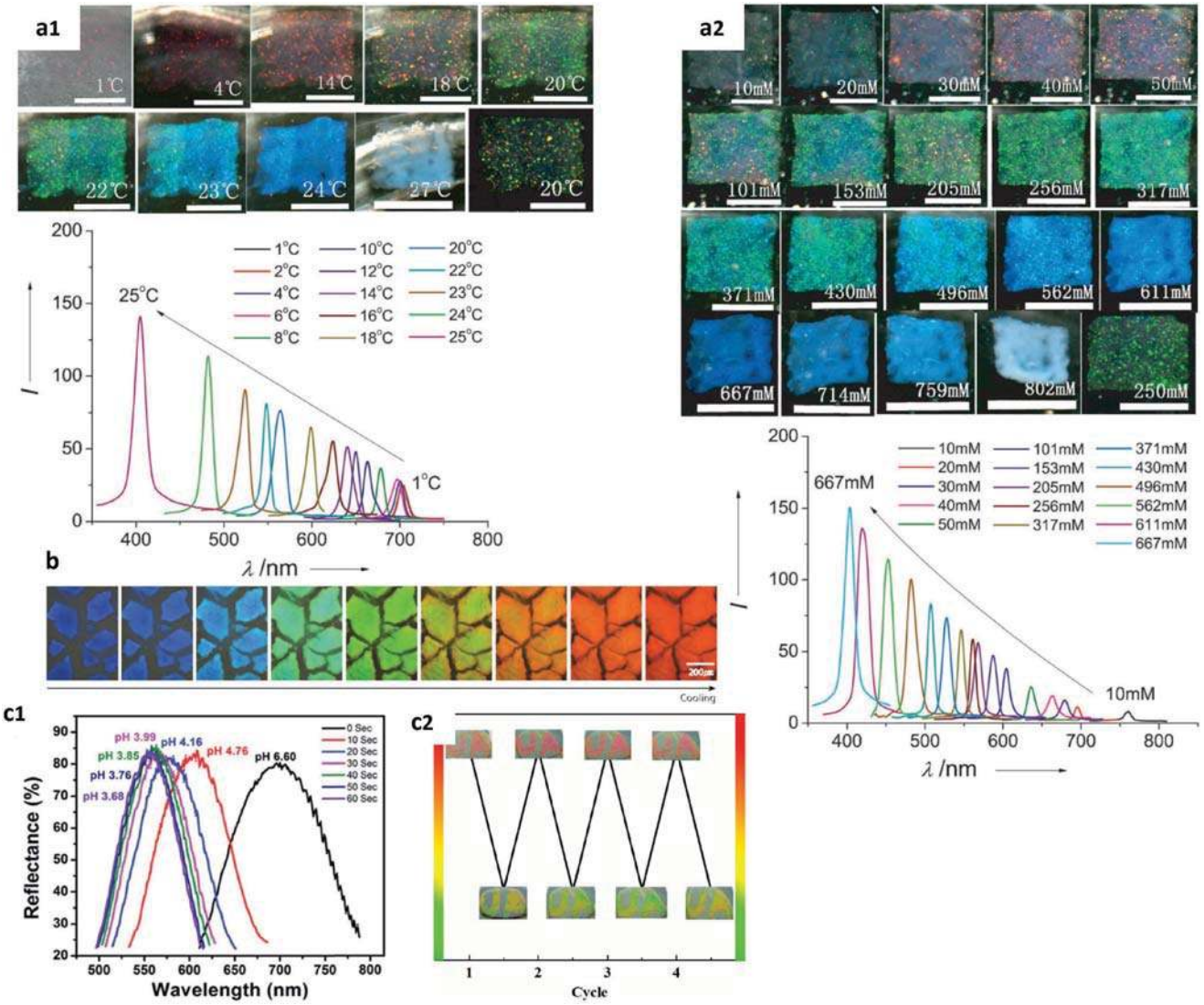

Figure 8. Color change patterns of P(NIPAM–AAc) systems. a) Photographs and reflection spectra of free-standing colloidal crystals films of HEMA-modified P(NIPAM–AAc) microgels: a_1) temperature increase. At the bottom right, the film was cooled back to 20 °C. The film was immersed in 0.5 M NaCl solution, pH 3.0. Scale bar is 0.5 cm. a_2) [NaCl] increase. At the bottom right [NaCl] was decreased back to 250×10^{-3} M. Scale bar is 0.5 cm, pH 3.0. $T = 23$ °C. Reproduced with permission.[30] Copyright 2013, Wiley-VCH. b) A uniform change of structural color in optical microscopy images of PS/P(NIPAM–AAc) hydrogel photonic crystals upon heating from 20 to 40 °C. Reproduced with permission.[37] Copyright 2017, Optical Society of America. c) Reflectance spectrum for a P(NIPAM–AAc)-based etalon in *o*-nitrobenzaldehyde (*o*-NBA) solution: c_1) after exposure to UV irradiation for the indicated times, color reversibility by repeated exposure to UV irradiation, c_2) followed by the addition of fresh *o*-NBA solution. Reproduced with permission.[58] Copyright 2014, American Chemical Society.

is changed and as a result the diffraction peak is shifted. PS colloidal crystals' array used as a template combined with a plasmonic material has been employed in the preparation of a pH-responsive polyacrylic acid (PAA)-based hydrogel. As a result, the diffraction peak is intensified with a better visual observation of the color change.[49] First, a 2D PS colloidal crystal monolayer array is prepared; then a thin layer of Au is sputtered on the PS monolayer. The PS spheres are removed and leave Au spherical nanoparticles on the surface. The polymerization of acrylic acid (AA) is performed on the 2D Au nanosphere array. The composite film shows different colors at different pH values. Gold thin layers have also been employed in responsive microgel-based etalons for the special optical properties that are endowed by the composite system, where Au serves as the mirrors and polymer microgels as the dielectric layer (**Figure 10**b). Serpe and co-workers have reviewed stimuli-responsive microgel-based etalons with various responsivities/functionalities.[58,163] With a different approach to make plasmonic hydrogels, Song and Cho have presented dual-responsive and multifunctional composites with high moldability, consisting of hybrid colloids (AuNPs assembled on a hydrogel colloid) and hydrogel colloids.[27] In both colloids, the hydrogel is the temperature- and ion-responsive poly(*N*-isopropylacrylamide-*co*-allyamine) (P(NIPAM-*co*-AAm)). A reversible color change is displayed by changing the stimuli, because AuNPs on the hydrogel colloids reversibly change their assembly structures accordingly (Figure 10c–e).

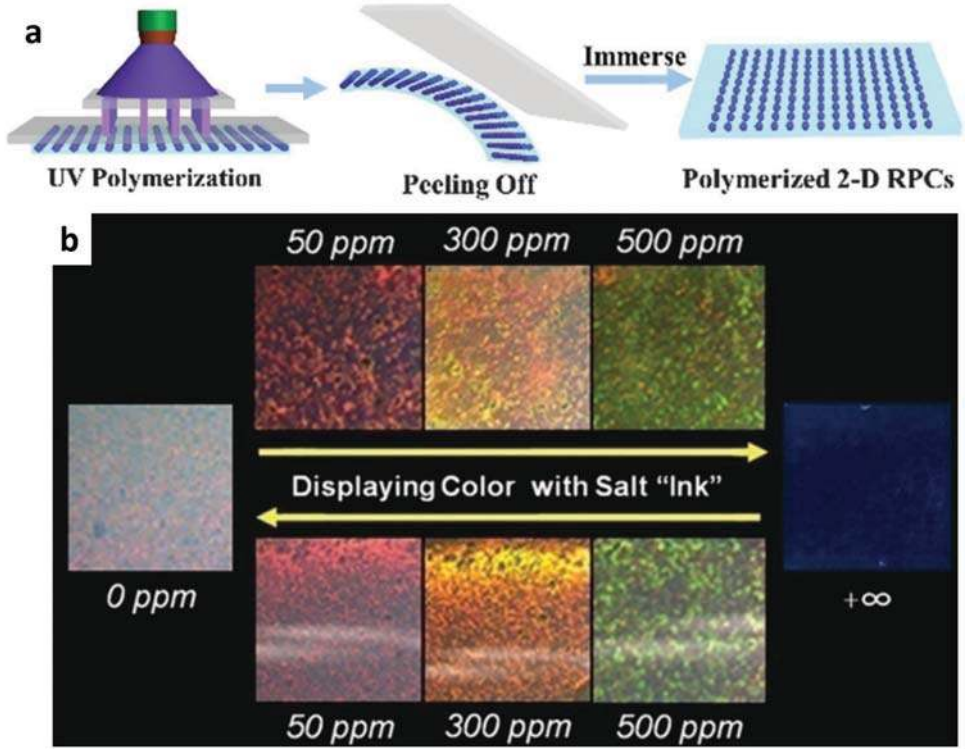

Figure 9. a) Schematic illustration of the preparation process of the 2D-responsive photonic crystals assemblies. b) Optical images of an electrolyte sensitive system ((PAm-*co*-PAA)/PS) immersed in a salt aqueous solution of different concentrations. Reproduced with permission.[56] Copyright 2016, Royal Society of Chemistry.

Taking inspiration from the photonic nanostructures in the butterfly, inverse opal films confined in microfluidic droplets have been prepared, in which the pores are created from silica nanoparticles.[164] The hydrogel used is PEGDA with acryloyl-modified aptamer crosslinker and the photonic crystal structures are used as colorimetric sensors to detect Hg^{2+} concentration in water.

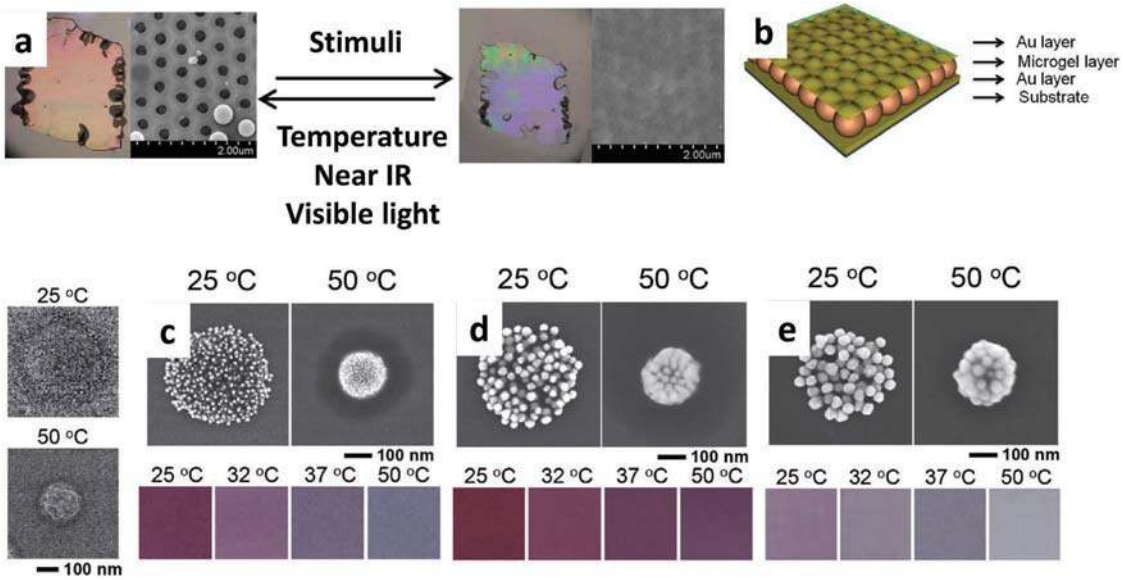

Figure 10. Plasmonic color-changing systems. a) A plasmonic P(NIPAM-*co*-MAA) hydrogel film responding to surroundings with color, volume, and conformation variation tuned by plasmonic nanoparticles. Reproduced with permission.[24] Copyright 2016, Springer Nature. b) Structure of microgel-based etalons. Reproduced with permission.[163] Copyright 2016, Royal Society of Chemistry. c–e) Top: SEM images of colloidal plasmonic microgel showing the temperature-dependent morphologies formed with a microgel colloid and Au NPs having c) 15 nm, d) 33 nm, and e) 50 nm. Bottom: colors of the plasmonic microgels in deionized water at various temperatures. Reproduced under the terms of the Creative Commons Attribution 4.0 International License.[27] Copyright 2016, The Authors; published by Springer Nature.

Photonic crystal structures have made it possible to detect and/or quantify metal ions in a more affordable, user-friendly, and faster way compared to complex spectroscopy techniques.[165] An optical sensor based on a CLC polymer has been developed. The polymer contains crown ether moieties, which provides the sensor with a great selectivity toward calcium.[54] A change of Ca^{2+} concentration between 10^{-4} and 10^{-2} M triggers a discernible color change in the film sample. Chen et al. have prepared colorimetric sensors based on 2D photonic films and 3D photonic (microfluidic) supraballs to detect 11 kinds of metal ions (Al^{3+}, Zn^{2+}, Cd^{2+}, Li^{+}, Mg^{2+}, Pb^{2+}, Mn^{2+}, Co^{2+}, Ni^{2+}, Fe^{3+}, and Cu^{2+}).[46] In another work, inverse opals of microfluidic supraballs based on polyionic liquids have been fabricated. The supraballs show different λ_{peak} when exposed to different counterions (BF_4^-, PF_6^-, Tf_2N^-, NO_3^-, and ClO_4^-).[45]

4.4. Magnetic-Field-Induced Structural Colors

4.4.1. Magnetic Particles

Magnetic nanoparticles based on magnetite (Fe_3O_4) can be easily prepared in a size range between 5 and 20 nm. These particles have been investigated during the past two decades for application in different fields, such as biomedicine, magnetic resonance imaging, water treatment, optics, and functional materials. The reason of their popularity is super-paramagnetism.[166] This means that they develop an internal magnetization rapidly only in the presence of an external magnetic field, and once the magnetic field is removed, they lose their net magnetization completely. Due to their rapid response to a magnetic field and the ability to form photonic crystal arrays precisely and conveniently with tunable optical properties in a liquid medium (aqueous or nonaqueous), they have been studied for their potential use as colorimetric sensors,[9] invisible photonic printing,[167] flexible color display,[168] security materials[60] and structurally colored fibers.[111] When Fe_3O_4 nanoparticles have sufficient surface charge, they maintain colloidal stability due to electrostatic interactions. Upon the application of a magnetic field, various assemblies of Fe_3O_4-based particles are formed. Dipolar interactions induce the formation of chains of particles. More complex field patterns, as well as the combination of magnetic dipolar interactions with other interactions, can form more sophisticated assemblies. These assemblies display different spacing among the particles, as well as different patterns, which both determine the diffracted color of the sample, according to Bragg's diffraction theory.

Diffraction gratings made of super-paramagnetic iron oxide nanoparticles (SPIONS) are one of the optical components with a great potential. A thermally tunable grating prepared using PNIPAM and SPIONS has been recently reported.[33] Nanoemulsions containing hydrophilic SPIONS of 10 nm in diameter were synthesized and topped with PNIPAM solution resulting in magnetic droplets covered by PNIPAM brushes. The grating spacing changes reversibly over heating and cooling above and below LCST because of conformational changes in PNIPAM chains. As a result, the Bragg peak shifts from 756 to 640 nm upon increasing the temperature from 5 to 32 °C due to the changes of inter-droplet array spacing.

Using pure magnetic materials as building blocks, instead of incorporating magnetic nanoparticles in a polymer carrier, e.g., PS,[169] or PNIPAM,[170] to fabricate colloidal photonic crystals, offers the advantage of having a high loading of magnetic nanoparticles in the materials and therefore a stronger response (high magnetization) in a shorter time. For this purpose, stabilized super-paramagnetic (Fe_3O_4) colloidal nanocrystal clusters with tunable sizes have been developed.[72,171] The size of the clusters composed of many small Fe_3O_4 nanocrystals, depending on the stabilizing agents, can vary up to the super-paramagnetic-ferromagnetic transition, so that sufficiently large clusters display ferromagnetic behavior.[171b] By applying a magnetic field gradient on a liquid sample containing sufficiently monodispersed and concentrated magnetic nanocrystals, different colors are reflected.

With an approach to fabricate wearable camouflage products, magnetically responsive stretchable/squeezable poly(dimethylsiloxane) (PDMS) fibers have been prepared. The fibers contain carbon-encapsulated Fe_3O_4@C super-paramagnetic colloidal nanocrystal clusters, which change color from brown to yellowish green in the presence of an external magnetic field.[75] The Fe_3O_4@C nanoclusters are embedded in ethylene glycol droplets, so they can freely move. Once the magnetic field is applied, they form 1D chain-like structures along the direction of the field. As a result, the color of the fiber is changed. Similarly, synthesized Fe_3O_4@C nanoclusters with different sizes have been used to prepare magnetic-field-induced structural color films for security applications.[65,66] Fe_3O_4@C are dispersed in a polymer precursor, e.g., a photocurable resin (ethoxylated trimethylolpropane triacrylate, ETPTA), and once they display the desired structural color pattern under a magnetic field, they get polymerized by UV exposure to form a homogeneous film (photolithography). Multicolor films can be prepared by using Fe_3O_4@C of different sizes. The photonic patterns display different colors based on the background and the angle of the incident of the light. Fe_3O_4@C nanoclusters have also been incorporated into responsive hydrogels, where the nanoclusters primarily self-assemble in a periodic order (1D chains) in a magnetic field and then are fixed within the hydrogel matrix. Now this photonic hydrogel changes its color due to the change in the 1D chain spacing, once the hydrogel swells or shrinks.[9,10] Fe_3O_4@C-P(Am-NIPAM) magnetic hydrogels are sensitive to temperature, humidity, mechanical stress, and alcohol.[172] In response of a change in each of the four parameters, the interplanar spacing of the pre-self-assembled Fe_3O_4@C in the photonic hydrogel is changed, and a different structural color is displayed. Release studies of such hydrogels have been reported as well for medical therapy applications, where an alternating magnetic field drives a controlled release.[173] Similarly, Fe_3O_4@C nanoclusters have been introduced into a PAm–PAA matrix where the photonic hydrogel changes its color in response to pH and ionic strength (**Figure 11**).[44]

The colloidal stability of super-paramagnetic Fe_3O_4 colloidal nanocrystal clusters is an important factor to be able to store them over a long period and use them over many cycles of applying and removing a magnetic field. Surface modification of the nanoclusters with a silica layer is one of the strategies that have been employed to prevent magnetic particles' chain coagulation and to improve dispersity in various solvents. Magnetic agarose hydrogel film with Fe_3O_4@SiO_2 core/shell colloids has

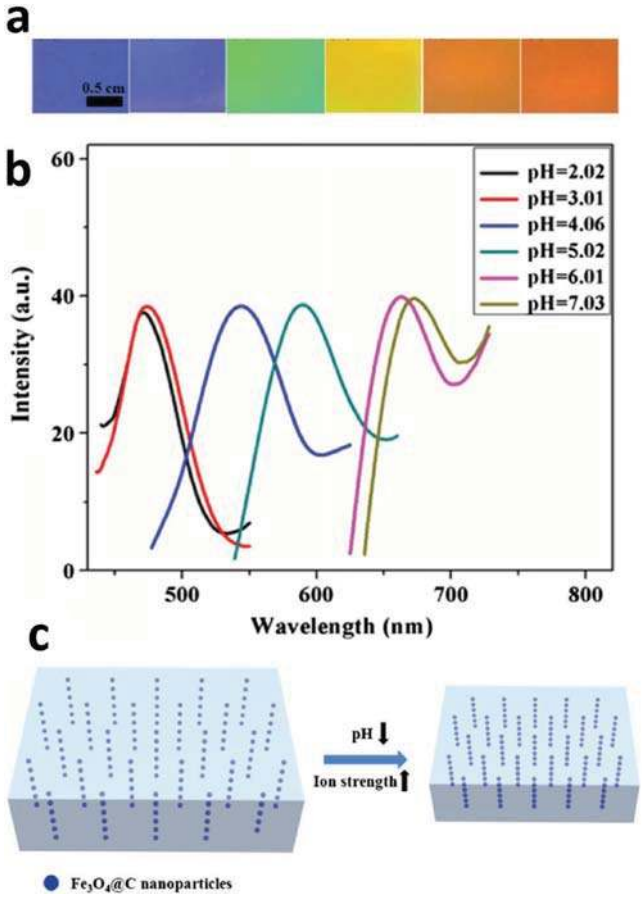

Figure 11. a) Photographs and b) corresponding reflection spectra of the Fe_3O_4@C/PAM–PAA hydrogels at different pH values: (left to right) pH = 2.02, 3.01, 4.06, 5.02, 6.01, and 7.03. The detector is fixed at an angle of 90°. c) Schematic illustration showing the structure of Fe_3O_4 nanoparticles in the PAM–PAA hydrogels when tuning the pH value or ionic strength in the aqueous solution. At low pH value or high ionic strength, the volume of photonic hydrogels shrunk, lattice spacing of the nanoparticles decreased and a blueshift in the reflection peak occurred. Reproduced with permission.[44] Copyright 2016, Elsevier Ltd.

been prepared.[67] Without a magnetic field, nanoclusters are randomly dispersed in the polymer film resulting in a brown color; once a magnetic field is applied, they self-assemble into linear chains along the field lines, creating a periodic structure, and the film turns green as a result. By varying the strength of the magnetic field, a broad range of reflection peak is realized. Similarly Fe_3O_4@SiO_2 core/shell colloids have been embedded in a hydrogel film made of NIPAM and PEGDA. The magnetic hydrogel exhibits different colors upon changing the temperature or the magnetic field strength.[174] The same logic can be used for structural color printing with magnetic particles. High-resolution magnetic patterns that have been fixed by lithography have been fabricated. The patterns can change their structural color in the presence of a magnetic field gradient.[60] The authors used an ink consisting of Fe_3O_4@SiO_2, a solvation liquid (ethanol), and a photocurable resin. The solvation liquid introduces a rather weak but long-range electrostatic force and a rather strong but short-range solvation force. Once the desired color is tuned by self-assembly of Fe_3O_4@SiO_2 into chains under the magnetic field, the resin is solidified through UV exposure. Multiple structural colors with different geometries are produced by adjusting the UV exposure and magnetic field strength. Flexible photonic crystal films have also been fabricated with the same strategy, and could be used as forgery protection.

A different approach to magnetically tune the color of the material has been proposed, where, instead of incorporating the magnetic clusters in the bulk, Fe_3O_4@SiO_2 nanoclusters have been incorporated into microspheres (opal balls) made of a photocurable resin (PEGDA).[61] Once the Fe_3O_4@SiO_2 nanoclusters self-assemble into 1D chains, the microdroplets of PEGDA precursor are UV-cured and fix the periodic structure inside the microsphere. By tuning the angle of the magnetic field, the orientation of the microspheres is changed and a different diffractive color is displayed. The rotation of microspheres being very rapid makes these microspheres promising for the preparation switchable color display.

Super-paramagnetic poly(vinylpyrrolidone)-coated Fe_3O_4 colloidal nanocrystal clusters, Fe_3O_4@PVP, are another type of stabilized magnetic nanoclusters, where the stabilization mechanism is the steric hindrance. 1D free-standing, flexible thermochromic films have been made with Fe_3O_4@PVP in a PNIPAM matrix.[28] After dispersing the nanocrystals in the monomer solution, a magnetic field is applied to create the structural color, followed by polymerization to fix the magnetic-field-generated patterns. The structural color of the magnetic photonic film is tunable by changing the temperature, thanks to the temperature-responsiveness imparted by PNIPAM. By decreasing the temperature from 35 to 10 °C, λ_{peak} shifts from 660 to 520 nm are observed. Similarly, it is possible to immobilize Fe_3O_4@PVP in PNIPAM microspheres to produce switchable structural colors.[43] The uniform structural color in the entire hydrogel ball can change both by magnetic field direction ("on" and "off" states) and temperature change (**Figure 12**).

Stabilization of nanoclusters by means of both PVP and SiO_2 has also been recently developed. Fe_3O_4@PVP@SiO_2 photonic nanorods made of nanoclusters have been generated by means of a magnetic field.[175] The nanorods are different in terms of both length (i.e., number of nanoclusters forming the chain) and interparticle distance. The interparticle distance, which is governed by the balance between the attractive magnetic force and repulsive electrostatic force, dictates the diffracted wavelength off the chain. An optical anticounterfeiting composed of a templated PDMS film filled with the photonic nanorods shows a color and brightness change upon applying a magnetic field gradient. Nanorods composed of magnetic nanoclusters have been also used as a rapid switch in color by tuning the direction or removal of the magnetic field.[68,69] Mixing chains of different length can result in distinct colors. It has been shown that, compared to polymer and silica shells, carbon shells offer much higher stability in most chemical and physical environments. Carbon coating and carboxyl group attachment on the surface of the carbon shells are shown to result in a high negative zeta potential on the magnetic nanoclusters.[176]

Switching the structural color by manipulating the direction of the external magnetic field—as it has been mentioned earlier—is known to be a promising strategy for reflective display applications.[73] Recently, a new type of photonic Janus microspheres has been reported, which is made magnetoresponsive by deposition of a thin ferromagnetic iron layer and optically anisotropic by alternately deposition of silica and

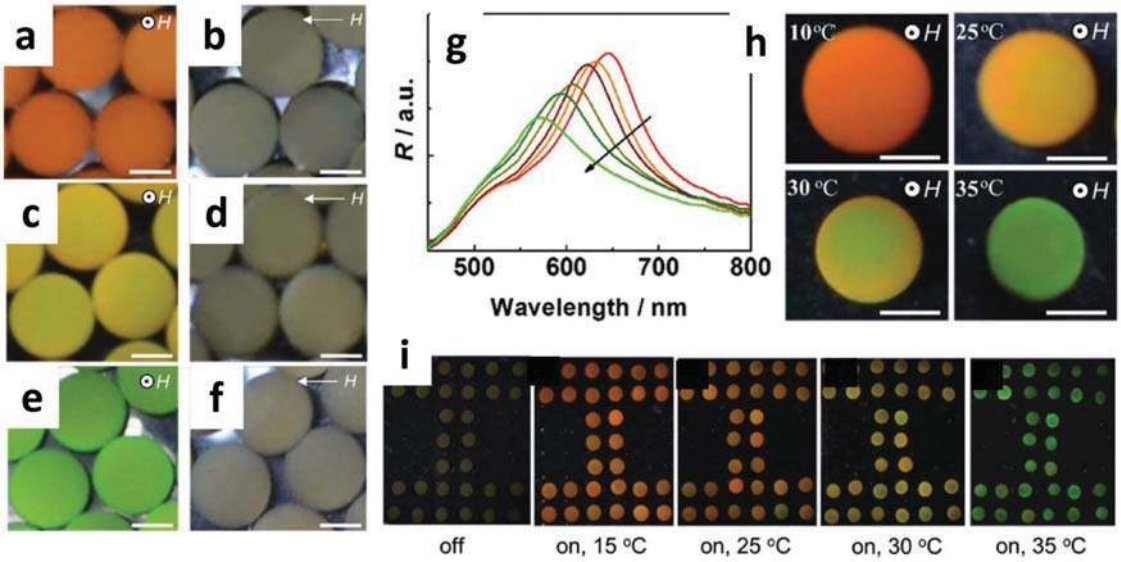

Figure 12. Digital photos of the Fe_3O_4@PVP–PNIPAM balls polymerized under magnetic field of a,b) 105 G s, c,d) 175 G s, and e,f) 340 G s, respectively, at magnetically switching a,c,e) "on" and b,d,f) "off" states. All the scale bars are 1 mm. g) Reflection spectra of the same balls polymerized under a 105 G s magnetic field along the arrow when the temperature is increased from 10 to 35 °C with a step of 5 °C. h) The typical digital photos at different temperatures. All scale bars are 1 mm. i) Digital photos of a bead pattern filled with the same balls formed under 105 G s at "off"/"on" states by rotating the external magnetic field between 0° and 90° at various temperatures. Reproduced with permission.[43] Copyright 2017, Royal Society of Chemistry.

titania layers.[70] The microfluidic microspheres made of the photocurable resin ETPTA of a size of about 100 μm show a gradient change of structural color because of the directional deposition on their curved surfaces and display different colors by changing the direction of the magnetic field. In another study, thin films of different thicknesses composed of Fe_3O_4 nanocrystals (11.5 nm in diameter) and polyurethane have been fabricated.[177] By tuning the magnetic field orientation, the structural color changes through thin-film interference effect. Fe@SiO_2 nanoellipsoids are another example of anisotropic building blocks that have been reported to change their diffraction properties in a magnetic field with variable directions.[71] Triple-responsive Janus supraballs (temperature, and magnetic and fluorescence-responsive) have been developed with the same concept.[64] The PS colloidal crystals with grafted poly(methacrylic acid) (PMA) chains are used as the seeds to couple with CdS quantum dots. The Cd^{2+}/PS particles are employed as a template to introduce Fe_3O_4 and PNIPAM hydrogels. The multiresponsive beads offer great potentials for displays and anticounterfeit applications.

The directional sensitivity in optical properties of the magnetic nanorods has been the cornerstone of fabricating magnetically actuated liquid crystals, where the polarization of light is altered instantly by a slight change in the magnetic field direction.[74] By using patterned templates in controllable magnetic fields, it is possible to create different polarizations in the area of choice inside the material, e.g., thin films, for different optical applications.

4.4.2. Nonmagnetic Particles

Another type of magnetic-field-induced structural colors is produced by an assembly of nonmagnetic particles. Taking advantage of numerous options for nonmagnetic particles in terms of size and materials, and integrating them with a compatible ferrofluid offer extended possibilities to develop magnetic-responsive materials ("magnetic hole" effect).[178] High-quality photonic crystal structures on large areas have been prepared by PS particles (180 nm in size) dispersed in a ferrofluid solution under different strengths of a magnetic field. 1D particle chains or 3D colloidal structures with various optical patterns and colors are formed in a matter of several minutes under magnetic fields of different strengths.[179] Similarly, a reversible on/off reflection switch based on P(S-*co*-AA) nanoparticles has been prepared. The nanoparticles of different sizes are dispersed in an aqueous ferrofluid made of highly surface-charged Fe_3O_4 nanocrystals.[63] The instant phase-separation colloidal assembly of the nonmagnetic particles upon applying and removing the magnetic field can find applications in photonic displays.[63,180] In another work, aqueous suspension of inverse opals of ETPTA-TPM dispersed in an aqueous ferrofluid of Fe_3O_4 nanocrystals has been used as colorimetric sensor to estimate the magnetic field strength.[62] The bright structural color of the inverse opals floating on the surface of the ferrofluid goes through a quenching of the reflection intensity. Based on the magnetic tuning, the quenching time and ratio are exploited to estimate the magnetic field strength in a more accurate, repeatable, and reliable way compared to traditional methods.

4.5. Electric-Field-Induced Structural Colors

The need to develop advanced display technology, smart windows, and camouflage devices has been a great motivation to fabricate electric-field-induced structural colors. An accurate and fast visual presentation of the system's dynamic is the first

requirement for application purposes. There are different strategies to produce materials with this ability. Different fabrication strategies of electroresponsive photonic crystals have already been reviewed, and advantages/disadvantages for each working principle have been presented.[181] Here we focus on examples of recent works published in the field.

4.5.1. Colloidal Suspensions

Colloidal crystal arrays with a nonclose-packed structure are a class of materials that are widely used in electrochromic (EC) devices where the lattice spacing can be changed by applying a bias voltage. Many PS- and SiO_2 particle-based colloidal crystals in electrochromic systems have been studied so far.[79,80,182] The particles' size and surface charge are the first two key factors that have to be taken into account when preparing such devices. Preparing tunable photonic crystals using high-refractive-index yet transparent materials, such as TiO_2, ZnS, and ZrO_2, is a promising yet challenging method for display applications. High density and polydispersity of these particles are some of the main issues that are the subjects of research in the field. Negatively charged ZnS– silica core–shell colloidal crystals stabilized by PVP have been developed. The long-range crystalline order of the particles is attributed to the highly charged shell. The ZnS–silica dispersion in water in an indium–tin oxide (ITO)–ITO cell shows a reflectance shift from λ_{peak} = 650–450 nm when the voltage is increased from 0 to 3.2 V, as a result of a change in the interparticle distance.[76]

Preparing and maintaining colloidal arrays ordered and stable in the long range is an important factor that has to be considered in order to have high-quality display pixel. One of the attempts to enhance the crystalline order is reported to be a modification of ITO surface, able to produce a significant number of ions at the cathode and anode, in which the ions interrupt the colloidal array. The enhancement has been done through ion exchange resins, which act like a barrier coating the ITO surface and increase the color-tuning switching cycles to over 800 times.[80] The ITO modification has been performed by thin films of Nafion proton-exchange membrane coated onto the cathode surface and fumasep (FAS) anion-exchange membrane coated onto the anode surface. In another study, conductive diamond-like carbon electrode and the boron-doped diamond electrode are used instead of one of ITO electrodes in the cell. As a result, a larger electrochemical potential is produced and the system has enhanced switching stability.[183]

As much as magnetic-field tuning is convenient to apply and control, it is not easy to restrict it within a small space, without having destructive interference effects. In that case, an electric field has several advantages over a magnetic field. Applying an electric field on a medium with proper dielectric properties can also drive self-assembly of magnetic nanoparticles. Color-changing magneto/electroresponsive Fe_3O_4@SiO_2 core–shell nanoparticles with hydrophobic surface have been prepared. The nanoparticles are dispersed in a low-dielectric medium. By changing the voltage from 0 to 10 V, the nanoparticle–nanoparticle distance is decreased; therefore, the reflective spectrum is shifted and various colors are displayed. This makes Fe_3O_4@SiO_2 nanoparticles promising for reflective display applications (**Figure 13**).[77] In order to create a material with lower density, higher optical contrast, and higher refractive index, hollow Fe_3O_4@C nanoparticles have been developed for photonic display applications.[78] The hallow nanoparticles are less than

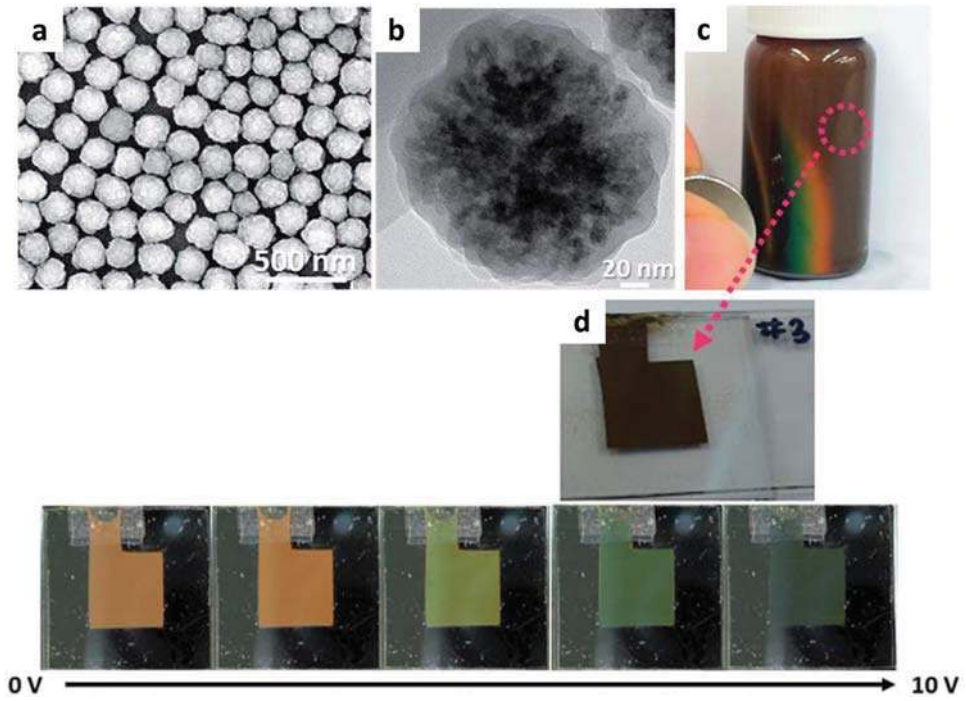

Figure 13. Magneto/electroresponsive hydrophobic surface modified Fe_3O_4@SiO_2 core–shell nanoparticles. a) SEM image, b) TEM image, and c) photo image of the reflective color changes under an applied magnetic field. d) Reflective color-change behavior of the same nanoparticle ink injected into the reflective display cells depending on the applied voltage. Reproduced under the terms of the Creative Commons attribution license.[77] Copyright 2017, Royal Society of Chemistry.

200 nm in size, and because of carbon coating and hydrophilic carboxyl group show great solvent dispersity and water stability. The photonic pixel made of hollow Fe_3O_4@C nanoparticles shows very fast (200 ms for "on" switching and 30 s for "off" switching) and reversible response to a low voltage change (0–1.5 V).

4.5.2. Electrochemical Processes

Electrochromism is a phenomenon displayed by certain materials, which can reversibly change their colors caused by electrochemical redox reactions. This physical phenomenon is used to build EC devices, i.e., systems that can change their optical transmission, absorption, reflectance, or emittance as a result of the application of a voltage. An electrochemically active component, conductive materials (electrodes), and an electrolyte are the main components in an electrochromic device. Several materials can be used as the electroactive component, such as polymers, metal oxides, liquid crystals, and polyaromatic hydrocarbons. When a polymer is used as the electrochemically active component, by applying an external voltage to the EC device, both the redox state of the polymers and its refractive index change. Conjugated polymers with various electron-donor and electron-acceptor structures show different colors, contrasts, and switching properties. The choice of the polymer is therefore important to design the desired EC device. Recently, polymeric donor–acceptor structures and characteristics for EC applications have been reviewed.[184] An EC device using a patterned film (diffraction grating) of propylenedioxythiophene phenylene copolymer has been prepared.[185] An EC with 770 nm thick polymer grating changes its color from green to magenta with an intermediate blue color by a change of voltage from −2 to 2 V. The patterned structure adds a possibility of creating tunable colors to the electroactive film. In another work, an EC device has been prepared that can reversibly show black color with a change of voltage between −2 and 2 V.[85] The EC device combines colors from conductive polymers to absorb the primary colors red, green, and blue (RGB) and an electrochromic polymer that produces a yellow color. The RGB covers the 450–750 nm wavelength range provided from poly(3-hexylthiophene) (P3HT) for red, poly(3,4-ethylenedioxythiophene) (PEDOT) for blue, and poly(aniline-*N*-butylsulfonate) (PANBS) for green, and the yellow provided from poly((1,3-bis(9,9-dihexylfluoren-20-yl)azulenyl)-*alt*-(2,7-(9″,9″ dihexylfluorenyl)) (PDHFA) covering below 450 nm completing the visible color spectrum. The EC device has a color memory, meaning it maintains the color state even after electric field removal. This makes the EC device special for energy-saving displays. An EC device has also been fabricated in fiber forms with a long time color memory (30 min).[86] The fibers show a great flexibility, can be used for weaving and patterning, and by using three kinds of π-conjugated organic polymers ((PEDOT), poly(3-methylthiophene) (P3MT), and poly(2,5-dimethoxyaniline)), the full RGB range is covered. The EC fibers can change their color from gray to dark blue in a millisecond scale in response to a change of voltage between 0 and −6 V.

Poly(vinyl alcohol) (PVA)–borax gel-based EC devices are successful examples of EC devices with polyelectrolyte gels. A rainbow-like EC device has been reported, which is prepared by two viologens (4,4′-bipyridine derivatives—nonpolymer electroactive component) with five different multiswitchable colors based on four-zoned electrodes. It can display green, pink–violet, orange, purple, and colorless by changing the voltage between 0 and −1.7 V.[87] This EC device with this zoning strategy has high potentials for applications in smart windows technology where users can optimize light transmission, thermal and visual properties of the glass on demand. In another recent study, a multicolored EC device based on two different viologens, monoheptyl viologen (MHV^+) and diheptyl viologen (DHV^{2+}), has been reported. Copolymers and ionic liquids have been used as electrolyte. The device is pale yellow in the bleached state (0 V) and turns blue in case of MHV^+ (−1.3 V) and blue in case of DHV^{2+} (−0.8 V).[186] EC devices with the ability to switch between a transparent state and black state (sometimes mirror as well) have been of a great importance for smart windows technology. Different strategies have been employed to produce EC devices with such properties.[187,188] Large luminance, high transmittance in the bleached state, and fast switching are important factors that need to be taken into account. An EC device based on electroactive polyamides, with *N*,*N*,*N*′,*N*′-tetraphenyl-*p*-phenylenediamine and tetraphenylbenzidine units in the backbone, has been produced, in which heptyl viologen (HV) is used as the supporting electrolyte. The device is completely transparent in the bleached state and turns to completely black in the redox state with the working voltage of <2 V.[88]

Polycyclic aromatic hydrocarbons (PAHs)-based EC devices are another class of EC devices with nonpolymer electroactive components. A large variety of PAHs exist in nature or are easy to synthesize compared to viologens and electroactive polymers. When neutral, most of PAHs are colorless and in charged states they show vivid colors. A multicolored EC device has been prepared based on a perylene ion gel that reversibly changes its color between royal blue (−3.5 V), olive (+4 V), and colorless (0 V) with a driving voltage of <5 V, as a result of molecular plasmon resonances.[189]

Electrochromic photonic crystal (EPC) display devices, which combine electrochromism with photonics, are known to show tunable reversible color change because of a combined trigger of a physical (changing the RI or the lattice size of the photonic structure), and chemical nature (the change in electronic structure of the electrochemical materials). For the first time, an EPC device made of TiO_2 inverse opals has been reported in which the color reversibly changes with insertion/extraction of lithium ions.[89] The inverse opal is prepared by atomic layer deposition using PS particles of 288 and 424 nm in diameter as a template. The EPC changes the color from blue to white/transparent upon charging (lithium extraction) with different voltages (1.5–2.3 V). The idea of having inverse opals used as an electroactive component, in which the electrolyte can freely infuse, has been already introduced before.[190]

The use of block copolymers in EC devices is another well-known method for color changing through different mechanisms. These include the ability to swell/shrink of the hydrophilic block in the copolymer and the change in spacing as a result. The behavior of block copolymers in electric fields has already been reviewed, in which, nanostructure alignment, macroscale order, and switching between various geometries have been elucidated.[191] The swelling mechanism of PS-*b*-P2VP has

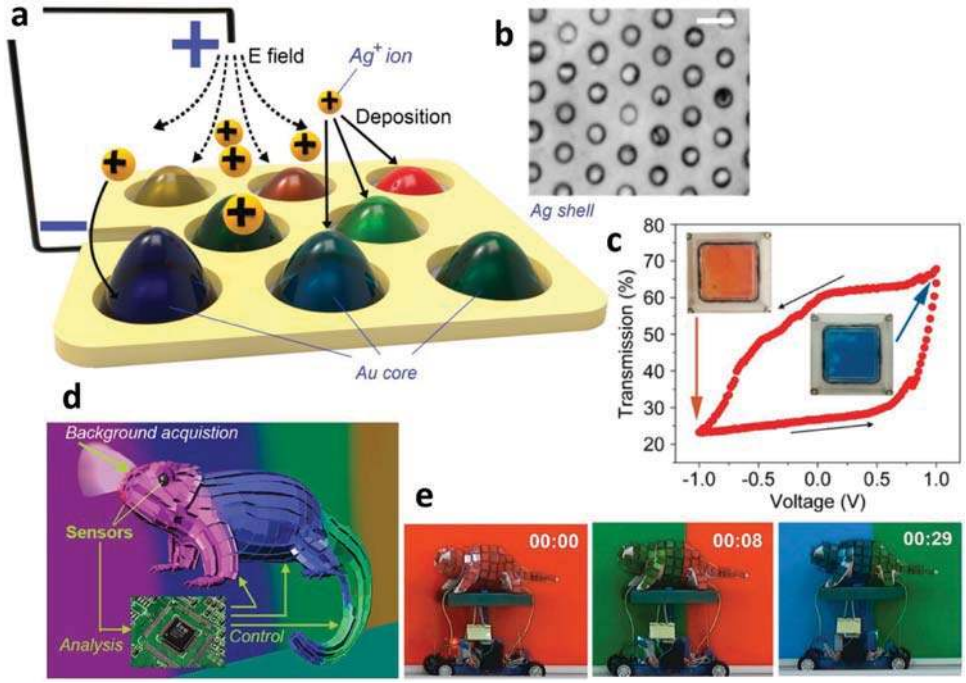

Figure 14. a) Schematic diagram of the plasmonic cell. The double-layered hemiellipsoids represent nanodomes with different Ag shell thickness. b) Top-view SEM image of the Au nanodome array. Scale bar is 100 nm. c) Transmission of 600 nm light as a function of electrodeposition voltage. Scan rate: 0.2 V s^{-1}. Inset: Photo of the plasmonic cell device at the starting and ending point. d) Schematic of the plastic chameleon covered with armor-like plasmonic cells and polyvinyl butyral as the host polymer. e) Screenshot of the plasmonic chameleon demonstration movie. The front and back parts of the chameleon are able to change color independently with respect to their color backgrounds. Reproduced with permission.[91] Copyright 2016, American Chemical Society.

been explained in Section 4.3. Inspired by cephalopod-layered reflectin protein, an EC device made of PS-*b*-P2VP, coated on the ITO bottom electrode with a fluoropolymer spacer filled with 2,2,2-trifluoroethanol (TFE) as an electrolyte, has been developed. Upon applying a voltage of 5V, P2VP swells with TFE, and then the film changes its color (from red to green) and trifluoroethoxide ions are produced by the electrochemical reaction. By increasing the voltage to 10 V, more ions are produced, causing P2VP shrink and a blueshift to occur (from green to blue).[90] In a similar fashion, EC based on quaternized PS-*b*-P2VP has been prepared which shows a response 1000 times faster than PS-*b*-P2VP without quaternization.[192] The fast switching originates from the charging of the P2VP block and it allows driving the system with lower voltages (from −4.50 to +2.36 V).

Combining electrochemical and plasmonic properties is a new approach that has been recently used to develop an EC device inspired by chameleon with the ability to manipulate light in real time to match it to the color setting in any given background (**Figure 14**).[91] The device can render colors in the entire visible region. The plasmonic contribution comes from highly ordered Au-core/Ag-shell nanodomes, integrated in a porous SiO_2 film, with a conductive ITO bottom. The whole cell is filled with gel electrolyte containing Ag^+ ions. The Ag-shell covers the Au-core through electrodepostion, in which the process duration and voltage have a great influence on the color reflected by the device.

In order to have a fast response (tens of milliseconds) and high contrast switching in EC devices, EC films based on surface plasmon polaritons have been developed. Two different electrochromic polymers, polyaniline (PANI) and poly(2,2-dimethyl-3,4 propylenedioxythiophene), are electrodeposited to form thin films and integrated with Au nanoslit arrays assembled on the electrode. PANI films are reduced ("on" state) and oxidized ("off" state) with −0.2 and 0.3 V, respectively. The color of the EC cell in the "on" state changes as the pitch of the nanoslit arrays varies.[92] In another multicolored EC device, localized surface plasmon resonance (LSPR) of Ag nanoparticles arising from their aggregation has been employed. Ionic liquids are use as electrolytes. Eight electrodes are used to display yellow, pink, purple–violet, dark blue, and transparent under constant voltages (2, −2 V). The device has a memory to maintain colors after removing the electric field.[193]

4.5.3. Liquid Crystal-Based Systems

LCs are an important class of electro-optical materials, which have also been subject to research for color-changing applications.[194] Filling inverse opal structures with LCs has been one of the strategies to produce 3D electro-optical photonic crystals.[195] Electrically induced color change in CLC materials has also been studied in recent years.[196] Recently, a polymer-stabilized CLC has been developed, in which the domain size distribution in its focal conic state (i.e., multiple-domain optical scattering state) is changed by applying an appropriate voltage. After applying the appropriate electric field pulse, a blueshift in the CLC molecule is caused. The polymer-stabilized CLC is made of E7 (Merck), mixed with a prepolymer (NOA65),

and a chiral dopant (R5011, Merck) to fill the ITO cells, which are then polymerized. Different concentrations of the chiral dopant result in different color cells in the focal conic states, induced by various applied voltages (5, 25, and 50 V).[81] Similarly, a negative dielectric anisotropy ($-\Delta\varepsilon$) polymer-based CLC has been prepared, in which the reflection color is changed from green to orange, and finally to red, as the electric field strength is changed to 0, 2, and 4 V μm^{-1}, respectively. It is shown that the reflection variations originate from an electrophoretic-based mechanism, resulting in charge trapping on the surface of the polymer.[197] An oblique, helicoidal (heliconical)-structured CLC has been developed in which colors are selectively reflected by electrical tuning. The CLC is made of two dimeric LCs (1′,7′-bis(4-cyanobiphenyl-4′-yl)heptane (CB7CB) and 1-(4-cyanobiphenyl-4′-yl)-6-(4-cyanobiphenyl-4′-yloxy)hexane (CB6OCB), and a standard LC pentylcyanobiphenyle (Merck), doped with a left-handed chiral additive S811 (Merck) and sandwiched between two ITO electrodes. Applying an electric field with different amplitudes results in color and texture changes in the CLC cell (**Figure 15**).[82] The choice of the dimeric LCs here with an elastic constant of bend K_3 smaller than elastic constant of twist assures the existence of the heliconical state under an electric field (Figure 15a_3,a_4,b_2–b_7), according to Meyer[198] and de Gennes.[199] The cholesteric structure shows a transition from a scattering state at zero electric field (Figure 15a_1) to another light-scattering structure (fingerprint texture) at an electric field (below 0.7 V μm^{-1}) only strong enough to rotate the cholesteric axis—which is responsible to reflect the light—perpendicularly to itself (Figure 15a_2,b_8). Upon applying a stronger electric field in a certain range and along the axis, the reorientation of the helicoid axis is preserved while the pitch P is changed, that is, where the reflected wavelength is changed from near-IR to visible colors and then to UV (Figure 15a_3,a_4,b_2–b_7). A further increase of the electric field (e.g., 5 V μm^{-1}) transforms the LC to a homeotropic state (Figure 15a_5,b_1). All the color changes are reversible and fast.

A recent study shows the effect of an electric field on CNC suspensions and investigates the iridescence properties of concentrated (35%) CNCs in an apolar solvent. Tuning of the iridescence, formation of a purely nematic phase and dynamic

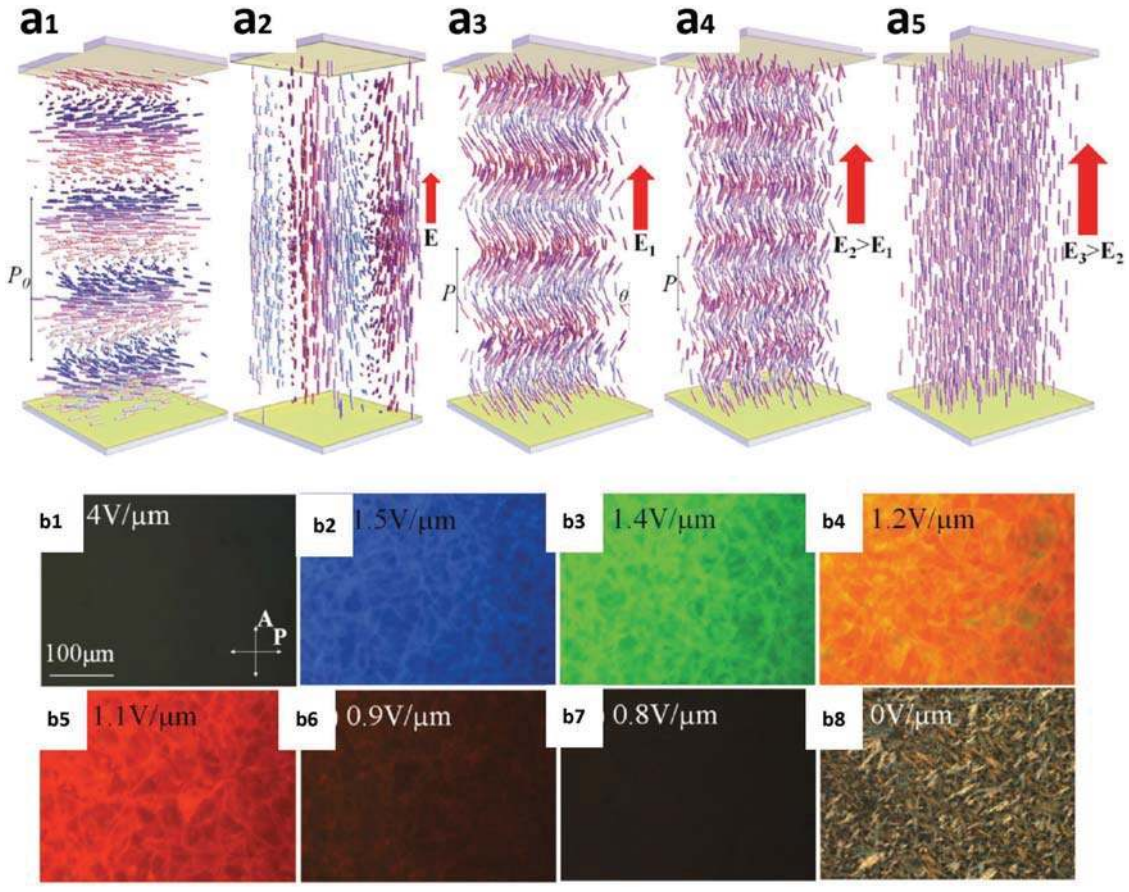

Figure 15. a) Field-induced behavior of cholesterics structures. a_1) Right-angle helicoidal cholesteric with a large bend constant and a positive local dielectric anisotropy in a planar cell. a_2) Sufficiently strong vertical electric field E realigns the cholesteric axis perpendicularly to itself, causing light-scattering fingerprint texture. a_3) Heliconical structure in a cholesteric with a small bend constant and positive dielectric anisotropy stabilized by the vertical electric field $\mathbf{E_1}$. a_4) The pitch P and tilt angle θ of the field-induced heliconical state both decrease as the electric field increases, $\mathbf{E_2} > \mathbf{E_1}$. a_5) As the field increases further, to some $\mathbf{E_3} > \mathbf{E_2}$, it unwinds the helical structure completely and forms a homeotropic nematic state. Polarizing optical microscopy textures of field-induced b_1) unwound nematic; b_2–b_7) heliconical states with reflected b_2) blue, b_3) green, b_4) orange, and b_5) red colors, b_6,b_7) two IR-reflective states; b_8) fingerprint state. The root mean square (RMS) amplitude of the electric field is indicated on the figures. Reproduced with permission.[82] Copyright 2015, The Authors; Published by Wiley-VCH.

color changes with time-modulated electric fields have been observed and thoroughly studied.[200]

4.6. Mechanoresponsive Structural Colors

Elastomers are a class of amorphous polymers that have viscoelastic properties above their glass transition temperature (T_g). Depending on the application, synthetic elastomers are classified as thermosets and thermoplastic. Thermosets (rubbers) are vulcanized to irreversibly crosslink individual chains together, and tend to burn or degrade at high temperatures. Thermoplastic elastomers are glassy or semicrystalline elastomers that can be processed like plastics at high temperatures because of having rigid domains covalently bonded to a soft matrix.[201] In a shape memory elastomer, i.e., an elastomer that has the ability to return from a deformed state to its original unperturbed state, when a mechanical stress is applied, the long polymer chains reconfigure themselves to compensate the stress. The elastomer retakes the original configuration once the stress is removed (reversible deformation).[202] If the elastomer does not return to the original configuration, permanent deformation occurs.[203] Here we focus on shape memory elastomers with structural coloration that is changed along the elastomer upon applying a stimulus, mainly mechanical force.

One basic method to prepare mechanochromic materials based on structural coloration is to embed photonic crystals in an elastomer compatible with the photonic crystals in terms of interface properties. One of the main applications of these mechanochromic materials is in stress-sensor technology where any slight change at the microscopic level, e.g., microcracks can be visually detected. Early works have focused more on the mechanical properties of the mechanochromic material.[204] Later on, composite systems emerged because of the need to develop multiresponsive materials for various applications, e.g., taking advantage of the responsive components in the material. Immobilizing colloidal crystals in hydrogels was explained earlier. However, for certain applications, weak mechanical properties of hydrogels and solvent evaporation are issues that need to be overcome. Therefore, strategies to improve elastic properties of the hydrogels have been emerging. The link between the polymer type, photonic gels structure, and their optical/mechanical properties has been reviewed before.[204b,205] Strain-responsive photonic elastomers have been prepared by fixing poly(ethyl acrylate-*co*-methyl methacrylate) (PEA-*co*-MMA) colloidal particles' film in poly(ethyl acrylate) (PEA) elastomer with interpenetrated polymer network structure.[100] The photonic film swells in the prepolymer solution, i.e., ethyl acrylate (EA) monomer, initiator (α,α'-azobis(isobutyronitrile)), and crosslinker (ethylene glycol dimethacrylate (EGDM)), and shows visible structural colors before EA polymerization. The amount of the crosslinker affects the original structural color. After polymerization an obvious change of color is seen when the crosslinked elastomer is stretched. Once the stress is removed the film goes back to the original color. The PEA chains penetrating into the (PEA-*co*-MMA) particles after polymerization are thought to be effective for the rubber elasticity of the photonic elastomer.

In another work, a multiresponsive photonic elastomer film with rigid-core-elastomeric shell particles has been prepared, in which a polymerizable fluorescent dye (rhodamine B methacrylamide (RhBMA)) is bound to either the core or the shell.[101] The dye adds light and temperature responsiveness to the elastomer, as it reversibly changes between a nonfluorescent state (closed spiroamide) and a fluorescent state (zwitterionic open) (**Figure 16**). The core is made of PS particles, with an interlayer of poly(ethyl acrylate-*co*-allyl methacrylate) and an elastomeric shell composed of a combination of PEA and poly(iso-butyl methacrylate). Similar works based on hard core–soft shell particles have been reported. PS core in poly(diethylene glycol methylether methacrylate-*co*-ethyl acrylate) (PDEGMEMA-co-PEA) shows a bandgap shift from 560 nm (stretched state) to 611 nm (swollen state).[102] In a similar work, core–interlayer–shell particles have been used to prepare a large photonic elastomer film with poly(butanediol diacrylate)) matrix, which shows a 160 nm bandgap upon deformation. Through a series of compression–relaxation cycles, the shape of core–interlayer–shell particles reversibly changes between spheres and oblate spheroids.[103] In a recent study, a series of bioinspired mechanochromic devices with different features have been developed: transparency change mechanochromism (TCM), luminescent mechanochromism (LM), color-alteration mechanochromism (CAM), and encryption mechanochromism (EM). The systems are based on simple soft and rigid bilayers with low-cost materials (PDMS, PVA, TiO_2, and laponite).[206] All devices show reversible behavior: TCM between transparent and opaque states; LM between nonemitting and fluorescence-emitting states; CAM between green and yellow colors; and EM between invisible and visible patterns. Photonic crystals made of different hard materials (metals), with various shapes, patterns, and lattice constants can be employed as templates embedded in flexible polymers (PDMS). Upon the removal of the hard materials, the flexible polymer can be used a colorimetric strain sensor.[207]

Poly(dodecylglyceryl itaconate) (PDGI)/PAm photonic hydrogel is one the most studied examples of mechanochromic hydrogels (**Figure 17**).[208] A tough and multiresponsive photonic hydrogel has been prepared with PAA network introduced into the PAm layer of a PDGI/PAm gel.[98] The soft PAA layer interpenetrates into the PAm layer and the hard PDGI layers toughen the gel. The alternately assembled hard (thickness = 4.7 nm) and soft layers (with a thickness of several hundred nanometers) make a temperature-, pH-, stress-responsive elastomeric hydrogel in which λ_{peak} shifts from 580 to 380 nm when the strain ε increases from 0% to 0.58%. In a similar work, a 1D photonic gel is reported, which is based on several thousand periodically aligned polymeric bilayers (PDGI) in a soft gel network of PAm in which the PAm gel can be partially and selectively hydrolyzed and makes the elastomer partially pH responsive.[209] To mimic natural camouflage behavior, the concept is used to make patterned elastomers, where a pH-induced color change is displayed only along the pattern, where it is being selectively hydrolyzed. The rigid bilayers of PDGI in the soft PAm hydrogel mimic the photonic structures in neon tetra fish, in which the PDGI bilayers act as "reflective platelets." This system has been used for display applications, where patterns are designed to change their color very

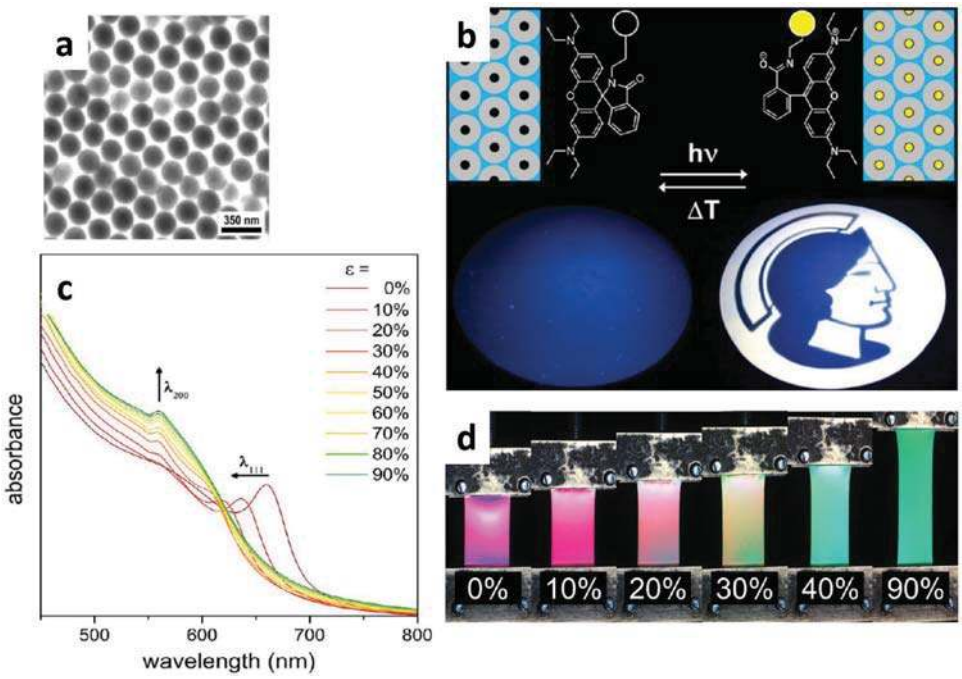

Figure 16. A light-, thermo-, and mechanoresponsive elastomeric polymer opal film. a) TEM image of an ultrathin section of a prepared elastomeric opal film with core–interlayer–shell beads with a temperature sensitive, fluorescent, and polymerizable rhodamine B derivative showing the hexagonally ordered 111 plane. b) Photo images of the same film at different strains ε. c) UV–vis transmission spectra of the same film at different strains ε. d) Optical images of a patterned elastomeric opal film after activation of RhBMA-labeled beads (right) and temperature-induced reversible erasing (left). Reproduced with permission.[101] Copyright 2013, American Chemical Society.

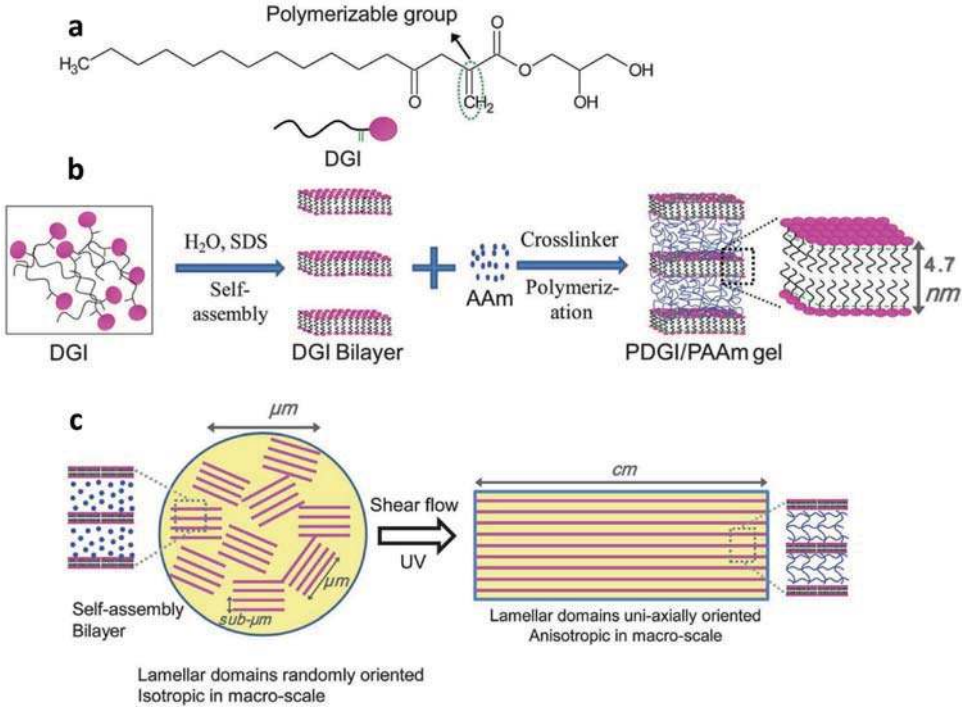

Figure 17. a) Molecular structure of dodecyl glyceryl itaconate (DGI) containing a polymerizable double bond. b) In the presence of an ionic surfactant, sodium dodecyl sulfate (SDS), DGI molecules self-assemble into a lamellar bilayer structure in water. This structure is retained in an aqueous solution of acrylamide (AAm) in the presence of a crosslinker and an initiator. By polymerization, polymeric-DGI (PDGI) lamellar bilayers are entrapped inside the amorphous polyacrylamide (PAAm) network and the hydride PDGI/PAAm hydrogel is obtained. c) Prior to the polymerization, randomly oriented self-assembled lamellar bilayer domains are aligned in one direction (anisotropic in the macroscale) by shear flow to the precursor solution. Reproduced with permission.[208] Copyright 2012, Royal Society of Chemistry.

fast with a slight stress applied on the film.[210] The same concept is reported in mechanochromic photonic papers made of silica photonic crystals embedded in PEGMA and EG matrix. Patterns created on the paper (photonic gel) are invisible in the relaxed state, while they appear upon stretching or squeezing, with a different color change in each state.[104]

Gold nanoparticles have been integrated into mechanoresponsive materials due to their optical properties. Patterned 1D arrays of AuNPs on PDMS substrate have been reported.[105] Stripes of AuNPs on the flexible film act similar to diffraction gratings. By applying an external mechanical stress, reflectance peak position and intensity change as a result of the change in spacing between the stripes. Height analysis based on atomic force microscopy (AFM) confirms a 60–70 nm height for the gold nanoparticles stripe and a 300 nm width. In a similar work, a high-refractive-index TiO_2 nanoparticles' layer is coated on an ≈60 μm thick PDMS membrane. Different concentrations of the TiO_2 nanoparticles result in different optical properties. Upon elongation up to 20% perpendicular to the grating direction, a 80 nm resonance shift is reported.[106]

Utilizing magnetic colloidal crystals in multiresponsive photonic elastomers has also been the subject of research in the past decade.[97] A hydrogel made of soft copolymer of *N*-hydroxymethyl acrylamide and *N*-vinylcaprolactam was designed to embed Fe_3O_4@C super-paramagnetic nanoclusters, which are self-assembled in 1D chain photonic structure under a magnetic field before polymerization.[95] The mechanochromic hydrogel shows a rapid and reversible color change with $\Delta\lambda_{peak} = 233$ nm and high mechanochromic sensitivity ($\Delta\lambda/\sigma = 53.1$ nm $(kPa)^{-1}$, where σ stands for compressive pressure). Similar work has been report on the preparation of mechanochromic hydrogel based on Am and EG, which shows an ultrafast color switching ($\Delta\lambda/\sigma = 1.2$ nm (nm ms^{-1})) with $\Delta\lambda_{peak} = 250$ nm and a mechanochromic sensitivity of $\Delta\lambda/\sigma = 20$–$40$ nm $(kPa)^{-1}$.[96]

Using an electric field to tune the color of photonic elastomers has also been reported.[211] For example, the preparation of elastomer-based systems mimicking the mechanism of expanding/contracting of chromatophores in cephalopods has been frequently studied. Artificial muscles have been designed by using artificial electroactuated chromatophores. They have used a dielectric elastomer (an electroactive polymer) actuator to mimic the cephalopods' radial expansion/contraction of chromatophores and the zebrafish fluid translocation of melanophores.[212] In another work, an electro-mechanochemically responsive elastomer system, with a panel size of 2 cm by 2 cm, has been developed by covalently attaching mechanochromic molecules (spiropyrans) to an elastomer (Sylgard). By applying an electrical field, a large deformation is produced within the elastomer, and various fluorescent patterns (line, circles, and letters) with a feature size of ≈100 μm appear on demand.[213]

4.6.1. Liquid Crystal Elastomers

Liquid crystal elastomers (LCEs) are well investigated as materials for artificial muscles and microactuators, due to their tunable mechanical properties through the nematic–isotropic transition.[214] Recent studies have summarized their synthesis methods, alignment techniques, and application of LCEs,[214d,215] as well as the progress and challenges, particularly, in the design of smart biomimetic micro/nanostructured systems.[216] A change in the orientational order of LCEs in response to an external stimulus is the design base of the LCE actuators. Inspired by chameleon's skin, a composite LCE based on single layer silver nanoparticles has been prepared.[107] Thanks to the presence of a closed packed array of AgNPs on the surface of the LCE film, under deformation or thermal actuation the LSPR peak blueshift because of the elongated spacing between the AgNPs. The reversible λ_{peak} shift occurs either through random (isotropic) to vertical alignment (nematic) or random (isotropic) to hybrid (nematic) alignment of the LC. In another work, a thermally actuated LCE has been developed by depositing a PS film on top a poly(methylhydrosiloxane)-based LCE.[108] The LCE–PS bilayer reversibly exhibits different levels of surface wrinkling upon changing the temperature, which on a macroscopic level is associated with a structural color change in the film sample. The wrinkling patterns are variable depending on the PS film thickness and preparation temperature.

As was previously mentioned, electric fields are also employed to tune the color the LCEs. Inverse opal materials have been used as a template to prepare LCEs.[217] A pure LCE in an inverse opal film has been reported for the first time, in which bright colors are displayed and can be changed by applying a voltage.[218] Later on, a bioinspired LCE based on micropatterned inverse opal films has been developed. Silica nanoparticles are fixed in a mixture of a nematic diacrylate monomer and a monoacrylate mesogenic monomer. After polymerization, the silica nanoparticles are etched and an LCE inverse opal film is formed. By locally polymerizing the mixture in two steps and by applying the electric field to change the spacing between the silica nanoparticles during the second step, a patterned LCE is fabricated. The patterned LCE shows a thermochromic behavior with dual structural colors.[83] Recently, alternate layers of an LCE and TiO_2 nanoparticles have been prepared, where in the top layer a fluorescent dye (rhodamin B) solution is deposited. The thickness of each layer affects the color change behavior. By applying a voltage, the matching degree between the photonic bandgap of the multilayer film and the emission spectrum of the dye on top of the film is changed. As a result, fluorescence intensity is reversibly and rapidly switched.[84] Inspirations from photomechanical, photo-thermomechanical, and magnetic LCE actuators[219] can also be used in the fabrication of novel color-changing LCEs.

4.6.2. Color-Changing Fibers

Taking advantage of electrical properties of graphene, bioinspired optical reflectors made of 2D graphene nanoplatelets have been developed for the first time, in which the structural colors are mechanically tunable.[109] The overlapping graphene nanoplatelets form a "fish-scale"-like structure, obtained through a special liquid-phase exfoliation method, on a single glass fiber surface, integrated in the epoxy resin. The deposition of graphene nanoplatelets can be applied up to a thickness of 500 nm. When a fiber glass/epoxy is stretched, its structural color dynamically changes. This process is reversible up to a certain deforma-

tion (safety region). By continuing the deformation, the platelets' contact points start to loosen up. That is where microcracks start to grow (alarm region), and finally a fracture occurs and is indicated by a permanent irreversible deformation developed in the composite (warning region). In another work, carbon-nanotube-based photonic fibers are reported. PS nanoparticles are electrophoretic-deposited onto continuous-aligned carbon-nanotube sheets (≈15 μm in thickness), which are then rolled on an elastic PDMS fiber (≈15 mm in diameter), and eventually embedded in a layer of PDMS.[110] Upon stretch/release, the PS nanoparticles' spacing changes and results in a visible color change along the fiber. The reversible and rapid color change of the elastic and conductive fiber over 1000 deformation cycles makes it very promising for weaving and for wearable electronic clothes.

Using magnetic particles to fabricate smart fiber, a flexible strain-responsive photonic fiber has been prepared, based on Fe_3O_4@C super-paramagnetic nanoclusters embedded in a PAm matrix.[111] The magnetic clusters form 1D chain-like photonic structures in the fiber, where the structural color reversibly changes upon stretching/squeezing. In order to make the elastomer fiber, Am and EG are mixed with a crosslinker (BIS), an initiator system (ammonium persulfate and *N,N,N′,N′*-tetramethylethylenediamine), and Fe_3O_4@C nanoclusters. The precursor is injected into a Teflon tube under a magnetic field to form the 1D chains. Once the polymerization is completed and the structural colors appear along the fiber, the sample is removed from the Teflon tube. The λ_{peak} of the fiber shifts from 637 to 515 nm when the $\Delta L/L$ changes from –20% to 40%, where L is the initial length of the fiber.

The hierarchical photonic structure of the seed coat of *Margaritaria nobilis* fruits has been a source of inspiration to fabricate structurally colored fibers. Its hue originates from interference effects within a concentrically layered architecture inside individual cells in the seed's exterior layers. Inspired by this effect, a photonic fiber made of elastomers has been reported. The two elastomeric dielectrics, PDMS and polyisoprene–polystyrene triblock copolymer, have sufficiently high RI contrast.[112] The technique has been used for the first time to make hollow multilayer fibers around a thin glass fiber (≈10–20 μm in diameter), which is later removed. The total multilayers' thickness directly affects the optical and mechanical performance of the fiber during elongation/release.

The use of commercially available fibers to prepare smart fibers, which can be used in fabrics and wearable products, is another strategy that has been reported. As an example, spandex fibers have been dip-coated by hard core–soft shell microspheres. The microspheres are made of PS core, PMMA interlayer, and PEA shell with a size of about 273 nm. The mechanochromic fibers can be fabricated in different diameters, ≈0.1–0.8 mm depending on the number of strands in multiple spandex fibers, different colors, and cross-sectional shapes. They can show various color changes, such as from red to green or from green to blue, upon stretching over 2000 cycles.[113]

5. Photonic Structures from Biotemplates

The idea of fabricating bioinspired color-changing systems is to mimic the hierarchical structure found in the natural species with structural coloration. A straightforward way to do this is to directly use the actual natural system as biotemplates, and functionalize/modify them to obtain the desired properties, which are not (easily) obtained using synthetic methods.[220] Butterfly wings have been frequently employed as biotemplates to prepare photonic materials. They have been modified by responsive polymers or by metal nanoparticles and actuated by different stimuli.[221] Usually, the wings need to be cleaned first and surface-treated. Here, we focus on recent works regarding reversible stimuli-responsive photonic materials and introducing fabrication ideas to prepare these materials. pH-responsive photonic structures based on *Morpho* butterfly wing have been fabricated. The hydrogen bond between the amine groups of chitosan in the wing and the MA monomer is used to deposit PMA through polymerization.[51] At certain pH values, charged groups of COO^- in PMA and $-NH_3^+$ in chitosan form an electrostatic pair of $-COO^-NH_3^+$, which leads to a contraction in the system. However, by increasing the pH to alkaline conditions, the electrostatic pair dissociates. Both groups are thus deprotonated, and result in a swelling of the system. In acidic environments, the protonation of the $-COO^-$ groups breaks up the electrostatic pair and that leads to swelling of the system as well. The swelling of the system is associated with a blue- to redshift in the reflection spectra once the pH is changed to acidic or alkaline conditions (**Figure 18**a). Similarly, a pH-responsive photonic structure has been developed based on the lamellar structure of *Papilio paris* wings.[52] The wings are coated with P(AA-*co*-Am), and similar to the previous work, a U transition in the reflectance from a swollen gel to a deswollen gel happens as a consequence of a pH change (Figure 18b).

The importance of angle-independent structural colors using amorphous photonic structures has already been discussed. Exploiting natural systems to create responsive systems showing angular-independent structural colors is therefore an obvious strategy, given the ability of natural systems to generate such features. Cuttlefish ink has been used as an additive to PS photonic crystals to break the long-range ordering of self-assembled PS colloidal structures.[222] Cuttlefish ink powder, which appears as black and is composed of many nonspherical melanin nanoparticles, when mixed with PS nanoparticles results in noniridescent colors. By using different proportions of the ink and different diameters of PS nanoparticles, a color palette with different color hues and visibility is produced. Inspired by the *Callophrys rubi* butterfly's wing, recently a different angle-independent pH-responsive composite has been reported.[53] A pH-responsive PMA is integrated into the natural gyroid structure of the wing to prepare the super-sensitive (18 nm reflection shift/pH) angle-independent composite.

Inspired by the photonic structure of the cuticle of *H. coerulea* beetle, which changes its color in response to humidity, recently 2D silk-titanate nanocomposites have been prepared.[17] The biotemplate is made of regenerated silk fibroin (RI = 1.55), which is cleaned, modified, and integrated with titanate nanosheets. Titanate nanosheets, i.e., 2D nanoparticle precursor of TiO_2, are synthesized using a sol–gel process and later mixed with silk solution to prepare high-RI silk solution. The regenerated silk fibroin and high-RI silk are alternately spin-coated on an SiO_2 slide to prepare a multilayer photonic composite. The layers' thickness changes when exposed to

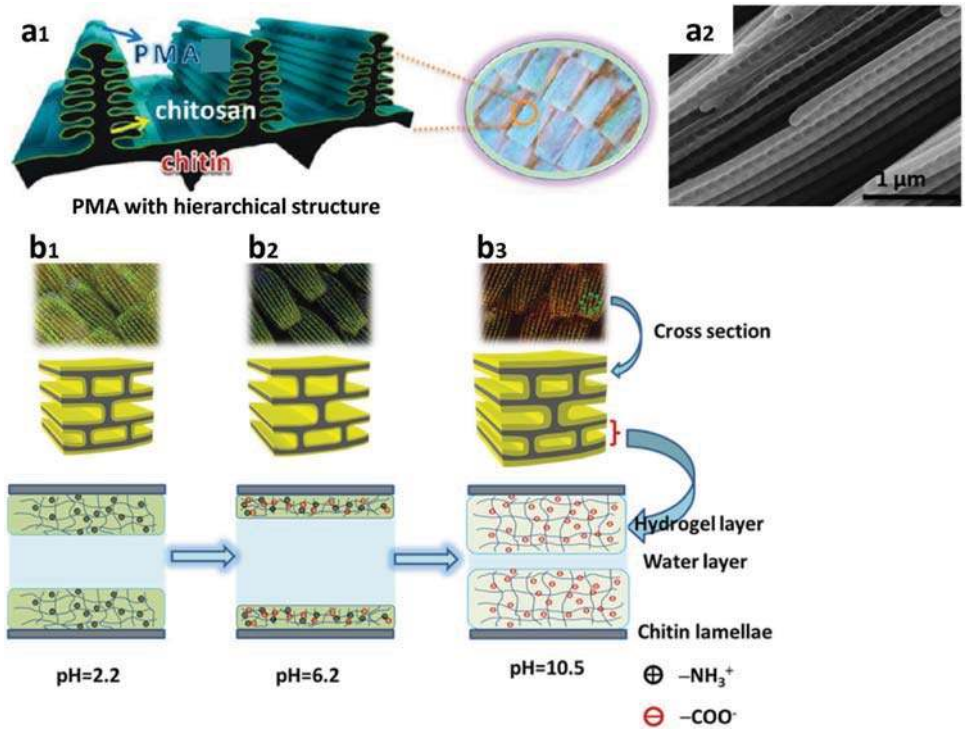

Figure 18. a_1) Schematic of modified *Morpho* butterfly wings. a_2) SEM images of alkali-treated template—PMA photonic structure. Reproduced with permission.[51] Copyright 2013, American Chemical Society. b) P(AA-*co*-Am)-modified *Papilio paris* wings: b_1) hydrogel swells slightly since amino groups protonate at pH 2.2, and digital image shows green color (λ_{max} = 555 nm). b_2) At pH value 6.2, positive and negative ions attract each other so the hydrogel shrinks drastically, leading to a reduction in the layer thickness. b_3) At pH 10.5, a large quantity of carboxylic acid deprotonate and the negative ions fill the whole hydrogel network, and such electronic repulsion makes the hydrogel swelling extremely. Reproduced with permission.[52] Copyright 2016, American Chemical Society.

humidity and the iridescent color is changed as a result. Silk fibroin has been used before as a template in humidity-responsive materials. Inspired by *Papilio blumei* and *Papilio Ullysess* butterflies, silk-fibroin-based inverse opals of different nanopore sizes have been prepared.[8] The butterflies display bistructural colors at different locations along their wings. In the fibroin-based inverse opals, by changing the lattice constant in a humid condition, the two λ_{peak} can be adjusted covering UV–visible, UV–IR, and visible–IR regions.

CLC chitosan nanofibrils derived from discarded crustacean exoskeletons and shells have also been employed for the first time to prepare photonic hydrogels.[223] Methyl methacrylate (MMA) monomer is polymerized on the twisted mesoporous chitosan nanofibril template to form PMMA/chitosan composite. As the composite swells to different extents in solvent environment, the iridescent color is changed as well.

6. Fabrication of Bioinspired Diffraction Elements: Methods and Ideas

So far, various examples of stimuli-responsive color-changing systems have been mentioned, in terms of materials, synthesis aspects, color-tuning mechanisms, efficiency, and potential applications. Here we focus on man-made diffraction elements based on optical principles behind the structural coloration in animals and plants and introducing ideas to mimic complex photonic structures in nature.

6.1. Technology

A recent study has reviewed different bioinspired technological strategies that have been exploited in the field.[1] Top-down strategies, e.g., lithographic techniques, and bottom-up approaches, based on self-assembly of micro/nanostructures, have been reviewed and compared. Self-assembly has been frequently exemplified here, while lithography needs to be highlighted. Considering whether it is a masked lithography or maskless lithography, the technique is classified into different types, some of them demonstrated in **Figure 19**. In the masked lithography, patterns are transferred from a template during lithography. It is performed on a large scale for mass fabrication. Photolithography, holographic lithography, nanoimprinting lithography, and soft lithography, all belong to this category. Maskless lithography is suitable for ultrahigh-resolution patterns (a few nanometers feature size), which are created by serial writing or etching. Electron beam lithography, focused ion beam lithography, and scanning probe lithography also fall in this category.[1,224]

Another powerful top-down technique used to fabricate hierarchical microparticles with high control over size, uniformity, shape, structure, and chemical composition is microfluidics, which over the past decade has been frequently used to prepare stimuli-responsive highly ordered structures.[225] Depending on the application, required resolution, precision of control over size, shape and spacing, cost and scale of use, one of these types of top-down or bottom-up strategies is selected.

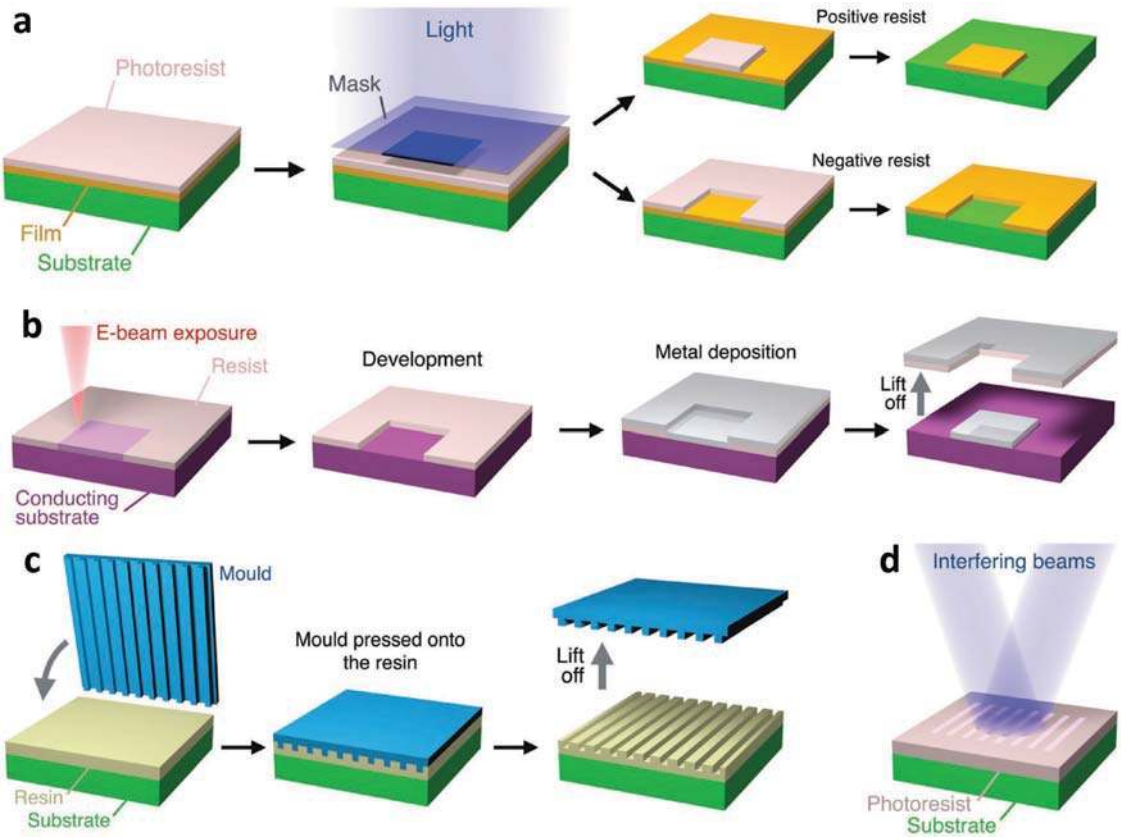

Figure 19. Some top-down, micro- and nanofabrication techniques used for the production of structurally colored biomimetic materials. a) In photolithography, a pattern is transferred from a mask to a photoresist by a curing light; further chemical treatment develops the profiled layer. b) Electron beam lithography serially registers a resist with a narrow, highly focused e-beam. c) Nanoimprint lithography press stamps a mold on a soft resin, which is then processed for its subsequent use. d) Interference lithography does not use a mask, but exploits interference patterns to print a photoresist. Reproduced with permission.[1] Copyright 2016, Royal Society of Chemistry.

A few more techniques, recently applied in the development of systems with responsive structural colors, are now briefly discussed. For the first time, structural color patterns have been recently created by electro-hydrodynamic jet printing with colloidal crystals as ink at adjusted voltage signals.[226] Different patterns can be designed by moving the printing stage. The wettability of the substrate can also be adjusted to create different shapes of the photonic units, while the jetting mode can be set to pulsating or continuous. The technique offers advantages over classical inkjet printing for micro/nanomanufacturing, and is promising for display technologies. By focusing on anticounterfeiting products, monodispersed CdS spheres of different diameters have been used as inks in inkjet printing (invisible at certain angles, single color and multicolor at other angles) to create computer-designed patterns on photo paper.[227]

Direct laser writing and electroless plating metallization techniques have been used together for the first time to produce metal-coated woodpile photonic crystals in the visible range, with a 600 nm periodicity and a resolution below 100 nm.[228] The 3D metallic structure is made of a photosensitive zirconium–silicon hybrid material doped with tertiary amine metal-binding monomers. The technique provides selective metallization, controlled density and distribution of the binding sites.

Microchannel technology has been reported to produce flexible structural color films. PNIPAM or PEGDA hydrogels containing monodispersed silica colloidal are micropatterned through single-layered PDMS microchannels, where a photopolymerization leading to the formation of a gel occurs. Microchannels prepared by soft lithography can have different geometries. The higher the number of photonic crystals gels, the higher the number of structural colors and therefore the pixel density on the film.[229]

A simple and effective rotational self-assembly technique has been used to prepare centimeter-scale opal films.[230] The technique benefits from both natural and rotational-forced drying and improves the structural order and lattice properties. A microchannel consisting of two glass substrates and a Parafilm spacer is dipped into a silica nanoparticles' suspension, left to dry for a short time (1 h), and is eventually subjected to rotation. Inspired by the optical feature of the longhorn beetle, the self-assembled opal film made of silica nanoparticles changes its color in response to humidity.

Butterfly wings have been frequently mentioned as a source of inspiration to fabricate hierarchical structures. Researchers have been looking into the wing structures from different angles to prepare bioinspired sensors.[142d,221a,231] Inspired by the reverse color-order diffraction effect observed in the

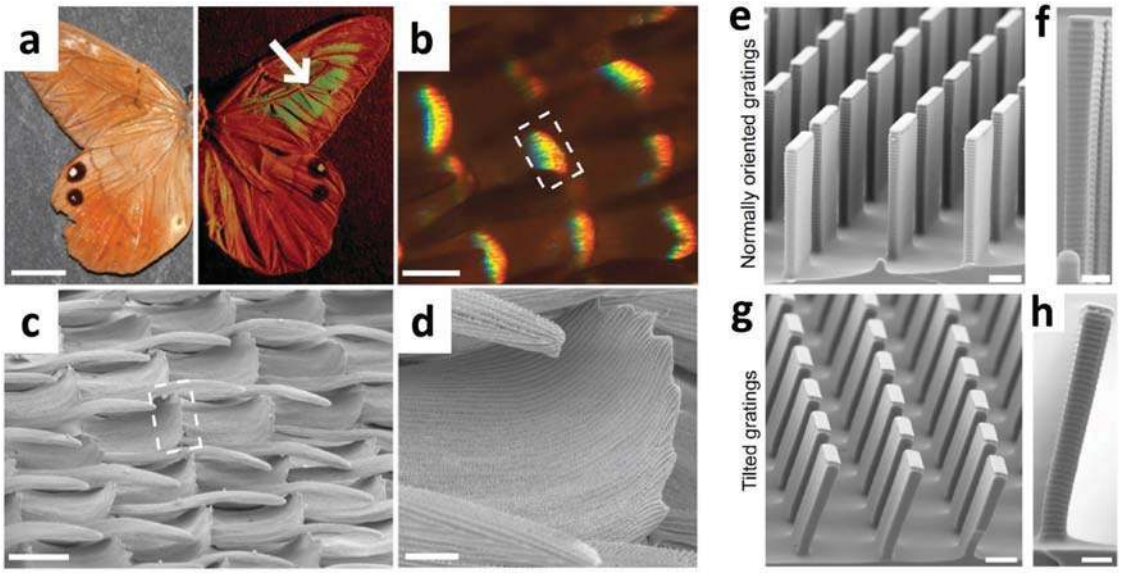

Figure 20. Optical properties of the curled scales in *P. luna* Butterfly. a) Optical image of *P. luna* under diffuse lighting (left) and directional lighting at grazing incidence (right). Scale bar is 10 mm. b) Optical microscopy image of *P. luna* scales under oblique illumination. Scale bar is 50 µm. c) SEM of scales in the colored wing region. Scale bar is 50 µm. White dashed boxes in panels (b) and (c) mark the curled tops of the scales from which the color originates. d) Closeup image of the curled region of the scale from which the color originates. Scale bar is 20 µm. Geometry and optical properties of the artificial photonic structure mimicking *P. luna* with vertically oriented (top) and tilted (bottom) diffraction gratings. e,g) SEM of the array of scalloped microplates. Scale bar is 5 µm. f,h) SEM of an individual plate with regular scallops. Scale bar is 2 µm. Reproduced with permission.[232] Copyright 2014, National Academy of Sciences.

Pierella luna butterfly, a mimic method has been developed using microdiffraction gratings in ordered arrays.[232] PDMS has been used as the mold, and a UV-curable epoxy resin as the replica. Bosch etching[233] and photolithography have been exploited to manufacture the microgratings (**Figure 20**). The vertically oriented microgratings are able to diffract different colors from red to blue as the observation angle is increased. The tilted microgratings show different optical characteristics.

Fabricating HAR nanostructures, like the one shown in Figure 3, has been introduced by Aizenberg and co-workers, who made the HARs in different geometries and patterns.[234] The method employed to create HARs is structural transformation by electrodeposition on patterned substrates, which can be employed for different applications. When an HAR nanopillar array is made, a step-by-step metal coating followed by metal evaporation on a desired angle/side/part is performed on the nanopillars. The result was the production of different shapes from the original nanopillars, nanoconical structures, for instance, with different conductivities, depending on the location of the nanopillars. Gold, platinum, or the conductive polymer, polypyrrole, have been deposited in different steps.

Metal-assisted chemical etching is a method that has been used to prepare vertically aligned silicon nanowires of different diameters, heights, and spacing.[235] The large-area ordered array of nanowires are assembled on P(NIPAM-*co*-MA) microgels (soft nanoparticle templating). By changing the spacing between the microgels, different colors are displayed. The Langmuir trough method is used to deposit the microgels on a silicon wafer. O_2 plasma etching with given durations has been used to tailor the mounted nanowires. Hierarchical structures with different patterns can be prepared by combining soft nanoparticle templating and photolithography.

6.2. Biomimetic Materials and Ideas

Other than butterfly wings, cephalopods are another species that have inspired many research works on the account of different aspects in their color-changing phenomenon.[138c] Some of the aspects have already been mentioned throughout this work. Manufacturing a device made of multiple independent stack layers is one of the suggested ideas.[120] Each layer (dielectric membrane) features an artificial chromatophore that can be (electrically) actuated independently on demand. As a result, different color hues and intensities can be displayed on the multilayer device. The concept has been exploited to develop an adaptive optoelectronic camouflage system made of flexible sheets, which can sense the surroundings and adapt the coloration without any user input.[93] The multilayer unit (e-skin) is equipped with photodetectors and actuators featuring pixelated color-changing elements on the top layer. The artificial chromatophore layers, the ultrathin silicon diode, the PDMS layer, and the Ag layer each resemble a component effective in the color-changing skin. In e-skin technology, color-changing mechanisms in chameleons are equally well studied. A highly stretchable, tactile sensing e-skin has been developed based on organic EC device (as chromatophore cells), with an elastic pyramidal microstructured layer (as tactile sensing) and PDMS layer. Both layers are coated by single-wall carbon nanotubes. The e-skin is equipped with a pressure sensor and the color is controlled by the applied pressure magnitude and duration, and therefore can be used as a colorimetric pressure sensor. The height of the micropyramids can be adjusted by the pressure sensor. The use of the EC device provides color memory and low power consumption.[94]

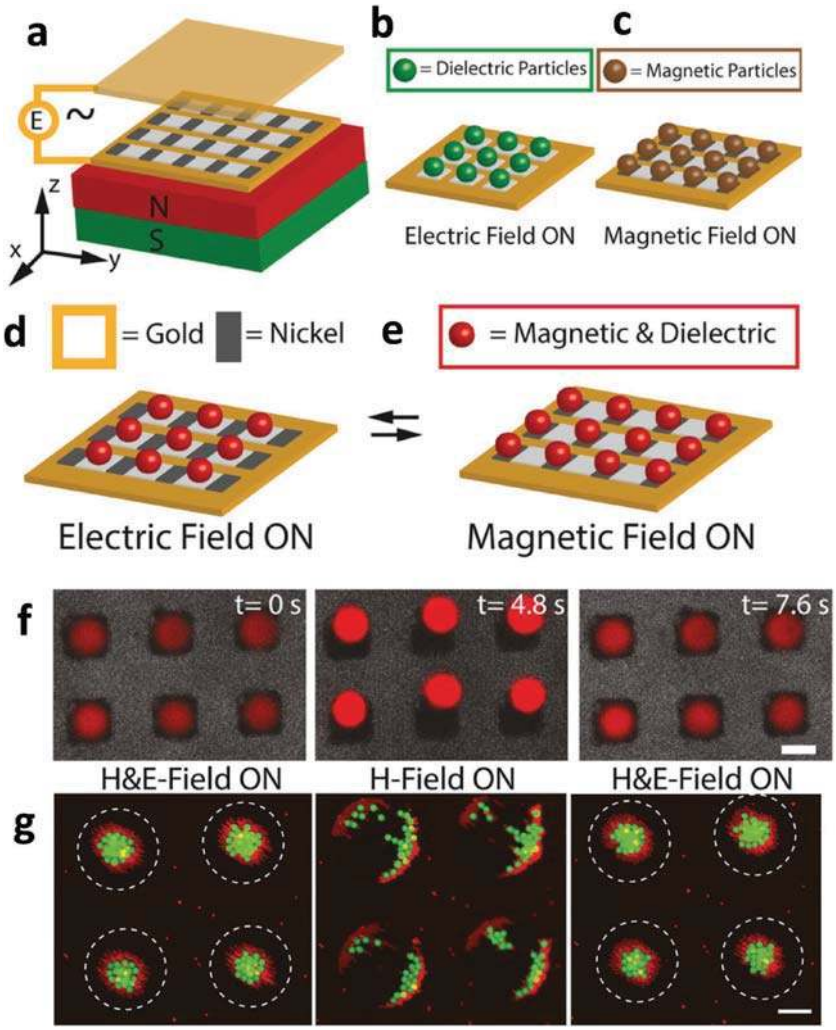

Figure 21. Electrode modeling and design. Setup with microfabricated Au and Ni patches a) with the expected behavior of a b) dielectric or c) magnetic particle. A particle with both magnetic susceptibility and dielectric contrast is expected to switch between the d) electric and e) magnetic potential minima. f) Time-lapse fluorescent microscopy images show the reversible switching of the position of 4.69 µm magneto-dielectric polystyrene particles between the two potential minima using magnetic and electric fields. g) Hierarchical assembly of binary-sized colloidal super-paramagnetic particles by electric field and the switching of the hierarchical assembly by turning the electric field on and off while keeping the magnetic field on. Dashed circles outline the voids of the microfabricated nickel-only electrode. The panels of the image show the field switching over time, namely, at (left) 0 s, (middle) 75 s, and (right) 95 s. The scale bar is 40 µm. Reproduced with permission.[237] Copyright 2017, American Chemical Society.

PDMS-based magnetic microplates similar to the micrograting in Figure 20 have been developed, with magnetic particles embedded in them, by means of lithography from a silicon wafer template.[236] The plates are coated with gold on one side. By applying a magnetic field, the microplates tilt, the gold-coated side is displayed, and the reflectance is changed as a result. A similar microplate system has been designed to change fluorescence by adding fluorescent coating on one side of the microplates.

Electroresponsive photonic crystal liquids based on metastable particles have been used as E-ink for photonic printing. The metastable system made of SiO_2/ETPTA–propylene carbonate has been applied as a single-component E-ink in lithographical printing and pixel printing to develop, respectively, multicolor and high-resolution photonic crystal patterns.[118] The color is tuned by a change in voltage; the grayscale is readily controlled and the structural colors are instantly fixed under the electric field, all simultaneously.

A mechanochromic photonic crystal paper based on similar metastable particles, i.e., SiO_2 colloidal crystals embedded in the PEGMA/EG gel have been utilized to prepare multicolor or high-resolution photonic patterns. The old relief printing technique has been combined with UV polymerization to produce this sensitive responsive system in which the structural color is tunable (multicolor) with slight/localized deformation (high resolution).[99]

Magnetophoresis and dielectrophoresis can be simultaneously used on colloidal particles to rapidly (tens of milliseconds) switch between their magnetic and electric potential minima. This idea has been implemented on a single chip, in which electric and magnetic fields are applied on magneto-dielectric PS particles (or on a binary particles' suspension) to change their position. In this manner, transparency/fluorescence of the sample can be tuned (**Figure 21**).[237]

Preparation of angle-independent noniridescent structural colors has been addressed above. The importance of colloidal amorphous arrays has also been reviewed before.[157,238] Different ideas to develop these systems have been presented. For the first time, it has been reported that polydopamine (PDA) black particles can be used to prepare amorphous colloidal structures and to mimic natural melanin granules.[239] By controlling the particles' concentration, diameter, and arrangement, different structural colors and textures are produced. In another recent work, melanin-like particles, i.e., PS core nanoparticle dip-coated with PDA layers as shell, have been used to produce bright structural colors that are independent of the background colors.[240] Different diameters of PS nanoparticles result in different structural colors, although this system is not as angle independent as the previous one.

An unconventional method to fabricate 3D-ordered structures has also been introduced, in which 1D layer structures are used as a building matrix for a 3D structure.[241] The number of layers and layer thickness tune the 3D structure properties. 1D heterogeneous laminar stacks of PVA and PMMA are doped with silver (high-RI component), and AgNPs aggregate (on PVA layers only), forming frameworks (such as dots, stripes, triangles, and letters) of different shapes via photomasking lithography, resulting in different optical properties.

7. Summary and Outlook

We have elucidated stimuli-responsive structural coloration by presenting examples from biological species. Our focus has been on animals that change the color of their skin, wing, and exoskeleton in response to an external stimulus (e.g., humidity and light) or for communication or protection through camouflage. Understanding the principles behind this color change is of paramount importance to replicate bioinspired stimuli-responsive materials. We have briefly explained possible architectures and structures of photonic materials such as thin films, Bragg stacks, photonic crystals, isotropic and anisotropic structures. We have reviewed how the structural color can be tuned through controlling the lattice constant, refractive index, orientation, and defect insertion.

Recent developments of bioinspired man-made photonic materials have then been discussed. Numerous examples of color-changing materials with the preparation methods have been presented and classified by the stimuli. There are still many systems with great potential to be explored in the field. For example, PNIPAM-based hydrogels/microgels have been frequently used as temperature-responsive materials. However, there are many other thermoresponsive polymers, with different LCST or upper critical solution temperature properties, that can be used in the fabrication of smart materials.[242] Preparation of inverse opals by removing silica/PS nanoparticles' templates is not the only route or necessarily the best one for certain applications to create ordered porous materials.[243] Clearly not all the smart color-changing systems could be classified in the above-mentioned categories. For instance, liquid crystals alone offer various possibilities of color change[194a] in terms of the nature of the LC, i.e., hydrophilic/hydrophobic or organic/inorganic and the stimuli to drive the isotropic–nematic transition, e.g., temperature,[194b] electric field, and light.[194c,244]

Stimuli/analytes such as light,[245] organic liquid,[246] biomolecules, bio-macromolecules, and small molecules have not been the main focus of this work either. Several authors prepared hydrogels and organogels,[247] designed from inverse opals and inspired by the Hercules beetle cuticle, to be used for detecting certain ions, small molecules, biological substances (e.g., proteins, vitamins, glucose, and DNA), or gases, for applications in medical diagnostics and environmental monitoring.[2,150a,164,248]

With emerging technologies, moving toward higher accuracy in sensing/visualization, and with an increasing number of fabrication methods, significant progress has been made in biomimetic materials, which in some cases even surpass the performance of the natural analogs. Various stimuli-responsive materials have been developed over the past two decades to meet market needs in different fields, such as displays, anti-counterfeiting materials, paints, flexible materials, wearable products, smart electronic/optical devices, and (temperature, pH, pressure, humidity, etc.) sensors. However, there are still many challenges to deal with, before some of the developed technologies will be ready to hit the market. Materials, methods, tools, and technologies must be customized to function in the complex environments, which are sometimes far from the ideal laboratory conditions where they are developed and tested. One should finally not forget that the major hurdle to be overcome before reaching the market is the cost of the solution. Highly complex solutions, though appealing and scientifically fascinating, are seldom the best choice.

Acknowledgements

Financial support from the Swiss National Science Foundation, though grant number PP00P2_159258 and especially through the National Center of Competence in Research Bio-Inspired Materials.

Conflict of Interest

The authors declare no conflict of interest.

Keywords

bioinspired materials, Bragg stacks, colloidal crystals, responsive hydrogels, structural colors

Received: December 3, 2017
Revised: January 16, 2018
Published online: April 27, 2018

[1] A. G. Dumanli, T. Savin, *Chem. Soc. Rev.* **2016**, *45*, 6698.
[2] S. Jung, J. L. Kaar, M. P. Stoykovich, *Mol. Syst. Des. Eng.* **2016**, *1*, 225.
[3] H. Inan, M. Poyraz, F. Inci, M. A. Lifson, M. Baday, B. T. Cunningham, U. Demirci, *Chem. Soc. Rev.* **2017**, *46*, 366.
[4] J. Sun, B. Bhushan, J. Tong, *RSC Adv.* **2013**, *3*, 14862.
[5] S.-N. Yin, C.-F. Wang, S.-S. Liu, S. Chen, *J. Mater. Chem. C* **2013**, *1*, 4685.
[6] A. Sidorenko, T. Krupenkin, A. Taylor, P. Fratzl, J. Aizenberg, *Science* **2007**, *315*, 487.
[7] P. Kim, L. D. Zarzar, M. Khan, M. Aizenberg, J. Aizenberg, in *SPIE Photonics West*, (Eds.: W. V. Schoenfeld, J. J. Wang, M. Loncar, T. J. Suleski), SPIE, San Francisco, CA **2011**, p. 792705.
[8] Y. Y. Diao, X. Y. Liu, G. W. Toh, L. Shi, J. Zi, *Adv. Funct. Mater.* **2013**, *23*, 5373.
[9] H. Hu, Q.-W. Chen, K. Cheng, J. Tang, *J. Mater. Chem.* **2012**, *22*, 1021.
[10] R. Xuan, Q. Wu, Y. Yin, J. Ge, *J. Mater. Chem.* **2011**, *21*, 3672.
[11] M. Xiao, Y. Li, J. Zhao, Z. Wang, M. Gao, N. C. Gianneschi, A. Dhinojwala, M. D. Shawkey, *Chem. Mater.* **2016**, *28*, 5516.
[12] K. Szendrei, P. Ganter, O. Sànchez-Sobrado, R. Eger, A. Kuhn, B. V. Lotsch, *Adv. Mater.* **2015**, *27*, 6341.
[13] P. Ganter, K. Szendrei, B. V. Lotsch, *Adv. Mater.* **2016**, *28*, 7436.
[14] Z. Wang, J. Zhang, J. Xie, Z. Wang, Y. Yin, J. Li, Y. Li, S. Liang, L. Zhang, L. Cui, *J. Mater. Chem.* **2012**, *22*, 7887.
[15] Y.-L. Ko, H.-P. Tsai, K.-Y. Lin, Y.-C. Chen, H. Yang, *J. Colloid Interface Sci.* **2017**, *487*, 360.
[16] R. Xuan, J. Ge, *J. Mater. Chem.* **2012**, *22*, 367.
[17] E. Colusso, G. Perotto, Y. Wang, M. Sturaro, F. Omenetto, A. Martucci, *J. Mater. Chem. C* **2017**, *5*, 3924.
[18] J. H. Kim, J. H. Moon, S.-Y. Lee, J. Park, *Appl. Phys. Lett.* **2010**, *97*, 103701.
[19] M. Giese, L. K. Blusch, M. K. Khan, W. Y. Hamad, M. J. MacLachlan, *Angew. Chem., Int. Ed.* **2014**, *53*, 8880.
[20] J. A. Kelly, A. M. Shukaliak, C. C. Y. Cheung, K. E. Shopsowitz, W. Y. Hamad, M. J. MacLachlan, *Angew. Chem., Int. Ed.* **2013**, *52*, 8912.

[21] B. Zhang, Y. Cheng, H. Wang, B. Ye, L. Shang, Y. Zhao, Z. Gu, *Nanoscale* **2015**, *7*, 10590.
[22] H. Sugiyama, T. Sawada, H. Yano, T. Kanai, *J. Mater. Chem. C* **2013**, *1*, 6103.
[23] T. Kanai, D. Lee, H. C. Shum, D. A. Weitz, *Small* **2010**, *6*, 807.
[24] Y. Yan, L. Liu, Z. Cai, J. Xu, Z. Xu, D. Zhang, X. Hu, *Sci. Rep.* **2016**, *6*, 31328.
[25] Y. Takeoka, *Polym. J.* **2016**, *49*, 301.
[26] H. Kye, Y. G. Koh, Y. Kim, S. G. Han, H. Lee, W. Lee, *Sensors* **2017**, *17*, 1398.
[27] J. E. Song, E. C. Cho, *Sci. Rep.* **2016**, *6*, 34622.
[28] H. Ma, M. Zhu, W. Luo, W. Li, K. Fang, F. Mou, J. Guan, *J. Mater. Chem. C* **2015**, *3*, 2848.
[29] M. C. Chiappelli, R. C. Hayward, *Adv. Mater.* **2012**, *24*, 6100.
[30] M. Chen, L. Zhou, Y. Guan, Y. Zhang, *Angew. Chem., Int. Ed.* **2013**, *52*, 9961.
[31] C. Liu, C. Yao, Y. Zhu, J. Ren, L. Ge, *Sens. Actuators, B* **2015**, *220*, 227.
[32] J. J. Walish, Y. Fan, A. Centrone, E. L. Thomas, *Macromol. Rapid Commun.* **2012**, *33*, 1504.
[33] A. W. Zaibudeen, J. Philip, *Opt. Mater.* **2017**, *66*, 117.
[34] Y. Gotoh, H. Suzuki, N. Kumano, T. Seki, K. Katagiri, Y. Takeoka, *New J. Chem.* **2012**, *36*, 2171.
[35] M. Zhou, F. Xing, M. Ren, Y. Feng, Y. Zhao, H. Qiu, X. Wang, C. Gao, F. Sun, Y. He, *ChemPhysChem* **2009**, *10*, 523.
[36] Y. Kim, D. Kim, G. Jang, J. Kim, T. S. Lee, *Sens. Actuators, B* **2015**, *207*, 623.
[37] J.-G. Park, W. B. Rogers, S. Magkiriadou, T. Kodger, S.-H. Kim, Y.-S. Kim, V. N. Manoharan, *Opt. Mater. Express* **2017**, *7*, 253.
[38] K. Lee, S. A. Asher, *J. Am. Chem. Soc.* **2000**, *122*, 9534.
[39] Y. J. Lee, P. V. Braun, *Adv. Mater.* **2003**, *15*, 563.
[40] C. Yao, J. Ren, C. Liu, T. Yin, Y. Zhu, L. Ge, *ACS Appl. Mater. Interfaces* **2014**, *6*, 16727.
[41] J. Shin, S. G. Han, W. Lee, *Sens. Actuators, B* **2012**, *168*, 20.
[42] M. Honda, T. Seki, Y. Takeoka, *Adv. Mater.* **2009**, *21*, 1801.
[43] W. Luo, J. Yan, Y. Tan, H. Ma, J. Guan, *Nanoscale* **2017**, *9*, 9548.
[44] X. Jia, K. Wang, J. Wang, Y. Hu, L. Shen, J. Zhu, *Eur. Polym. J.* **2016**, *83*, 60.
[45] J. Cui, W. Zhu, N. Gao, J. Li, H. Yang, Y. Jiang, P. Seidel, B. J. Ravoo, G. Li, *Angew. Chem., Int. Ed.* **2014**, *53*, 3844.
[46] T. Chen, Z.-Y. Deng, S.-N. Yin, S. Chen, C. Xu, *J. Mater. Chem. C* **2016**, *4*, 1398.
[47] Y. Zhang, Q. Fu, J. Ge, *Nat. Commun.* **2015**, *6*, 7510.
[48] S. Yu, Z. Han, X. Jiao, D. Chen, C. Li, *RSC Adv.* **2016**, *6*, 66191.
[49] D. Men, F. Zhou, L. Hang, X. Li, G. Duan, W. Cai, Y. Li, *J. Mater. Chem. C* **2016**, *4*, 2117.
[50] A. K. Yetisen, H. Butt, S.-H. Yun, *ACS Sens.* **2016**, *1*, 493.
[51] Q. Yang, S. Zhu, W. Peng, C. Yin, W. Wang, J. Gu, W. Zhang, J. Ma, T. Deng, C. Feng, *ACS Nano* **2013**, *7*, 4911.
[52] X. Fei, T. Lu, J. Ma, W. Wang, S. Zhu, D. Zhang, *ACS Appl. Mater. Interfaces* **2016**, *8*, 27091.
[53] R. Xue, W. Zhang, P. Sun, I. Zada, C. Guo, Q. Liu, J. Gu, H. Su, D. Zhang, *Sci. Rep.* **2017**, *7*, 42207.
[54] M. Moirangthem, R. Arts, M. Merkx, A. P. H. J. Schenning, *Adv. Funct. Mater.* **2016**, *26*, 1154.
[55] D. Men, H. Zhang, L. Hang, D. Liu, X. Li, W. Cai, Q. Xiong, Y. Li, *J. Mater. Chem. C* **2015**, *3*, 3659.
[56] J. Zhang, Y. Tian, W.-Q. Ji, Z. Zhu, C.-F. Wang, S. Chen, *J. Mater. Chem. C* **2016**, *4*, 6750.
[57] B. Yu, F. Zhai, H. Cong, D. Yang, *J. Mater. Chem. C* **2016**, *4*, 1386.
[58] Y. Gao, M. J. Serpe, *ACS Appl. Mater. Interfaces* **2014**, *6*, 8461.
[59] L. Hu, M. J. Serpe, *J. Mater. Chem.* **2012**, *22*, 8199.
[60] H. Kim, J. Ge, J. Kim, S.-e. Choi, H. Lee, H. Lee, W. Park, Y. Yin, S. Kwon, *Nat. Photonics* **2009**, *3*, 534.
[61] J. Ge, H. Lee, L. He, J. Kim, Z. Lu, H. Kim, J. Goebl, S. Kwon, Y. Yin, *J. Am. Chem. Soc.* **2009**, *131*, 15687.
[62] Y. Zhang, Y. Jiang, X. Wu, J. Ge, *J. Mater. Chem. C* **2017**, *5*, 9288.
[63] J. Liu, Y. Mao, J. Ge, *Nanoscale* **2012**, *4*, 1598.
[64] H. Wang, S. Yang, S.-N. Yin, L. Chen, S. Chen, *ACS Appl. Mater. Interfaces* **2015**, *7*, 8827.
[65] S. Shang, Q. Zhang, H. Wang, Y. Li, *J. Colloid Interface Sci.* **2017**, *485*, 18.
[66] H. Hu, Q.-W. Chen, J. Tang, X.-Y. Hu, X.-H. Zhou, *J. Mater. Chem.* **2012**, *22*, 11048.
[67] Y. Hu, L. He, X. Han, M. Wang, Y. Yin, *Nano Res.* **2015**, *8*, 611.
[68] M. Wang, L. He, Y. Hu, Y. Yin, *J. Mater. Chem. C* **2013**, *1*, 6151.
[69] Y. Hu, L. He, Y. Yin, *Angew. Chem., Int. Ed.* **2011**, *50*, 3747.
[70] S. Y. Lee, J. Choi, J.-R. Jeong, J. H. Shin, S.-H. Kim, *Adv. Mater.* **2017**, *29*, 1605450.
[71] M. Wang, L. He, W. Xu, X. Wang, Y. Yin, *Angew. Chem., Int. Ed.* **2015**, *54*, 7077.
[72] W. Luo, H. Ma, F. Mou, M. Zhu, J. Yan, J. Guan, *Adv. Mater.* **2014**, *26*, 1058.
[73] J. Kim, Y. Song, L. He, H. Kim, H. Lee, W. Park, Y. Yin, S. Kwon, *Small* **2011**, *7*, 1163.
[74] M. Wang, L. He, S. Zorba, Y. Yin, *Nano Lett.* **2014**, *14*, 3966.
[75] S. Shang, Q. Zhang, H. Wang, Y. Li, *J. Colloid Interface Sci.* **2016**, *483*, 11.
[76] M. G. Han, C. G. Shin, S. J. Jeon, H. Shim, C. J. Heo, H. Jin, J. W. Kim, S. Lee, *Adv. Mater.* **2012**, *24*, 6438.
[77] S. Lee, J. Y. Kim, S. Cheon, S. Kim, D. Kim, H. Ryu, *RSC Adv.* **2017**, *7*, 6988.
[78] X. Qiao, A. Sun, C. Wang, C. Chu, S. Ma, X. Tang, J. Guo, G. Xu, *Colloids Surf., A* **2016**, *498*, 74.
[79] M. G. Han, C.-J. Heo, C. G. Shin, H. Shim, J. W. Kim, Y. W. Jin, S. Lee, *J. Mater. Chem. C* **2013**, *1*, 5791.
[80] M. G. Han, C. J. Heo, H. Shim, C. G. Shin, S. J. Lim, J. W. Kim, Y. W. Jin, S. Lee, *Adv. Opt. Mater.* **2014**, *2*, 535.
[81] Y.-C. Hsiao, W. Lee, *Opt. Lett.* **2015**, *40*, 1201.
[82] J. Xiang, Y. Li, Q. Li, D. A. Paterson, J. Storey, C. T. Imrie, O. D. Lavrentovich, *Adv. Mater.* **2015**, *27*, 3014.
[83] H. Xing, J. Li, J. Guo, J. Wei, *J. Mater. Chem. C* **2015**, *3*, 4424.
[84] C. Lin, Y. Jiang, C.-a. Tao, X. Yin, Y. Lan, C. Wang, S. Wang, X. Liu, G. Li, *ACS Appl. Mater. Interfaces* **2017**, *9*, 11770.
[85] H. Shin, Y. Kim, T. Bhuvana, J. Lee, X. Yang, C. Park, E. Kim, *ACS Appl. Mater. Interfaces* **2011**, *4*, 185.
[86] K. Li, Q. Zhang, H. Wang, Y. Li, *ACS Appl. Mater. Interfaces* **2014**, *6*, 13043.
[87] Y. Alesanco, A. Viñuales, J. s. Palenzuela, I. Odriozola, G. n. Cabañero, J. Rodriguez, R. n. Tena-Zaera, *ACS Appl. Mater. Interfaces* **2016**, *8*, 14795.
[88] H.-S. Liu, B.-C. Pan, D.-C. Huang, Y.-R. Kung, C.-M. Leu, G.-S. Liou, *NPG Asia Mater.* **2017**, *9*, e388.
[89] L. Liu, S. K. Karuturi, L. T. Su, Q. Wang, A. I. Y. Tok, *Electrochem. Commun.* **2011**, *13*, 1163.
[90] J. J. Walish, Y. Kang, R. A. Mickiewicz, E. L. Thomas, *Adv. Mater.* **2009**, *21*, 3078.
[91] G. Wang, X. Chen, S. Liu, C. Wong, S. Chu, *ACS Nano* **2016**, *10*, 1788.
[92] T. Xu, E. C. Walter, A. Agrawal, C. Bohn, J. Velmurugan, W. Zhu, H. J. Lezec, A. A. Talin, *Nat. Commun.* **2016**, *7*, 10479.
[93] C. Yu, Y. Li, X. Zhang, X. Huang, V. Malyarchuk, S. Wang, Y. Shi, L. Gao, Y. Su, Y. Zhang, *Proc. Natl. Acad. Sci. USA* **2014**, *111*, 12998.
[94] H.-H. Chou, A. Nguyen, A. Chortos, J. W. F. To, C. Lu, J. Mei, T. Kurosawa, W.-G. Bae, J. B. H. Tok, Z. Bao, *Nat. Commun.* **2015**, *6*, 8011.
[95] R. Hong, Y. Shi, X.-Q. Wang, L. Peng, X. Wu, H. Cheng, S. Chen, *RSC Adv.* **2017**, *7*, 33258.

[96] X.-Q. Wang, R. Hong, C.-F. Wang, P.-F. Tan, W.-Q. Ji, S. Chen, *Mater. Lett.* **2017**, *189*, 321.
[97] X. Jia, J. Wang, K. Wang, J. Zhu, *Langmuir* **2015**, *31*, 8732.
[98] Y. F. Yue, M. A. Haque, T. Kurokawa, T. Nakajima, J. P. Gong, *Adv. Mater.* **2013**, *25*, 3106.
[99] D. Yang, S. Ye, J. Ge, *Chem. Commun.* **2015**, *51*, 16972.
[100] T. Ito, C. Katsura, H. Sugimoto, E. Nakanishi, K. Inomata, *Langmuir* **2013**, *29*, 13951.
[101] C. G. Schäfer, M. Gallei, J. T. Zahn, J. Engelhardt, G. t. P. Hellmann, M. Rehahn, *Chem. Mater.* **2013**, *25*, 2309.
[102] C. G. Schäfer, C. Lederle, K. Zentel, B. Stühn, M. Gallei, *Macromol. Rapid Commun.* **2014**, *35*, 1852.
[103] C. G. Schäfer, D. A. Smolin, G. P. Hellmann, M. Gallei, *Langmuir* **2013**, *29*, 11275.
[104] a) S. Ye, Q. Fu, J. Ge, *Adv. Funct. Mater.* **2014**, *24*, 6430; b) D. Yang, S. Ye, J. Ge, *Adv. Funct. Mater.* **2014**, *24*, 3197.
[105] L. Minati, A. Chiappini, C. Armellini, A. Carpentiero, D. Maniglio, A. Vaccari, L. Zur, A. Lukowiak, M. Ferrari, G. Speranza, *Mater. Chem. Phys.* **2017**, *192*, 94.
[106] T. Karrock, M. Paulsen, M. Gerken, *Beilstein J. Nanotechnol.* **2017**, *8*, 203.
[107] Y. Shi, C. Zhu, J. Li, J. Wei, J. Guo, *New J. Chem.* **2016**, *40*, 7311.
[108] A. Agrawal, P. Luchette, P. Palffy-Muhoray, S. L. Biswal, W. G. Chapman, R. Verduzco, *Soft Matter* **2012**, *8*, 7138.
[109] Y. Deng, S. Gao, J. Liu, U. Gohs, E. Mäder, G. Heinrich, *Mater. Horiz.* **2017**, *4*, 389.
[110] X. Sun, J. Zhang, X. Lu, X. Fang, H. Peng, *Angew. Chem., Int. Ed.* **2015**, *54*, 3630.
[111] S. Shang, Z. Liu, Q. Zhang, H. Wang, Y. Li, *J. Mater. Chem. A* **2015**, *3*, 11093.
[112] M. Kolle, A. Lethbridge, M. Kreysing, J. J. Baumberg, J. Aizenberg, P. Vukusic, *Adv. Mater.* **2013**, *25*, 2239.
[113] J. Zhang, S. He, L. Liu, G. Guan, X. Lu, X. Sun, H. Peng, *J. Mater. Chem. C* **2016**, *4*, 2127.
[114] H. Wang, K.-Q. Zhang, *Sensors* **2013**, *13*, 4192.
[115] S. Kinoshita, S. Yoshioka, J. Miyazaki, *Rep. Prog. Phys.* **2008**, *71*, 076401.
[116] J. D. Joannopoulos, S. G. Johnson, J. N. Winn, R. D. Meade, *Photonic Crystals: Molding theFlow of Light*, Princeton University Press, Princeton, NJ **2011**.
[117] J. C. Berg, *An Introduction to Interfaces and Colloids: The Bridge to Nanoscience*, World Scientific, Singapore **2010**.
[118] D. Yang, S. Ye, J. Ge, *J. Am. Chem. Soc.* **2013**, *135*, 18370.
[119] T. Lu, W. Peng, S. Zhu, D. Zhang, *Nanotechnology* **2016**, *27*, 122001.
[120] Y. Fu, C. A. Tippets, E. U. Donev, R. Lopez, *Wiley Interdiscip. Rev.: Nanomed. Nanobiotechnol.* **2016**, *8*, 758.
[121] W. Yi, D.-B. Xiong, D. Zhang, *Nano Adv.* **2016**, *1*, 62.
[122] H. Nilsson Sköld, S. Aspengren, M. Wallin, *Pigm. Cell Melanoma Res.* **2013**, *26*, 29.
[123] L. Wu, J. He, W. Shang, T. Deng, J. Gu, H. Su, Q. Liu, W. Zhang, D. Zhang, *Adv. Opt. Mater.* **2016**, *4*, 195.
[124] R. A. Potyrailo, H. Ghiradella, A. Vertiatchikh, K. Dovidenko, J. R. Cournoyer, E. Olson, *Nat. Photonics* **2007**, *1*, 123.
[125] E. Shevtsova, C. Hansson, D. H. Janzen, J. Kjærandsen, *Proc. Natl. Acad. Sci. USA* **2011**, *108*, 668.
[126] L. M. Mäthger, C.-C. Chiao, A. Barbosa, R. T. Hanlon, *J. Comp. Physiol., A* **2008**, *194*, 577.
[127] J. Teyssier, S. V. Saenko, D. van der Marel, M. C. Milinkovitch, *Nat. Commun.* **2015**, *6*, 6368.
[128] C. M. Eliason, M. D. Shawkey, *Opt. Express* **2010**, *18*, 21284.
[129] F. Liu, B. Q. Dong, X. H. Liu, Y. M. Zheng, J. Zi, *Opt. Express* **2009**, *17*, 16183.
[130] J. P. Vigneron, J. M. Pasteels, D. M. Windsor, Z. Vértesy, M. Rassart, T. Seldrum, J. Dumont, O. Deparis, V. Lousse, L. P. Biró, *Phys. Rev. E* **2007**, *76*, 031907.
[131] M. Rassart, P. Simonis, A. Bay, O. Deparis, J. P. Vigneron, *Phys. Rev. E* **2009**, *80*, 031910.
[132] D. Gur, B. A. Palmer, B. Leshem, D. Oron, P. Fratzl, S. Weiner, L. Addadi, *Angew. Chem., Int. Ed.* **2015**, *54*, 12426.
[133] J. F. F. Boyer, L. Swierk, *Can. J. Zool.* **2017**, *95*, 213.
[134] R. C. Duarte, A. A. V. Flores, M. Stevens, *Philos. Trans. R. Soc., B* **2017**, *372*, 20160342.
[135] D. Akkaynak, L. A. Siemann, A. Barbosa, L. M. Mäthger, *R. Soc. Open Sci.* **2017**, *4*, 160824.
[136] L. M. Mäthger, S. L. Senft, M. Gao, S. Karaveli, G. R. R. Bell, R. Zia, A. M. Kuzirian, P. B. Dennis, W. J. Crookes-Goodson, R. R. Naik, G. W. Kattawar, R. T. Hanlon, *Adv. Funct. Mater.* **2013**, *23*, 3980.
[137] L. F. Deravi, A. P. Magyar, S. P. Sheehy, G. R. R. Bell, L. M. Mäthger, S. L. Senft, T. J. Wardill, W. S. Lane, A. M. Kuzirian, R. T. Hanlon, E. L. Hu, K. K. Parker, *J. R. Soc., Interface* **2014**, *11*, 20130942.
[138] a) L. M. Mäthger, E. J. Denton, N. J. Marshall, R. T. Hanlon, *J. R. Soc., Interface* **2009**, *6*, S149; b) E. Kreit, L. M. Mäthger, R. T. Hanlon, P. B. Dennis, R. R. Naik, E. Forsythe, J. Heikenfeld, *J. R. Soc., Interface* **2012**, *10*, 20120601; c) L. Phan, R. Kautz, E. M. Leung, K. L. Naughton, Y. Van Dyke, A. A. Gorodetsky, *Chem. Mater.* **2016**, *28*, 6804.
[139] M. Goda, *Pigm. Cell Melanoma Res.* **2017**, *30*, 368.
[140] D. Gur, B. Leshem, V. Farstey, D. Oron, L. Addadi, S. Weiner, *Adv. Funct. Mater.* **2016**, *26*, 1393.
[141] D. Gur, B. A. Palmer, S. Weiner, L. Addadi, *Adv. Funct. Mater.* **2017**, *27*, 1603514.
[142] a) C. Chatterjee, A. Sen, *J. Mater. Chem. A* **2015**, *3*, 5642; b) J. Li, C. Hou, D. Huo, M. Yang, H.-b. Fa, P. Yang, *Sens. Actuators, B* **2014**, *196*, 10; c) O. Dalstein, D. R. Ceratti, C. Boissière, D. Grosso, A. Cattoni, M. Faustini, *Adv. Funct. Mater.* **2016**, *26*, 81; d) R. A. Potyrailo, R. K. Bonam, J. G. Hartley, T. A. Starkey, P. Vukusic, M. Vasudev, T. Bunning, R. R. Naik, Z. Tang, M. A. Palacios, M. Larsen, L. A. Le Tarte, J. C. Grande, S. Zhong, T. Deng, *Nat. Commun.* **2015**, *6*, 7959.
[143] a) Y. S. Zhang, A. Khademhosseini, *Science* **2017**, *356*, eaaf3627; b) L. Ionov, *Adv. Funct. Mater.* **2013**, *23*, 4555.
[144] W. Wang, Y. Zhang, W. Liu, *Prog. Polym. Sci.* **2017**, *71*, 1.
[145] P. Kim, L. D. Zarzar, X. He, A. Grinthal, J. Aizenberg, *Curr. Opin. Solid State Mater. Sci.* **2011**, *15*, 236.
[146] J. E. Stumpel, D. J. Broer, A. P. H. J. Schenning, *RSC Adv.* **2015**, *5*, 94650.
[147] a) C. Salas, T. Nypelö, C. Rodriguez-Abreu, C. Carrillo, O. J. Rojas, *Curr. Opin. Colloid Interface Sci.* **2014**, *19*, 383; b) M. Giese, L. K. Blusch, M. K. Khan, M. J. MacLachlan, *Angew. Chem., Int. Ed.* **2015**, *54*, 2888.
[148] K. Yao, Q. Meng, V. Bulone, Q. Zhou, *Adv. Mater.* **2017**, *29*, 1701323.
[149] T. Wu, J. Li, J. Li, S. Ye, J. Wei, J. Guo, *J. Mater. Chem. C* **2016**, *4*, 9687.
[150] a) J. Liu, Y. Zhang, R. Zhou, L. Gao, *J. Mater. Chem. C* **2017**, *5*, 6071; b) Y. Ohtsuka, T. Seki, Y. Takeoka, *Angew. Chem.* **2015**, *127*, 15588; c) K. Ueno, K. Matsubara, M. Watanabe, Y. Takeoka, *Adv. Mater.* **2007**, *19*, 2807.
[151] a) R. H. Pelton, P. Chibante, *Colloids Surf.* **1986**, *20*, 247; b) H. Kawaguchi, K. Fujimoto, Y. Mizuhara, *Colloid Polym. Sci.* **1992**, *270*, 53; c) R. Acciaro, T. Gilányi, I. Varga, *Langmuir* **2011**, *27*, 7917.
[152] a) S. Tsuji, H. Kawaguchi, *Langmuir* **2005**, *21*, 8439; b) J. Zhou, G. Wang, M. Marquez, Z. Hu, *Soft Matter* **2009**, *5*, 820.
[153] D. Suzuki, T. Yamagata, K. Horigome, K. Shibata, A. Tsuchida, T. Okubo, *Colloid Polym. Sci.* **2012**, *290*, 107.
[154] a) J. Wu, B. Zhou, Z. Hu, *Phys. Rev. Lett.* **2003**, *90*, 048304; b) H. Senff, W. Richtering, *J. Chem. Phys.* **1999**, *111*, 1705.
[155] X. Li, Y. Gao, M. J. Serpe, *Macromol. Rapid Commun.* **2015**, *36*, 1382.

[156] J. M. Weissman, H. B. Sunkara, S. T. Albert, S. A. Asher, *Science* **1996**, *274*, 959.
[157] Y. Takeoka, *J. Mater. Chem.* **2012**, *22*, 23299.
[158] a) I. Lee, D. Kim, J. Kal, H. Baek, D. Kwak, D. Go, E. Kim, C. Kang, J. Chung, Y. Jang, S. Ji, J. Joo, Y. Kang, *Adv. Mater.* **2010**, *22*, 4973; b) K. Ueno, A. Inaba, Y. Sano, M. Kondoh, M. Watanabe, *Chem. Commun.* **2009**, 3603.
[159] H. Gu, Y. Zhao, Y. Cheng, Z. Xie, F. Rong, J. Li, B. Wang, D. Fu, Z. Gu, *Small* **2013**, *9*, 2266.
[160] A. K. Yetisen, Y. Montelongo, M. M. Qasim, H. Butt, T. D. Wilkinson, M. J. Monteiro, S. H. Yun, *Anal. Chem.* **2015**, *87*, 5101.
[161] T. Okubo, S. Fujii, K. Aono, Y. Nakamura, *Colloid Polym. Sci.* **2013**, *291*, 2569.
[162] C. Kang, E. Kim, H. Baek, K. Hwang, D. Kwak, Y. Kang, E. L. Thomas, *J. Am. Chem. Soc.* **2009**, *131*, 7538.
[163] Y. Gao, X. Li, M. J. Serpe, *RSC Adv.* **2015**, *5*, 44074.
[164] B. Ye, F. Rong, H. Gu, Z. Xie, Y. Cheng, Y. Zhao, Z. Gu, *Chem. Commun.* **2013**, *49*, 5331.
[165] a) B.-F. Ye, Y.-J. Zhao, Y. Cheng, T.-T. Li, Z.-Y. Xie, X.-W. Zhao, Z.-Z. Gu, *Nanoscale* **2012**, *4*, 5998; b) D. Arunbabu, A. Sannigrahi, T. Jana, *Soft Matter* **2011**, *7*, 2592.
[166] a) L. Zhang, W.-F. Dong, H.-B. Sun, *Nanoscale* **2013**, *5*, 7664; b) M. Mahmoudi, S. Sant, B. Wang, S. Laurent, T. Sen, *Adv. Drug Delivery Rev.* **2011**, *63*, 24; c) A.-H. Lu, E. L. Salabas, F. Schüth, *Angew. Chem., Int. Ed.* **2007**, *46*, 1222; d) M. Faraji, Y. Yamini, M. Rezaee, *J. Iran. Chem. Soc.* **2010**, *7*, 1.
[167] H. Hu, J. Tang, H. Zhong, Z. Xi, C. Chen, Q. Chen, *Sci. Rep.* **2013**, *3*, 1484.
[168] J. Ge, J. Goebl, L. He, Z. Lu, Y. Yin, *Adv. Mater.* **2009**, *21*, 4259.
[169] X. Xu, G. Friedman, K. D. Humfeld, S. A. Majetich, S. A. Asher, *Adv. Mater.* **2001**, *13*, 1681.
[170] J. Zhang, S. Xu, E. Kumacheva, *J. Am. Chem. Soc.* **2004**, *126*, 7908.
[171] a) J. Ge, Y. Hu, Y. Yin, *Angew. Chem.* **2007**, *119*, 7572; b) H. Deng, X. Li, Q. Peng, X. Wang, J. Chen, Y. Li, *Angew. Chem.* **2005**, *117*, 2842.
[172] X. Tang, A. Sun, C. Chu, C. Wang, Z. Liu, J. Guo, G. Xu, *Sens. Actuators, B* **2016**, *236*, 399.
[173] X. Q. Wang, S. Yang, C. F. Wang, L. Chen, S. Chen, *Macromol. Rapid Commun.* **2016**, *37*, 759.
[174] W. Wang, X. Fan, F. Li, J. Qiu, M. M. Umair, W. Ren, B. Ju, S. Zhang, B. Tang, *Adv. Opt. Mater.* **2018**, *6*, 1701093.
[175] H. Ma, K. Tang, W. Luo, L. Ma, Q. Cui, W. Li, J. Guan, *Nanoscale* **2017**, *9*, 3105.
[176] H. Wang, Y.-B. Sun, Q.-W. Chen, Y.-F. Yu, K. Cheng, *Dalton Trans.* **2010**, *39*, 9565.
[177] L. He, M. Janner, Q. Lu, M. Wang, H. Ma, Y. Yin, *Adv. Mater.* **2015**, *27*, 86.
[178] a) L. He, M. Wang, J. Ge, Y. Yin, *Acc. Chem. Res.* **2012**, *45*, 1431; b) H. Takahashi, D. Nagao, K. Watanabe, H. Ishii, M. Konno, *Langmuir* **2015**, *31*, 5590.
[179] L. He, Y. Hu, H. Kim, J. Ge, S. Kwon, Y. Yin, *Nano Lett.* **2010**, *10*, 4708.
[180] L. He, M. Wang, Q. Zhang, Y. Lu, Y. Yin, *Nano Lett.* **2013**, *13*, 264.
[181] L. Nucara, F. Greco, V. Mattoli, *J. Mater. Chem. C* **2015**, *3*, 8449.
[182] A. C. Arsenault, D. P. Puzzo, I. Manners, G. A. Ozin, *Nat. Photonics* **2007**, *1*, 468.
[183] H. Shim, C. Gyun Shin, C.-J. Heo, S.-J. Jeon, H. Jin, J. Woo Kim, Y. Jin, S. Lee, J. Lim, M. Gyu Han, *Appl. Phys. Lett.* **2014**, *104*, 051104.
[184] X. Lv, W. Li, M. Ouyang, Y. Zhang, D. S. Wright, C. Zhang, *J. Mater. Chem. C* **2017**, *5*, 12.
[185] T. Bhuvana, B. Kim, X. Yang, H. Shin, E. Kim, *Angew. Chem., Int. Ed.* **2013**, *52*, 1180.
[186] H. Oh, D. G. Seo, T. Y. Yun, C. Y. Kim, H. C. Moon, *ACS Appl. Mater. Interfaces* **2017**, *9*, 7658.
[187] S. Araki, K. Nakamura, K. Kobayashi, A. Tsuboi, N. Kobayashi, *Adv. Mater.* **2012**, *22*, OP122.
[188] S. V. Vasilyeva, P. M. Beaujuge, S. Wang, J. E. Babiarz, V. W. Ballarotto, J. R. Reynolds, *ACS Appl. Mater. Interfaces* **2011**, *3*, 1022.
[189] G. J. Stec, A. Lauchner, Y. Cui, P. Nordlander, N. J. Halas, *ACS Nano* **2017**, *11*, 3254.
[190] D. P. Puzzo, A. C. Arsenault, I. Manners, G. A. Ozin, *Angew. Chem.* **2009**, *121*, 961.
[191] C. W. Pester, C. Liedel, M. Ruppel, A. Böker, *Prog. Polym. Sci.* **2017**, *64*, 182.
[192] Y. Lu, C. Meng, H. Xia, G. Zhang, C. Wu, *J. Mater. Chem. C* **2013**, *1*, 6107.
[193] Z. He, X. Yuan, Q. Wang, L. Yu, C. Zou, C. Li, Y. Zhao, B. He, L. Zhang, H. Zhang, *Adv. Opt. Mater.* **2016**, *4*, 106.
[194] a) T. J. White, M. E. McConney, T. J. Bunning, *J. Mater. Chem.* **2010**, *20*, 9832; b) S. Carrasco-Hernandez, J. Gutierrez, A. Tercjak, *Eur. Polym. J.* **2017**, *91*, 187; c) M. Brehmer, J. Lub, P. van de Witte, *Adv. Mater.* **1998**, *10*, 1438.
[195] a) D. Kang, J. E. Maclennan, N. A. Clark, A. A. Zakhidov, R. H. Baughman, *Phys. Rev. Lett.* **2001**, *86*, 4052; b) V. P. Tondiglia, L. V. Natarajan, R. L. Sutherland, D. Tomlin, T. J. Bunning, *Adv. Mater.* **2002**, *14*, 187.
[196] a) H. Xianyu, T.-H. Lin, S.-T. Wu, *Appl. Phys. Lett.* **2006**, *89*, 091124; b) S.-Y. Lu, L.-C. Chien, *Appl. Phys. Lett.* **2007**, *91*, 131119.
[197] M. E. McConney, V. P. Tondiglia, L. V. Natarajan, K. M. Lee, T. J. White, T. J. Bunning, *Adv. Opt. Mater.* **2013**, *1*, 417.
[198] R. B. Meyer, *Appl. Phys. Lett.* **1968**, *12*, 281.
[199] P. G. de Gennes, *Solid State Commun.* **1968**, *6*, 163.
[200] B. Frka-Petesic, H. Radavidson, B. Jean, L. Heux, *Adv. Mater.* **2017**, *29*, 1606208.
[201] R. J. Spontak, N. P. Patel, *Curr. Opin. Colloid Interface Sci.* **2000**, *5*, 333.
[202] T. Xie, *Polymer* **2011**, *52*, 4985.
[203] C. L. Lewis, E. M. Dell, *J. Polym. Sci., Part B: Polym. Phys.* **2016**, *54*, 1340.
[204] a) A. C. Arsenault, T. J. Clark, G. von Freymann, L. Cademartiri, R. Sapienza, J. Bertolotti, E. Vekris, S. Wong, V. Kitaev, I. Manners, *Nat. Mater.* **2006**, *5*, 179; b) A. Chiappini, A. Piotrowska, M. Marciniak, M. Ferrari, D. Zonta, in *Proc. of SPIE—The Int. Society for Optical Engineering, Sensors and Smart Structures Technologies for Civil, Mechanical, and Aerospace Systems 2015* (Ed.: J. P. Lynch), Vol. *9435*, SPIE, Bellingham, WA **2015**, p. 94350J.
[205] a) E. P. Chan, J. J. Walish, A. M. Urbas, E. L. Thomas, *Adv. Mater.* **2013**, *25*, 3934; b) E. P. Chan, J. J. Walish, E. L. Thomas, C. M. Stafford, *Adv. Mater.* **2011**, *23*, 4702.
[206] S. Zeng, D. Zhang, W. Huang, Z. Wang, S. G. Freire, X. Yu, A. T. Smith, E. Y. Huang, H. Nguon, L. Sun, *Nat. Commun.* **2016**, *7*, 11802.
[207] J.-H. Choi, Y.-S. No, J.-P. So, J. M. Lee, K.-H. Kim, M.-S. Hwang, S.-H. Kwon, H.-G. Park, *Nat. Commun.* **2016**, *7*, 11569.
[208] M. A. Haque, T. Kurokawa, J. P. Gong, *Soft Matter* **2012**, *8*, 8008.
[209] Y. Yue, X. Li, T. Kurokawa, M. A. Haque, J. P. Gong, *J. Mater. Chem. B* **2016**, *4*, 4104.
[210] Y. Yue, T. Kurokawa, M. A. Haque, T. Nakajima, T. Nonoyama, X. Li, I. Kajiwara, J. P. Gong, *Nat. Commun.* **2014**, *5*, 4659.
[211] Q. Zhao, A. Haines, D. Snoswell, C. Keplinger, R. Kaltseis, S. Bauer, I. Graz, R. Denk, P. Spahn, G. Hellmann, *Appl. Phys. Lett.* **2012**, *100*, 101902.
[212] J. Rossiter, B. Yap, A. Conn, *Bioinspiration Biomimetics* **2012**, *7*, 036009.
[213] Q. Wang, G. R. Gossweiler, S. L. Craig, X. Zhao, *Nat. Commun.* **2014**, *5*, 4899.

[214] a) H. Shahsavan, S. M. Salili, A. Jákli, B. Zhao, *Adv. Mater.* **2015**, *27*, 6828; b) H. Yu, T. Ikeda, *Adv. Mater.* **2011**, *23*, 2149; c) H. Jiang, C. Li, X. Huang, *Nanoscale* **2013**, *5*, 5225; d) C. Ohm, M. Brehmer, R. Zentel, *Adv. Mater.* **2010**, *22*, 3366; e) H. Yang, G. Ye, X. Wang, P. Keller, *Soft Matter* **2011**, *7*, 815.
[215] R. S. Kularatne, H. Kim, J. M. Boothby, T. H. Ware, *J. Polym. Sci., Part B: Polym. Phys.* **2017**, *55*, 395.
[216] H. Shahsavan, L. Yu, A. Jakli, B. Zhao, *Soft Matter* **2017**, *13*, 8006.
[217] G. Wu, Y. Jiang, D. Xu, H. Tang, X. Liang, G. Li, *Langmuir* **2010**, *27*, 1505.
[218] Y. Jiang, D. Xu, X. Li, C. Lin, W. Li, Q. An, C.-a. Tao, H. Tang, G. Li, *J. Mater. Chem.* **2012**, *22*, 11943.
[219] a) A. Kaiser, M. Winkler, S. Krause, H. Finkelmann, A. M. Schmidt, *J. Mater. Chem.* **2009**, *19*, 538; b) M. Winkler, A. Kaiser, S. Krause, H. Finkelmann, A. M. Schmidt, *Macromol. Symp.* **2010**, *291–292*, 186.
[220] J. Gu, W. Zhang, H. Su, T. Fan, S. Zhu, Q. Liu, D. Zhang, *Adv. Mater.* **2015**, *27*, 464.
[221] a) Y. Zhu, W. Zhang, D. Zhang, *Adv. Mater. Technol.* **2017**, *2*, 1600209; b) D. Zhang, W. Zhang, J. Gu, T. Fan, Q. Liu, H. Su, S. Zhu, *Prog. Mater Sci.* **2015**, *68*, 67; c) Y. Chen, X. Zang, J. Gu, S. Zhu, H. Su, D. Zhang, X. Hu, Q. Liu, W. Zhang, D. Liu, *J. Mater. Chem.* **2011**, *21*, 6140; d) Y. Chen, J. Gu, D. Zhang, S. Zhu, H. Su, X. Hu, C. Feng, W. Zhang, Q. Liu, A. R. Parker, *J. Mater. Chem.* **2011**, *21*, 15237; e) X. Zang, Y. Ge, J. Gu, S. Zhu, H. Su, C. Feng, W. Zhang, Q. Liu, D. Zhang, *J. Mater. Chem.* **2011**, *21*, 13913; f) Z. Zhang, K. Yu, L. Lou, H. Yin, B. Li, Z. Zhu, *Nanoscale* **2012**, *4*, 2606; g) W. Peng, S. Zhu, W. Wang, W. Zhang, J. Gu, X. Hu, D. Zhang, Z. Chen, *Adv. Funct. Mater.* **2012**, *22*, 2072.
[222] Y. Zhang, B. Dong, A. Chen, X. Liu, L. Shi, J. Zi, *Adv. Mater.* **2015**, *27*, 4719.
[223] T. D. Nguyen, B. U. Peres, R. M. Carvalho, M. J. MacLachlan, *Adv. Funct. Mater.* **2016**, *26*, 2875.
[224] B. Ai, H. Möhwald, D. Wang, G. Zhang, *Adv. Mater. Interfaces* **2017**, *4*, 1600271.
[225] J. Wang, J. C. T. Eijkel, M. Jin, S. Xie, D. Yuan, G. Zhou, A. van den Berg, L. Shui, *Sens. Actuators, B* **2017**, *247*, 78.
[226] H. Ding, C. Zhu, L. Tian, C. Liu, G. Fu, L. Shang, Z. Gu, *ACS Appl. Mater. Interfaces* **2017**, *9*, 11933.
[227] S. Wu, B. Liu, X. Su, S. Zhang, *J. Phys. Chem. Lett.* **2017**, *8*, 2835.
[228] N. Vasilantonakis, K. Terzaki, I. Sakellari, V. Purlys, D. Gray, C. M. Soukoulis, M. Vamvakaki, M. Kafesaki, M. Farsari, *Adv. Mater.* **2012**, *24*, 1101.
[229] N. Suzuki, E. Iwase, H. Onoe, *Langmuir* **2017**, *33*, 6102.
[230] H.-b. Seo, S.-Y. Lee, *Sci. Rep.* **2017**, *7*, 44927.
[231] Q. Li, Q. Zeng, L. Shi, X. Zhang, K.-Q. Zhang, *J. Mater. Chem. C* **2016**, *4*, 1752.
[232] G. England, M. Kolle, P. Kim, M. Khan, P. Muñoz, E. Mazur, J. Aizenberg, *Proc. Natl. Acad. Sci. USA* **2014**, *111*, 15630.
[233] F. Laermer, A. Schilp, *US5501893*, **1996**.
[234] P. Kim, A. K. Epstein, M. Khan, L. D. Zarzar, D. J. Lipomi, G. M. Whitesides, J. Aizenberg, *Nano Lett.* **2011**, *12*, 527.
[235] B. M. Rey, R. Elnathan, R. Ditcovski, K. Geisel, M. Zanini, M.-A. Fernandez-Rodriguez, V. V. Naik, A. Frutiger, W. Richtering, T. Ellenbogen, *Nano Lett.* **2015**, *16*, 157.
[236] S. Liu, Y. Long, C. Liu, Z. Chen, K. Song, *Adv. Opt. Mater.* **2017**, *5*, 1601043.
[237] A. F. Demirörs, P. J. Beltramo, H. R. Vutukuri, *ACS Appl. Mater. Interfaces* **2017**, *9*, 17238.
[238] Y. Takeoka, *J. Mater. Chem. C* **2013**, *1*, 6059.
[239] M. Kohri, Y. Nannichi, T. Taniguchi, K. Kishikawa, *J. Mater. Chem. C* **2015**, *3*, 720.
[240] M. Kohri, S. Yamazaki, A. Kawamura, T. Taniguchi, K. Kishikawa, *Colloids Surf., A* **2017**, *532*, 564.
[241] H. Shen, Y. Wu, L. Fang, S. Ye, Z. Wang, W. Liu, Z. Cheng, J. Zhang, Z. Wang, B. Yang, *RSC Adv.* **2015**, *5*, 28633.
[242] a) Y.-J. Kim, Y. T. Matsunaga, *J. Mater. Chem. B* **2017**, *5*, 4307; b) F. D. Jochum, P. Theato, *Chem. Soc. Rev.* **2013**, *42*, 7468.
[243] A. Zhang, H. Bai, L. Li, *Chem. Rev.* **2015**, *115*, 9801.
[244] a) Y. Wang, Z.-g. Zheng, H. K. Bisoyi, K. G. Gutierrez-Cuevas, L. Wang, R. S. Zola, Q. Li, *Mater. Horiz.* **2016**, *3*, 442; b) S. H. Ryu, M.-J. Gim, W. Lee, S.-W. Choi, D. K. Yoon, *ACS Appl. Mater. Interfaces* **2017**, *9*, 3186.
[245] a) H. Ge, G. Wang, Y. He, X. Wang, Y. Song, L. Jiang, D. Zhu, *ChemPhysChem* **2006**, *7*, 575; b) M. Kamenjicki, I. K. Lednev, S. A. Asher, *J. Phys. Chem. B* **2004**, *108*, 12637.
[246] Y. W. Chiang, J. J. Chang, C. Y. Chou, C. S. Wu, E. L. Lin, E. L. Thomas, *Adv. Opt. Mater.* **2015**, *3*, 1517.
[247] N. L. Smith, Z. Hong, S. A. Asher, *Analyst* **2014**, *139*, 6379.
[248] a) J.-T. Zhang, X. Chao, X. Liu, S. A. Asher, *Chem. Commun.* **2013**, *49*, 6337; b) Z. Cai, J.-T. Zhang, F. Xue, Z. Hong, D. Punihaole, S. A. Asher, *Anal. Chem.* **2014**, *86*, 4840.